JAERI-M
4707

Recovery of Lattice Defects after Plastic Deformation and Neutron Irradiation at Low Temperature

February 1972

Saburo Takamura

日本原子力研究所
Japan Atomic Energy Research Institute

JAERI—M 4707

Recovery of Lattice Defects after Plastic Deformation and Neutron Irradiation at Low Temperature

Saburo Takamura

Div. of Physics, Tokai, JAERI
(Received 1 February 1972)

The recovery of electrical resistivity in polycrystalline copper, gold, aluminum, vanadium and iron, deformed at 4.2°K and in polycrystalline copper, gold, aluminum, iron, molybdenum and tungsten after fast neutron irradiation at about 5°K has been studied and the recovery structure was determined from 4.2°K to about 400°K.

For the recovery stage after deformation, the initial recovery stage (stage I) was attributed to the dislocation rearrangement rather than the annihilation of Frenkel pairs both in f.c.c. metals (Cu, Au, Al) and in b.c.c. metals (V, Fe). The stage II recovery was considered to be due to the migration or dissociation of interstitial clusters in both metals.

For the recovery of f.c.c. metals after fast neutron irradiation at about 5°K, cold work before irradiation enhanced the recovery above 150°K in Cu and above 50°K in Au. In Au, the stage III recovery shifted by about 30°K toward lower temperature for cold worked specimens. The effect of deformation after irradiation on the recovery spectra was studied on Cu, Au and Al. In Cu, the recovery below 43°K was retarded. But this large retardation could not be observed in Al and Au. Two current mechanisms for the recovery stages were discussed in relation with these observations.

For the recovery of Mo and W after neutron irradiation, the effect of

radiation doping on recovery stages was discussed. The radiation doping was found to increase the amount of stage I recovery in both Mo and W. The effect of radiation doping vanished in Mo when doped specimen was annealed above stage III, but not in W. This result suggested that the type of the so-called stage III defects of Mo were different from those of W. The effect of deformation on the mixed state of superconductor (V) was studied and the flux line pinning by defects was discussed.

JAERI－M 4707

低温で加工および中性子照射した後の格子欠陥の回復

日本原子力研究所東海研究所物理部
高村　三郎

（１９７２年２月１日受理）

加工および照射によって作られた格子欠陥の回復過程を電気抵抗法によって測定し，その解析を行った。銅，金，アルミニウム（面心立方金属），鉄，バナジウム（体心立方金属）を4.2°Kで加工した後の回復段階のステージⅠはフレンケル対の消滅，格子間原子の移動によるとするより，転位の再配列によると考えた方がよい。ステージⅡは格子間原子のクラスターの移動あるいは分解によると考えられる。銅，金，アルミニウムおよびモリブデン，タングステン，鉄を極低温で中性子照射した後の欠陥の回復の結果についても合せて議論した。

This report is based on the works which were published in the following journals:

Phys. Letters 25A (1967) 239, S. Okuda and S. Takamura; "Low temperature recovery in cold worked f.c.c. metals"

J. Phys. Soc. Japan 25 (1968) 418, S. Takamura, H. Maeta and S. Okuda; "Recovery of fast neutron irradiated molybdenum at low temperatures"

J. Phys. Soc. Japan 25 (1968) 714, S. Takamura and S. Okuda; "Electrical resistivity measurements of f.c.c. metals deformed at 4.2°K"

J. Phys. Soc. Japan 26 (1969) 1120, S. Takamura, H. Maeta and S. Okuda; "Recovery of fast neutron irradiated copper and gold at low temperatures"

J. Phys. Soc. Japan 26 (1969) 1125, S. Takamura, H. Maeta and S. Okuda; "Recovery of fast neutron irradiated iron at low temperatures"

Phys. Stat. Sol. 36 (1969) 531, S. Okuda, S. Takamura and H. Maeta; " "Effect of plastic deformation on the recovery of stage I after neutron irradiation"

Trans. Japan Inst. Metals 11 (1970) 434, R. Hanada, S. Takamura, S. Okuda and H. Kimura; "Recovery of fast neutron irradiated molybdenum"

J. Phys. Soc. Japan 30 (1971) 1091, S. Takamura, R. Hanada, S. Okuda and H. Kimura; "Recovery of low temperature fast neutron irradiated tungsten"

J. Phys. Soc. Japan 30 (1971) 1360, S. Takamura, R. Hanada and S. Okuda; "Electrical resistivity measurements of deformed metals after low temperature neutron irradiation"

J. Phys. Soc. Japan 30 (1971) 1367, S. Takamura; "Electrical resistivity measurements of vanadium and iron deformed at 4.2°K"

Contents

1. Introduction

The problem of atomic displacements from the normal crystal lattice sites in crystalline solids by irradiation are of technological importance and are also important for research on the physical properties of solids. Wigner[1] deduced in 1946, prior to the construction of the first nuclear reactors, that the structural materials exposured by the intense radiation in reactors would lead to pronounced changes in the physical properties. The graphite used as a reactor materials showed that very large effects could occur. The effects of irradiation have been investigated on many solids at a fundamental and a technological regions. Thus, the research of radiation damage are of importance on the reactor materials. It is generally observed that the stress at which yield occurs is increased and the marked yielding phenomenon occurs by irradiations. These change in mechanical properties are due to the interaction between dislocations and irradiation induced defects.

The point defects in metal crystals play an important role for the strain aging and diffusion, in addition to having influence on the physical and mechanical behaviour of metal and alloy as a consequence of point defect-dislocation interactions or point defect-solute atom interactions. The studies associated with the behaviour of point defects are able to be gained from the annealing process of excess point defects present over thermal equilibrium. The methods obtaining the excess point defects in crystal are to quench the specimen from an elevated temperature to a low temperature rapidly enough to freeze in the defects, the ratiation damage and generation of defects by plastic deformation. The most simple study in these experiments is quenching and a number of quantitative informations

about vacancy defects are given from quenching experiments.

The irradiation produces Frenkel defects in the lattice, vacancies and interstitials in equal numbers. The defects in specimens react with each other. Some of the reactions are annihilation of vacancies and interstitials by recombination, aggregation of defects and trapping of defects at impurities upon warming. The annealing stages depend on the activation energy of the mobile defect, the initial distribution of defects and sinks. The interpretation of recovery stage is still a matter of discussion. One of the question is whether a sort of interstitial present in crystal is one or two. This dispute continues for more than ten years even though extensive effort has been made.

The studies of point defects formed by plastic deformation are few compared with the amount of research in quenching and radiation damage experiments. Deformation introduces complex defect structure, particularly the recovery phenomena at low temperature remain as unknown problem. In the present work, the defects produced by deformation and irradiation in metals are studied by means of the measurements of electrical resistivity, particularly the mechanisms of recovery at low temperatures and the interaction between these defects and dislocations.

1. 1. Production of defects by plastic deformation at low temperature.

There are many experimental observations of the formation of point defects by plastic deformation.[2,3] The motion of dislocations during plastic deformation can generate point defects by several mechanisms. Two important mechanisms are considered at present. (a) The formation by the nonconservative motion of jog on screw dislocations.[4~6] Short jogs are produced by the intersection of a dislocation with a second dislocation. Edge dis-

location is able to slide on the slip plane freely with jog. Jog on screw dislocation is small edge dislocation which have Burgers vector parallel to screw dislocation. The jog on screw dislocation can slide along screw dislocation, but the formation of a row of vacancies or of interstitials results behind the jog because of movement of edge dislocation slided out slip plane if the jog slides out the plane involving the screw dislocation and the jog. (b) When two edge dislocations of opposite sign lie on glide planes separated by one lattice spacing, their configuration is equivalent to a row of vacancies or a row of interstitials.[7] If two screw dislocations with different Burgers vectors meet and are unable to intersect one another, one dislocation sweeps around the other, forming edge segments which are separated by the Burgers vector. The rows of interstitials or vacancies produced by these two mechanisms may be dispersed with the amount of edge component but it has been suggested that in the resulting distribution, point defect pairs and larger clusters may be favored over single defects.

1. 2. Production of defects by low temperature irradiation.

The irradiation of a crystal with energetic particles produces Frenkel defects in the lattice. This phenomenon is said as radiation damage and it plays an important role in the research of point defects. Neutron interacts only with the nuclei of the lattice since it has no charge. The total cross sections are of the order of 10^{-24} cm^2. A displaced primary atom is slowed down by interaction with the other atoms of the lattice.

There is minimum energy to be required in order to displace the lattice atom from its original site. This displacement energy, E_d, is approximately between 20 and 50 ev for most metals. As long as the lattice atom is tranferred the energies between E_d and $2E_d$, it is expected to produce one

displaced atom. The number $\nu(T)$ of displacements produced by a primary displacement of initial energy T can be calculated by Kinchin-Pease model.[8] $\nu(T) = T/2\ E_d$. In this model, when the energy of primary is above a limited value T_c, all the energy is lost in electronic excitation, and below T_c all the energy is used in producing displacements. In neutron irradiation in thermal reactor, the average energy of primary knock on atom is below T_c. In a elastic collision, the maximum energy T_m, which is transferred by a neutron of energy E_n to a nucleus of atomic weight A is $T_m = 4A \cdot E_n/(A+1)^2$. For 2 MeV neutrons the average number of displacements per collision is 700 when an atomic weight A = 100. The damage produced by a primary knock-on due to neutron in the lattice is generally very concentrated. Damaged zone will consist of a region with a high vacancy density surrounded by a shell with a high density of interstitial atoms. This zone with high vacancy concentration is called as a depleted zone or Seeger zone.[9] Recent studies have shown that the crystal lattice structure can play an important role in the atomic displacement process. The lines of close packed stoms in the crystal littice are able to transfer energy. The first atom on a close packed line in a lattice gives an impulse the second atom at an angle ψ to the line, and the sequence of collision along the line is propagated if ψ is less than the critical value ψ_c. A component of the initial momentum is focused into the close packed line of atoms. This process is a focusing collision which are able to remove energy from a displacement cascade.[10] Replacement collision occurs when the initially moving atom retains an energy less than E_d after collision and the struck atom move to neighbouring site from the initial site.[8] The collision sequence due to focusing collision are distorted in the neighbourhood of

a dislocation and end abruptly at the stacking fault region. This process tends to generate more damage in the vicinity of a dislocation line.[11] Thus, the increasing rate of defect production depends on deformed structure of the solids. There exists one further effect known as channelling.[12] A moving atom in a cascade may be deflected by a collision into a channel through the lattice and then continue in motion along it. Such channelled atoms are unlikely to be as effective in producing displacements. Oen et al.[13] calculated the effect of channelling on the number of displacements assuming channelled atoms produces no further displacements. The total number of atoms displaced by the primary knock on of energy T is

$$\frac{1}{1-2p}\left[(1-P)\left(\frac{T}{2E_d}\right)^{1-2p} - P\right] \qquad \text{for } T > 2E_d$$

where p is the probability of being channelled following a collision. The number of displacements is reduced about a fifth if P = 0.1.

1. 3. Recovery processes of point defects

If a solid contains a defect concentration in excess of the thermal equilibrium, these defects will react. Its changes are a function of temperature, defect concentration and time. The property change due to defects is generally formulated using equations similar to those of chemical kinetics.[3] The annealing rate of the recovery may be described by

$$-\frac{dn}{dt} = n^{\gamma} \cdot \nu \cdot \exp(-E/kT)$$

where n is the number of defects per unit volume, γ the order of reaction, E the activation energy of migration, ν the atomic frequency and t the time. The number of defect changed is obtained by resistivity measurements as long as the resistivity is proportional to the defect concentration.

a dislocation and end abruptly at the stacking fault region. This process tends to generate more damage in the vicinity of a dislocation line.[11] Thus, the increasing rate of defect production depends on deformed structure of the solids. There exists one further effect known as channelling.[12] A moving atom in a cascade may be deflected by a collision into a channel through the lattice and then continue in motion along it. Such channelled atoms are unlikely to be as effective in producing displacements. Oen et al.[13] calculated the effect of channelling on the number of displacements assuming channelled atoms produces no further displacements. The total number of atoms displaced by the primary knock on of energy T is

$$\frac{1}{1-2p}\left[(1 - P)\left(\frac{T}{2E_d}\right)^{1-2p} - P\right] \qquad \text{for } T > 2E_d$$

where p is the probability of being channelled following a collision. The number of displacements is reduced about a fifth if P = 0.1.

1. 3. Recovery processes of point defects

If a solid contains a defect concentration in excess of the thermal equilibrium, these defects will react. Its changes are a function of temperature, defect concentration and time. The property change due to defects is generally formulated using equations similar to those of chemical kinetics.[3] The annealing rate of the recovery may be described by

$$-\frac{dn}{dt} = n^{\gamma} \cdot \nu \cdot \exp(-E/kT)$$

where n is the number of defects per unit volume, γ the order of reaction, E the activation energy of migration, ν the atomic frequency and t the time. The number of defect changed is obtained by resistivity measurements as long as the resistivity is proportional to the defect concentration.

For isochronal annealing, which is the stepwise increase of temperature in equal time interval, the integrated forms at a temperature T_i may be given as follows:

$$\frac{1}{n_0^{\gamma-1}} - \frac{1}{n_i^{\gamma-1}} = \nu \cdot \Delta t \cdot \exp(-E/kT_i) \qquad \text{for } \gamma \neq 1$$

$$n_i/n_0 = \nu \cdot \Delta t \cdot \exp(-E/kT_i) \qquad \text{for } \gamma = 1$$

The relative concentration change with temperature, n_i/n_0, does not depend on the initial concentration, n_0, when γ is equal to 1, but for $\gamma \neq 1$ n_i/n_0 depends on n_0 where the isochronal recovery curve is shift to low temperature with increasing n_0.

Since irradiation produces two primary defects, vacancies and interstitials, in a crystal, the annealing of radiation damage is expected to exhibit stages corresponding to mutual annihilation in a simple case. The interstitial is the faster moving defect and its jump rate is the rate control at low temperature. Let the jump frequency in any direction ν_i and the vacancy is surrounded by Z sites from which interstitial jumps toward the vacancy. If I' is the probability that an interstitial is on one of these Z sites, then the rate of vacancy annihilated by recombination with interstitials is

$$-dV/dt = Z\nu_i VI'$$

where V is the concentration of vacancies in atomic fractions. The number of interstitials disappeared must equal the number of vacancies annihilated. If interstitials are randomly distributed in the biginning and the diffusion continually redistributes the remaining ones, I' is equal to I. I is the

concentration of interstitials.

$$-dV/dt = Z\nu_i V(I_0 - V_0 + V)$$

when the initial concentrations are equal, the reaction rate of defects is described by the simple second order equation, e.g.

$$dV/dt = Z\nu_i V^2$$

1. 4. Recovery in face centered cubic metals and body centered cubic metals

The discovery of a large annealing stage below 60°K in Cu and Ag was made by Cooper et al. in 1955.[14] The pioneering experiments which clarified the nature of the recovery processes in the low temperature range of electron irradiated Cu were performed by Corbett et al. in 1959.[15]

The damage produces in the form of randomly distributed interstitial vacancy pairs by electron irradiation at low temperature. Stage I consists of at least five sub-peaks which were first found by Corbett et al. for Cu.[15] A number of small subpeaks have been reported by Kauffman et al.,[16] but this fine structure may be due to the experimental procedure since the fine structure have never reproduced. Stages I_A, I_B and I_C are due to the recombination of close Frenkel pairs. This interpretation is based on the observation that the reaction kinetics of these stages obeys a first order reaction law. This reaction is not dependent on the total number of defects produced by the irradiation or on the addition of doping agents which could act as sinks for interstitials. Stage I_D, independent of irradiation dose and doping, is assigned as the correlated recombination of non-interacting interstitials and vacancies. That the activation energy in

stage I_D is the same as that of stage I_E has been proved by Corbett et al. for Cu.[15] Stage I_E is shown to be dose-dependent and requires a large number of lattice jumps. In this stage, interstitial escape from the neighbourhood of its original vacancy partner and annihilate with some other vacancy.

Several different interstitial configurations are possible in f.c.c. metals. The interstitial configurations are the body-center, the activated crowdion and the tetrahedral, the split <100> interstitial configuration, the split <110> interstitial crowdion and the split <111> interstitial. The calculations indicate that the lowest energy and the stable configuration is the split <100> configuration.[17] The crowdion appears as metastable, but near the limit of instability. There are many possible configurations for di-interstitial. The most stabe di-interstitial has two split interstitials parallel to each other at nearest-neighbor lattice sites. Similar calculations have been done for the interstitial configurations in Fe, which is b.c.c. metals.[18] Six types of interstitial configurations can be distinguished as in the f.c.c. lattice, e.g. activatived crowdion, octahedral interstitial, tetrahedral interstitial, <100> split, <110> split and <111> split interstitial (crowdion). Calculations show the <110> split interstitial as the stable configuration. The calculated motion energies are 0.33 and 0.18 ev for split interstitial and di-interstitial respectively.[18] The most stable di-vacancy according to the calculation is one in which two vacancies are at second nearest neighbouring lattice sites. The motion energies are 0.66 and 0.78 ev for vacancy and di-vacancy, respectively.[18] The most striking discrimination of the configuration of defect should be obtained by anelastic observations which can reveal the symmetry of the defect

involved. The anelastic experiments are the measurement of internal friction and magnetic after effects.

In Ni, the position of stages I_B and I_C in the magnetic relaxation curves are almost independent of the irradiation dose, whereas the peaks I_E is shifted to lower temperatures with increasing dose.[19] These results seem to indicate that relaxation peaks I_B and I_C are due to Frenkel pairs whereas I_E peak is caused by freely migrating interstitials. Also the experimental results suggest that the defects of stage I_E would be in the split configuration in the <100> direction.

For Fe,[20] stages I_A, I_B and I_C are considered to be due to the recombination of close pairs by the following facts: a) the relative retardation of stages I_A, I_B and I_C and growth of stage I_D after neutron irradiation comparing with electron. b) the kinetics are observed to be of first order. The recovery peak I_D in internal friction measurements is observed only after neutron irradiation. After electron irradiation, stage I_D does not appear whilst stage I_D in the resistivity measurement is present after electron irradiation. An interpretation for the <100> orientation of this defect have not been found. The defects associated with stage I_D in Fe and Ni relax mechanically but not magnetically, because of the absence of magnetic after effect corresponding to stage I_D in both Ni (f.c.c. metal) and Fe (b.c.c. metal). It is therefore concluded that stage I_D cannot be attributed to a simple defect. For stage I_E in Fe, the point defect responsible for this stage has an orientation which is probably <110> and this defect is able to reorientate both magnetically and mechanically. Its annealing kinetics are of order two. The fact that the internal friction peak II and magnetic after effect at 128°K exist

involved. The anelastic experiments are the measurement of internal friction and magnetic after effects.

In Ni, the position of stages I_B and I_C in the magnetic relaxation curves are almost independent of the irradiation dose, whereas the peaks I_E is shifted to lower temperatures with increasing dose.[19] These results seem to indicate that relaxation peaks I_B and I_C are due to Frenkel pairs whereas I_E peak is caused by freely migrating interstitials. Also the experimental results suggest that the defects of stage I_E would be in the split configuration in the <100> direction.

For Fe,[20] stages I_A, I_B and I_C are considered to be due to the recombination of close pairs by the following facts: a) the relative retardation of stages I_A, I_B and I_C and growth of stage I_D after neutron irradiation comparing with electron. b) the kinetics are observed to be of first order. The recovery peak I_D in internal friction measurements is observed only after neutron irradiation. After electron irradiation, stage I_D does not appear whilst stage I_D in the resistivity measurement is present after electron irradiation. An interpretation for the <100> orientation of this defect have not been found. The defects associated with stage I_D in Fe and Ni relax mechanically but not magnetically, because of the absence of magnetic after effect corresponding to stage I_D in both Ni (f.c.c. metal) and Fe (b.c.c. metal). It is therefore concluded that stage I_D cannot be attributed to a simple defect. For stage I_E in Fe, the point defect responsible for this stage has an orientation which is probably <110> and this defect is able to reorientate both magnetically and mechanically. Its annealing kinetics are of order two. The fact that the internal friction peak II and magnetic after effect at 128°K exist

only after neutron irradiation indicates that the associated defect is not a simple point defect. Interstitials happen to find each other and form di-interstitials. Since di-interstitials are the dominant form in which interstitials survive above stage I after low dose damage, it would be expected that either dissociation or migration of di-interstitials occur in stage II.

There are two main models of the stage III recovery for the radiation damage in f.c.c. metals, namely, a) the one-interstitial model, (b) the conversion-two-interstitial model. The one interstitial model assumes the existence of only one configuration of the interstitial. This defect migrates at about 50°K (stage I_E) in Cu. The conversion-two-interstitial model postulates that two configurations of the interstitial are present, a metastable one migrates freely in stage I_E and a stable one migrates in stage III, and the stage I_E interstitial can be transformed into the stage III interstitial by thermal activation.

The b.c.c. metals have a tendency to pick up interstitial impurities because of their open structure. This causes a difficulty in the interpretation of recovery stages. Besides, most of b.c.c. metals have high melting points and quenching experiments are very difficult to perform on these metals. For b.c.c. metals, controversial interpretations for recovery are mainly centred around stage III. There are two interpretations ascribing stage III to migration of free vacancies and of free interstitials.

Stage III of W and Mo was generally ascribed to vacancy migration with first order kinetics until 1962.[21] Later, the reaction corresponding to second order kinetics was found and it was proposed that stage III is caused by free interstitial migration to vacancies in analogy with the two interstitial

model of f.c.c. metals.[22] In addition, stage III is sometimes explained in terms of interstitial impurity migration, since interstitial impurities have a migration energy being equal to the observed stage III activation energy.[23] For Nb,[24] Ta[25] and α-Fe,[26] considerable evidence of impurity migration in stage III has given. Evidence has been given for the absence of a pronounced stage III recovery in neutron irradiated Nb[24] and in plastically deformed Nb, Ta,[25] and α-Fe,[26] if very pure specimens were used. These results seem to leave no doubt about interstitial impurities playing an important part in stage III of α-Fe, Ta and Nb.

However, it has been shown that neutron irradiation of very carefully decarburized W gave rise to a normal prominent stage III recovery.[27] It may be concluded that for W and Mo the stage III recovery corresponds to an intrinsic process. Thus controversy of interpretation of stage III of b.c.c. metals is in a similar situation to that of stage III in f.c.c. metals.

In the present experiments, annealing studies of the electrical resistivity of f.c.c. metals and b.c.c. metals are made. The detailed mechanisms in the recovery after deformation have not been made clear yet. Recovery studies after deformation of f.c.c. metals and b.c.c. metals are discussed at first. Secondly effects of dislocation doping, impurity doping and radiation doping on the recovery stages are discussed for a various metals after fast neutron irradiation at low temperature. Then stages I and III in b.c.c. metals are discussed from these results.

1.5. Interaction between point defects and dislocations

The distortions around point defects and dislocations cause an

interaction between them. The defects are attracted to the region where they can relieve the stress. The region immediately below the half plane of an edge dislocation is a region of dilatation, while the region immediately above is one of compression. A vacancy will be attracted to a region of compression and an interstitial to one of dilation. The elastic interaction is calculated in the following manner.[28] If $r(1+\varepsilon)$ is the radius of a defect and r is the radius for this defect in the parent crystal, the interaction energy of defect with any stress field is given by

$$U = -\frac{4}{3}\pi\varepsilon r^3(\sigma_x + \sigma_y + \sigma_z)$$

where the σ_s are the normal stresses at the site of defect. The interaction energy at the defect position given by radius vector R and angle θ from edge dislocation is

$$U = 4G\varepsilon r^3\lambda(1 + \nu)\sin\theta/(3R\cdot(1 - \nu))$$

where G is the shear modulus, ν possion's ratio and λ the slip distance in the dislocation. For most metals, the value at one atomic distance from dislocation is about 0.1 ev and 0.02 ev for $\varepsilon = 0.1$ of interstitial and $\varepsilon = 0.02$ of vacancies, respectively.

The electrical interaction arising from the redistribution of electrons caused by any volume dilation is much smaller than the elastic interaction and is typical of the order of 0.02 ev for vacancies and interstitials in the monovalent metals.[29] The screw dislocation does not possess an dilational strain field. A non-spherical distortion around an interstitial is able to provide an interaction with a screw dislocation. Replacing an atom of the matrix by an atom of different elastic constants changes the

elastic energy stored in the atom. The interaction energy between a dislocation and the atom is proportional to the difference of the elastic constants.[30]

Thus, dislocations can act as traps for point defects. The jogs in dislocations, which occur when the dislocation changes its slip plane abruptly by one interatomic spacing, absorb vacancies or interstitials by moving along the dislocation. Deformation changes the annealing recovery.[31,32] Some interstitials are trapped at dislocation lines in stage I and the interstitials trapped at dislocations may be able to move along dislocations to annihilate in stage II. In stage III, the interstitials release from trapping at dislocation lines and migrate to fixed vacancies. These dislocation trapping model was suggested by Sosin.[33]

The methods to examine the point defects-dislocations interaction are tensile test, internal friction and modulus measurements. The accurate measurements of electrical resistivity would also apply to examination of the interaction between defects produced by fast neutron and dislocations.

1. 6 Infuence of defects on the superconducting properties.

For type II superconductors, the exclusion of magnetic field from the specimen occurs for values of field H smaller than H_{c1}, where H_{c1} is a critical lower field. For $H_{c1} < H < H_{c2}$, magnetic flux gradually penetrates into the specimen. In this range, a lattice of quantized flux-enclosing supercurrent vortices is formed. This state is commonly called as the mixed state. For $H < H_{c2}$, the specimen becomes normal.

Abrikosov[34] proposed a structure of the mixed state containing a two-dimensional periodic array of normal regions of small radius, in which the core of line contains magnetic flux and is surrounded by a vortex of

superconducting electrons. The radius of a core is of the order of coherence length and each flux line carries one quantum of flux. Essmann et al.[35] have observed the flux line pattern directly in Pb-In and in Nb by depositing small ferromagnetic particles on the specimen and observing these with an electron mircroscope using a replica technique. The flux lines in the mixed state may be subject to a number of forces: (1) Coulomb interaction will produce a force between two flux lines, (2) there is a Lorentz force perpendicular to the direction of the current in the presence of transport current, (3) if there are pinning points in the specimen these will impede the movement of flux lines.

The electric voltage can be observed between two point along a specimen when the magnetic field and the current are kept constant, which may be interpreted as a steady movement of flux across the specimen under the action of the Lorentz force.

Type-II superconductors containing defects exhibit high transport current, and this property is discussed in terms of the interaction of flux lines in the mixed state with dislocations and defect clusters. The flux lines are pinned by these defects so that the movement of flux lines occurs when the Lorentz force exceeds the pinning force. The voltage produced by flux line motion in the mixed state is changed by the concentration of defects, which are removed by annealing above a certain temperature. One purpose of the present experiments is to study the influence of defects on the superconducting properties of vanadium after deformation at liquid helium temperature.

2. Experimental Procedures

2. 1 Specimens

2. 1. 1. Specimens used for deformation experiments

The specimens of Au, Cu and Al used for deformation at low temperature were of 99.999% purity and wires of 0.3 ∿ 0.4 mm dia and 30 ∿ 35 mm length. As-received cold drown wires of Cu and Al were annealed in vacuum (about 4×10^{-6} mm Hg) for 70 min at 900°C and for 120 min at 350°C and Au wires were in air for about 50 hr at 980°C, before deformation at low temperature. The resistivity ratios of annealed specimens at room temperature and 4.2°K ($\rho_{R.T}/\rho_{4.2}$) were about 900 for Cu and Au.

For V, the foil of 0.005 in thickness was obtained from Materials Research Corporation (M.R.C.). Nominal purity was 99.98% and gaseous impurities was 57, 3 and 112 ppm for carbon, nitrogen and oxygen, respectively. Specimens of about 1 mm wide were cut from the foil, and wound into helical form. Then, the specimens were annealed by current heating under high vacuum (10^{-8} mmHg) for about 1 hr at 1200°C; the temperature was estimated from the resistivity of specimens and also with an optical pyrometer. The current and potential leads were spot welded to the specimen. The resistivity ratio between room temperature and 4.2°K was about 15.

Fe wire of 0.005 in dia. of 99.99% purity was from M.R.C. Specimens were annealed for 3 days at 850°C in hydrogen purified by zirconium hydride. Current and potential leads for resistivity measurement were soldered to the specimen. The resistivity ratio between room temperature and 4.2°K was about 200. The resistivity of specimens of V and Fe at 4.2°K was obtained from the resistance at 4.2°K and room temperature and the resistivity of the pure metal at room temperature.[36)]

2. 1. 2. Specimens used for irradiation experiments

The specimens of Cu and Au were of 99.999% purity. They were wires of 0.3 ∿ 0.4 mm dia. and about 80 mm length. Cu specimens were annealed in vacuum for 90 min. at 900°C, and Au specimens annealed in air for about 40 hr at 980°C. The resistivity ratios of annealed specimens between room temperature and 4.2°K were about 1000 for Cu and Au. Deformed specimens of Cu were prepared by twisting at room temperature and annealed at 50°C, and those of Au by drawing and annealed at 100°C.

Mo wire of 50 μm diameter was purchased from M.R.C. and the resistivity ratio between room temperature and 4.2°K was 5 to 10 in the as-received state. The specimen was first annealed at 1800°C in wet and dry hydrogen for 5 hr. Next, the specimen was annealed under ultra high vacuum (10^{-9} Torr.) for 5 ∿ 6 days at 1700°C. After these treatments, the final resistivity ratio was increased to 400 ∿ 1000 without any size correction. The following specimens were used for the experiments on the effect of deformation. The specimens were wires of 0.005 in dia and about 80 mm length. Nominal purity of the as-received wires obtained from M.R.C. was 99.992%. Annealing was performed at 1150°C for 4 hr in vacuum (3×10^{-6} mmHg). Deformation was given at room temperature by twisting the annealed specimen by about 50% surface shear strain.

For W, specimens in the wire form of 0.005 in dia were used. The wires of nominal purity 99.97% were obtained from M.R.C. They were annealed about 5 days at 1700°C in ultra high vacuum (10^{-9} mmHg) after hydrogen annealing at 1500°C. After this treatment, the resistivity ratio of specimens at room temperature and 4.2°K were about 200.

The specimen was mounted on a mica strip protected by a silica tube. Both ends of the specimen were soldered on heads of 1 mm screws using Mo solder as described by Dejong and Afman.[37]

For Fe, specimens used for irradiation were obtained from M.R.C. in the wire form of 0.005 in dia. The nominal purity of this material was 99.995% including 8 ppm carbon, 7 ppm oxygen and 7 ppm nitrogen. They were annealed in vacuum for 1 hr at 900°C and then 1 hr at 700°C. The resistivity ratio of specimens at room temperature and 4.2°K was 110 ∿ 170. Deformed specimens were prepared by twisting at room temperature. This treatment gave 18% and 46% surface shear strain. The resistivity of specimen at 4.2°K was calculated from the resistance measured at 4.2°K and room temperature and the value of the resistivity of pure metal at room temperature.

2. 1. 3. Specimens deformed after irradiation at low temperature.

The specimens used were wires of diameter about 0.1 mm (Cu), 0.06 mm (Au) and 0.3 mm (Al). They were all of 99.999% purity. Cu and Al specimens were annealed in vacuum of 10^{-5} mmHg for about 2 hr at 900°C and 600°C, respectively. Au specimens were annealed in air for about 20 hr at 980°C.

2. 2. Irradiation experiment at low temperature

The liquid Helium Temperature Loop (LHTL) was set in the horizontal experimental hole of JRR-3. The loop is shown in Fig. 1. The facility was designed to cool the temperature of capsule down to as low as 4.5°K. In the facility, high pressure helium gas was expanded to a lower pressure and the temperature was reduced further by Joule-Thomson cooling. The inmost tube of irradiation facility was cooled by circulating helium mist. Surrounding this tube, there was an intermediate tube through which helium gas cooled

by liquid nitrogen was circulated. The end of the irradiation tube was surrounded by a fast converter to reduce the thermal neutron flux. The fast converter was designed to yield fission neutron spectrum. The reactor neutrons were converted into fission neutrons by a cylinder of uranium which contained 95% enriched uranium-zircaloy with zicaloy cladding. Inside the uranium there was cylinder of boron carbide. The thermal neutron absorbed by boron resulted a pure fission neutron spectrum. The fast converter system was cooled with water. Capsule was inserted from a casule inlet and sent to the other end in the irradiation tube. After irradiation, the capsule was dropped into liquid He in a transporting container. The irradiated capsule was transferred into the glass Dewar from a transporting container through the specially designed cryostat cooled by mist of liquid helium. The specimen removed from inside a capsule in the liquid helium of the glass Dewar using the long tongs and were inserted into sample chamber where the annealing treatment could be made.

It is important to know the energy spectrum of the neutrons as well as their number for the interpretation of radiation damage measurements. Reactor neutrons can be divided into three regions; thermal, epithermal and fission neutrons. The thermal neutron flux can be measured from the activity induced by thermal neutron. Gold was used as thermal detector. The activation was a product of the neutron flux and the cross section. The activity with and without Cd cover of the detector was measured. The latter activation corresponds to that from thermal and epithermal neutrons, and the former represents the activation from the epithermal neutrons. The measurement of the fast neutron flux was done by the use of threshold detectors Al, Fe and Ni. Neutron spectrum was obtained from

these results.

Specimens were irradiated mostly by fast neutrons: fast neutron flux in the irradiated space was about 1 x 10^{12} n/cm^2·sec (>0.1 MeV), epithermal neutron flux about 1.4 x 10^{10} n/cm^2 sec, and thermal neutron flux below 10^9 n/cm^2 sec.

2. 3. Annealing apparatus and temperature control

The apparatus used in the early experiments for deformation at 4.2°K in f.c.c. metals and following isochronal annealing is shown in Fig. 2. A specimen was mounted in specimen chamber (3), and deformed by pulling the stainless steel tube (7). The amount of deformation was determined by measuring the difference in length between the potential probes before and after deformation. After the deformation, the specimen was annealed isochronally with a manganin heater (2) after evacuating the space (4). The annealing temperatures, measured by a copper-constantan thermocouple, were held constant for 6 minutes within ±0.2°K. Thermoelectric voltage was measured by P-7 potentiometer of Yokokawa Electric Corp. The resistivity of specimens was measured after liquid helium was introduced into the specimen chamber through the needle valve (5) and helium gas into the vacuum space (4). Since this early appartus spent a large amount of liquid helium during annealings, in the later stage of the experiments, the method for annealings was improved as shown in Fig. 3. In this apparatus, specimens were annealed by raising the chamber above the liquid helium level and passing a electric current through the heater. After each pulse annealing, the specimen were cooled by immersing the specimen chamber into liquid helium.

For deformation of V, the torsional deformation was applied in liquid

helium by pulling one end of a helical specimen with the other end fixed. The specimen of Fe were deformed in liquid helium and 79°K by twisting the one end of the specimen.

For annealing studies of the electrical resistivity after neutron irradiation at low temperature , the irradiated specimens were transferred to the glass Dewar as described above where the annealing experiments and resistivity measurements were made. During the transfer of the specimens, special care was taken not to warm up the specimens. In the Dewar, the specimens were placed in a small box wound by heater and were annealed by raising the box from the liquid helium level and passing a electric current through the heater. Annealing temperatures of 6 minutes pulses were controlled manually within ±0.2°K. Later, the control of temperature were made by automatic electric controller of PID type of Okura Electric Corp. Annealing temperature were controlled within ±0.2°K. A copper-constantan thermocouple placed in the specimen box was used to measure the temperature. After each pulse annealing, the specimens were cooled by immersing the specimen box into liquid helium.

2. 4. Measurement of electrical resistivity

The electrical resistivity of specimens were measured in liquid helium by the standard potentiometric method. A Diesselhorst-type potentiometer (Otto Wolff KDE 8) was used with a high sensitivity photocell-amplified galvanometer. The effect of thermal emf's was eliminated by taking the forward and reverse current readings. The reproducibility of measurements was within 2×10^{-8} V. Since V is superconductor, the electrical resistivity of V was measured in liquid helium with the magnetic field of 5000 Oe applied perpendicular to the axis of a helical specimen.

For Fe after deformation at low temperature, the electrical resistivity was measured in liquid helium with a magnetic field of 140 Oe parallel to the specimen axis. A magnetic field was kept constant by constant current supply to a coil placed outside the Dewar.

3. Experimental Results

3.1 Plastic deformation in f.c.c. metals

a. Au

The isochronal recovery curves of the residual resistivity induced by deformation at 4.2°K are shown in Fig. 4. The recovery of specimen 1, fully annealed prior to deformation, is in good agreement with the results by Schumacher et al.[38]; the initial continuous recovery up to about 120°K and a reverse annealing from 120°K to 150°K are followed by a large recovery stage. The amount of reverse annealing for fully-annealed different specimens are different. Specimens 5 and 6, deformed at room temperature and annealed at 100°C to anneal out only the point defects prior to deformation at 4.2°K, recover continuously without any reverse annealing.

The effect of additional deformation is shown in Fig. 5. Increase of the dislocation density is seen to enhance the recovery, when the curves 2 and 4 are compared with the curves 1 and 3, respectively. The curves 2 and 4 are for the specimens deformed additionally after partial annealing. Similarly, the large dislocation density in the specimens of the curves 5 and 6 increases the slope of the recovery curves.

b. Cu

The isochronal recovery curves of the resistivity induced by deformation are shown in Fig. 6. In Cu, the initial continuous recovery is followed by a large recovery in the range 100°$\sim$ 200°K where the most prominent recovery occurs at 130°K. No reverse annealing is observed on the contrary to Dawson's results.[39]

c. Al

The isochronal recovery curves of Al are shown in Fig. 7. The initial recovery, up to about 50°K, is followed by a large recovery centered at 80°K. Similar results are also obtained by Swanson.[40]

In Fig. 8, fractional isochronal recovery curves of deformed Au, Cu and Al are compared with one another.

3.2 Vanadium and iron after deformation at low temperature.

a. V

The isochronal recovery curves after deformation at 4.2°K are shown in Fig. 9. Here, the resistivity increases immediately after deformation are 4.5, 0.7, 2.9 and 1.5 x $10^{-8}\Omega$cm, respectively. The latter two specimens have been deformed at 4.2°K after deformation at room temperature. For small amount of deformation (0.7 x $10^{-8}\Omega$cm) in the specimen as-annealed, the recovery is seen to be enhanced although the measurement is less accurate (curve 4). The recovery rate increases with decreasing amount of deformation given to specimens. This behaviour is in contrast to that of f.c.c. metals in which the rate of recovery increases with increasing amount of deformation. The differential isochronal curves, calculated from Fig. 9, are shown in Fig. 10.

b. Fe

The dependence of the resistivity at 4.2°K of specimens on the applied magnetic field is shown in Fig. 11. The resistivity ratio of this specimen at 273°K and 4.2°K without a magnetic field is 200 and that with a magnetic field of 140 Oe is 290. The amount of deformation is such that the resistivity increase is 8 x 10^{-10} Ωcm. The negative magnetoresistance is due to movement of magnetic domain walls and the rotation of the magnetization direction

of domains into the applied field. The decrease in electrical resistivity with the applied magnetic field is smaller in the specimen deformed at 4.2°K than for an as-annealed specimen. This is considered to be due to the interaction between the domain wall and internal stresses. The resistivity change due to the negative magnetoresistance is so large at 4.2°K in Fe that the measurements on recovery stages must be carried out under a constant magnetic field, particularly for the recovery after deformation. Therefore, in the present experiments, resistivity measurement is made in a magnetic field of 140 Oe, which is kept constant by constant current supply. In Fig. 12, the isochronal recovery curve after deformation at 4.2°K is shown. Because of brittleness, the deformation of Fe at 4.2°K is difficult and the possible amount of deformation is very small. About 90% of resistivity given by deformation at 4.2°K is restored by annealing at 300°K. The isochronal recovery curve after deformation at 79°K is also shown in Fig. 12. The recovery stage observed at about 200°K is similar to that of Cuddy.[41]

3.3 F.c.c. metals after irradiation at low temperature.

a. Damage rates

The damage rates of Cu are considerably enhanced by cold work (enhancement of more than 10%). On the other hand, the damage rates of Au are decreased by cold work and also by alloying. The decrease amounts to about 10%.

b. Recovery of Cu

The isochronal recovery curves and their differential curves are shown in Figs. 13 and 14, respectively. The differences between fractional recovery of the cold worked specimens and annealed ones against temperature are plotted in Fig. 15. The main features are as follows. (a) The recovery

in the temperature range above 150°K is enhanced by cold work. (b) The recovery below 60°K is somewhat retarded by cold work. (c) Recovery peak at 300°K is shifted toward a low temperature by cold work, whereas no shift in temperature is observed for the peak at 225°K (Fig. 14).

c. Recovery of Au

The isochronal recovery curves and their differential curves are shown in Figs. 16 and 17. The differences between fractional recovery of cold worked specimens, Au-0.1% Cu alloy and annealed one against temperature are plotted in Fig. 18. It is noted that: (a) The recovery in the temperature range between 50° and 315°K is enhanced by cold work. The recovery below 28°K seems to be suppressed a little by cold work. (b) The recovery peak at 320°K in annealed specimen is apparently shifted by about 30°K toward a lower temperature by cold work. (c) In Au-0.1% Cu ally, recovery is retarded below 70°K and the retained resistivity seems to recover in stage III. Recovery is, however, suppressed again at 370°K.

3.4 F.c.c. metals deformed after irradiation at low temperature

To study the effect of low temperature deformation on the recovery spectra after low temperature irradiation the following treatments are given to each specimens; 1, an annealed specimen is irradiated; 2, an annealed specimen is deformed at 4.2°K without irradiation; 3, an annealed specimen is first irradiated, then deformed by twisting at 4.2°K; 4, an annealed specimen is deformed at room temperature, then irradiated; 5, an annealed specimen is annealed at moderate temperature after irradiation, then deformed at 4.2°K. After irradiation, isochronal annealing are carried out by annealing the specimens. In order to attain an accurate comparison, the specimen of treatment 1 is simultaneously irradiated with the specimens of treatments 3, 4 and 5, then they are simultaneously isochronally annealed.

a. Cu

The isochronal recovery curves after treatments 1, 2 and 3 with 30 hr irradiation are shown in Fig. 19. In this figure, the resistivity increase after irradiation (ρ_I) of treatment 3 specimen is normalized to that of treatment 1 specimen. The same normalization procedure is applied also in Al and Au. The resistivity increase after deformation of the specimen of treatment 2 is 7.1×10^{-9} Ωcm. The difference of the isochronal recovery curves, after treatments 1 and 3 with 30 hr irradiation ($\Delta\rho_{I+D}-\Delta\rho_I$) and the isochronal recovery curve of the only deformed (treatment 2) specimen $(\Delta\rho_D)_2$ are shown in Fig. 20. Whereas the resistivity increase after deformation of treatment 2 specimen $(\Delta\rho_D)_2$ is 7.1×10^{-9}Ωcm, the resistivity increase after deformation in treatment 3 specimen $(\Delta\rho_D)_3$ is 2.0×10^{-9} Ωcm. In this Fig. 20, $(\Delta\rho_D)_2$ is normalized to $(\Delta\rho_D)_3$ = 2.0×10^{-9} Ωcm. This procedure is justified from the experimental results on low temperature deformed specimens, where the fractional resistivity recovery in stages II and III is not strongly dependent on the amount of deformation induced resistivity.

In the following, the notation shown below will be used.

$\Delta\rho_I$; the resistivity increase due to irradiation.

$(\Delta\rho_D)_{2,3,4,5}$; the resistivity increase due to deformation in treatments 2, 3, 4 and 5, respectively.

$(\Delta\rho_D)'_2$; resistivity increase after deformation normalized to $(\Delta\rho_D)_3$.

$\Delta\rho_{I+D}$; The total resistivity increase of treatments 3 and 5.

$\Delta\rho_{D+I}$; the total resistivity increase of treatment 4 specimen.

The difference of the isochronal recovery curves of treatments 4 and 1

after 30 hr irradiation ($\Delta\rho_{D+I}-\Delta\rho_I$) is shown together in Fig. 20. The differential curve of the difference between isochronal recovery curves of treatments 3 and 1 ($\Delta\rho_{I+D}-\Delta\rho_I$) is shown in Fig. 21. In Fig. 21, the differential curves of isochronal curves of the resistivity increases $(\Delta\rho_D)'_2$ and $\Delta\rho_I$ (30 hr irradiation) are shown together.

We summarize the features of these results as follows.

(1) The reduction corresponding to 5% surface shear strain is found to be about 20% of stage I.

(2) The specimen of treatment 4 also shows a little reduction in stage I, below about 43°K, similar suppression of stage I is also observed in specimens, which are given more heavy deformation before irradiation.

b. Al

The isochronal recovery curves of treatments 1, 2 and 3 after 10 hr irradiation are shown in Fig. 22. The resistivity increase after deformation of treatment 2 specimen $(\Delta\rho_D)_2$ is 0.52×10^{-9} Ωcm. The isochronal recovery curves of only deformed specimen $(\Delta\rho_D)'_2$, of difference between treatments 3 and 1 ($\Delta\rho_{I+D}-\Delta\rho_I$) are shown in Fig. 23. In this figure, as it was done for Cu, $(\Delta\rho_D)_2$ is normalized to the amount of the resistivity increase after deformation in treatment 3 specimen $(\Delta\rho_D)_3 = 1.0 \times 10^{-9}$ Ωcm. The differential curve of the difference between the isochronal recovery curves of treatments 3 and 1 ($\Delta\rho_{I+D}-\Delta\rho_I$) is shown in Fig. 24. The differential curves of isochronal curves of the resistivity increases $(\Delta\rho_D)'_2$ and $\Delta\rho_I$ (10 hr irradiation) are also shown together in Fig. 24.

Different from Cu, the retardation of stage I recovery by deformation at 4.2°K is not observed in Al. Also, no reduction of stage I is observed in the specimen deformed (about 20% surface shear strain) at room temperature

before irradiation in Al. On the contrary, the deformation seems to enhance a little the amount of stage I recovery.

c. Au

The isochronal recovery curves of treatments 1, 2 and 3 after 10 hr irradiation are shown in Fig. 25. The isochronal recovery curves of only deformed specimen and the difference between isochronal recovery curves of treatments 3 and 1 ($\Delta\rho_{I+D}$-$\Delta\rho_I$) are shown in Fig. 26. In this figure, $(\Delta\rho_D)_2 = 1.9 \times 10^{-9}$ Ωcm is also normalized to $(\Delta\rho_D)_3 = 2.3 \times 10^{-9}$ Ωcm as in Cu and Al. The differential curves of the difference between isochronal curves of treatments 3 and 1 ($\Delta\rho_{I+D}$-$\Delta\rho_I$) and of the deformed specimen $(\Delta\rho_D)_2'$ is shown in Fig. 27 together with the differential curve of isochronal curve of $\Delta\rho_I$.

A little reduction in the amount of recovery below 30°K is observed in treatment 3. If stage I in Au is assumed to be below 30°K, the effect of deformation on stage I is similar in Au and Cu.

d. Effect of annealing at moderate temperatures (Cu)

(d.1) The difference between the isochronal recovery of specimens, which are annealed at 30°K and at 40°K after low temperature irradiation then deformed at 4.2°K and that of treatment 1 specimen after 30 hr irradiation are shown in Fig. 28. These results show a similar reduction as treatment 3 specimen but, this time, the shape of the curves around 45°K is a little different from that of treatment 3 specimen.

(d.2) Specimens, which are annealed at 125°, 253° and 293°K after irradiation then deformed at 4.2°K, show a little increase in recovery amount below 105°K if compared with specimens only deformed at 4.2°K (treatment 2). This is shown in Fig. 29.

This last result seems to suggest that moving dislocations have transformed the stable defects, possibly defect clusters which formed after moderate annealing, into the more unstable defects. For Al, such effect is not observed in the present experiments, i.e. Al specimens annealed at 120° and 220°K after irradiation give the same recovery amount (below 100°K) as an unirradiated specimen after deformation at 4.2°K. On the other hand, Dimitrov et al.[42] found that the deformation at 78°K of Al specimen neutron-irradiated at the same temperature, decreases the amount of stage III recovery. According to them, possibly interstitial clusters are transformed into stage I defects by the movement of dislocations. The difference could be due to the difference in temperature of deformation in these two works.

e. Stages II and III

When the amount of recovery of $\Delta\rho_{I+D}-\Delta\rho_{I}$ in stages II and III is compared with that of the only deformed specimen, the amount of recovery in stages II and III increases in treatment 3 specimen for all metals studied in the present works. For Cu, if we assume that the disappearance of a certain fraction of the defects by deformation in treatment 3 specimen can be neglected, the amount of recovery enhancement in stages II and III should be compared with the amount of stage I reduction. However, as the former is larger or smaller than the latter in the three specimens of treatment 3, no reasonable comparison of both amounts can be made in the present results. Since no reduction of stage I in treatment 3 is observed in Al, enhancement of stages II and III can not be attributed to transformation of the stage I defects. Similarly, for Au, the reduction of stage I in

treatment 3 appears to be too small compared to the increased amount of stages II and III.

Damage rates and resistivity recovered in moderate temperature ranges for Cu, Al and Au specimens are shown in Table I.

3.5 B.c.c. metals after irradiation at low temperature.

a. Recovery in as-annealed specimens of Mo.

Fig. 30 shows the recovery structure in stage I (4.2° -70°K), stage II (70°-300°K) and stage III (300°-600°K) in a 10 hr irradiated specimen . The three recovery curves correspond to those of three different purity specimens. As shown in Fig. 30, the recovery structure is not strongly dependent on the purity of the specimen except for the substage between 50° and 70°K. In this substage, a systematic decrease of the amount of recovery with impurity content is observed.

Most of the peaks in stage II are not reproducible except the one at 120°K, which is also observed by Coltman et al.[43)]

b. Recovery in doped specimens.

Fig. 31 shows the typical recovery structures in three Mo specimens with different treatments before low temperature irradiation. These treatments are (1) as-annealed (2) doped for 64 hr (3) doped for 64 hr and annealed at 400°C for 1 hr.

As seen from Fig. 31, the doped specimen shows a remarkable increase of recovery amount in stages I, II, whereas the specimen doped and subsequently annealed at 400°C almost loses the effect of the doping. No change in the temperature positions of the peaks is detected in the doped specimen compared with the annealed specimen.

By changing the doping time by 12, 22 and 64 hr, it is found that the enhancement tends to saturate with increasing doping dose (see Table II).

This will be discussed later in conjunction with the damage rate at room temperature, which also shows the saturation tendency.

One should also note that the enhancement is not due to the preferred production of stages I, II defects in the doped specimens. If this were the case, the damage rate would be enhanced by the doping treatment. No such an enhancement of the damage rate is observed in the present experiment.

As shown in Fig. 32, where the ratio of the differential recovery curves in the doped to the as-annealed specimens are plotted, the enhancement starts at about 30°K and continues to proceed up to room temperature.

c. Stage III recovery in doped specimens.

Fig. 33 shows the differential isochronal recovery curves of stage III in two specimens with different treatments, namely, one doped at room temperature without any further irradiation and one doped at room temperature and further irradiated at liquid helium temperature. The actual procedure is as follows; two specimens are given radiation doping at the same time at room temperature for a given time. After measurement of the induced resistivity, one of the doped specimens is again irradiated at liquid helium temperature. After the isochronal annealing at stages I and II, where the enhancement of recovery due to the doping treatment is observed, the specimens are brought up to the room temperature and annealed further at higher temperatures to investigate stage III. Before the onset of the stage III recovery, the resistivity remaining in the as-doped specimen (specimen 1) is given by,

$$\Delta\rho_1 = \Delta\rho_D(\mathrm{III}) + \Delta\rho_D(\mathrm{IV,V})$$

where $\Delta\rho_D(\mathrm{III})$ is the resistivity to recover in stage III and $\Delta\rho_D(\mathrm{IV,V})$ is the resistivity to recover above stage III.

In the second specimen (specimen 2), to which the doping and low temperature irradiation are given, the resistivity remaining is given as,

$$\Delta\rho_2 = \Delta\rho'_D(III) + \Delta\rho'_{LI}(III) + \Delta\rho'_D(IV,V) + \Delta\rho'_{LI}(IV,V)$$

where $\Delta\rho'_{LI}(III)$ is the resistivity due to low temperature irradiation to recover in stage III.

The resistivity remaining in the specimen (specimen 3), which is only irradiated at low temperature, is given as,

$$\Delta\rho_3 = \Delta\rho_{LI}(III) + \Delta\rho_{LI}(IV,V)$$

If it is assumed that the stage III defect is not lost during the processes of stages I, II enhancement due to doping, we should have a relation.

$$\Delta\rho'_D(III) + \Delta\rho'_{LI}(III) = \Delta\rho_D(III) + \Delta\rho_{LI}(III)$$

In order to test the relation, $\Delta\rho'_D(III) + \Delta\rho'_{LI}(III) - \Delta\rho_D(III)$ is calculated and compared with $\Delta\rho_{LI}(III)$. Fig. 34 shows the results of comparison, where doping time is chosen to be 27.5 and 54 hr and low temperature irradiation time is 18.7 hr. Note that the specimens 1 and 2 are simultaneously irradiated at room temperature and also specimens 2 and 3 are also simultaneously irradiated at liquid helium temperature. As seen from Fig. 34, the difference of the differential recovery curves,

$\frac{d}{dT}(\Delta\rho'_D(III) + \Delta\rho'_{LI}(III)) - \frac{d}{dT}\Delta\rho_D(III)$, shifts to lower temperature with increasing doping dose. However, the difference of the recovery amount, $\Delta\rho'_D(III) + \Delta\rho'_{LI}(III) - \Delta\rho_D(III)$, is almost comparable with $\Delta\rho_{LI}(III)$ (see Table III). This result seems to indicate that the stage III defect is not lost during the process of the enhancement in stages I, II.

The results of the doping experiments are summarized as follows;

(1) The amounts of stages I and II are increased by radiation doping at room temperature.

(2) The increase tends to saturate with increasing doping dose.

(3) The effect of the doping treatment is almost lost if the doped specimen is annealed at 400°C prior to the low temperature irradiation.

(4) The amount of stage III recovery in the doped and low temperature irradiated specimen is close to the sum of the only low temperature irradiated specimen and the only doped specimen. No decrease or enhancement of the stage could be detected in the present experiment.

The damage rates of annealed, deformed and as-received specimens are shown in Table IV. The resistivity ratio of these specimens at room temperature and 4.2°K are about 6. Fractional isochronal recovery curves for specimens (1) as-annealed, (2) deformed and (3) as-received are shown in Fig. 35. Annealing peak at 28°K in deformed and as-received specimens are retarded with respect to the annealed one. This is more clearly shown in Fig. 36, in which the differences in percentage of recovery between the deformed and as-received specimens and the annealed one at each temperature are plotted.

d. W

The isochronal recovery curves and their differential curves after 6 hr irradiation for specimens with three kinds of pre-irradiation treatments, namely, (a) annealed, (b) radiation doped for 64 hr and (c) radiation doped for 64 hr followed by aging at 400°C for 1 hr, are shown in Figs. 37 and 38. The isochronal recovery curves for specimens with different amount of irradiation doping and also different amount of low temperature irradiation

are shown in Fig. 39. The differential curves for specimens with three kinds of pre-irradiation treatments, namely, (a) annealed, (b) radiation doped for 112 hr and (c) radiation doped for 112 hr followed by aging at 890°C for 1 hr are shown in Fig. 40. The recovery curves can be divided into two prominent stages; stage I ($<$ 90°K) and stage II (90°K $\sim$ 400°K). At least five substages are observed below 90°K. Such substages are also observed by Coltman et al.[43] and Burger et al.[44] The amount of recovery in stage I is increased by radiation doping. This is shown more clearly in Fig. 32, where the ratio of the differential isochronal curves of the specimen doped for 64 hr to the annealed one are plotted against annealing temperature, together with similar result on Mo. The ratio of recovery rates rapidly increases from 18°K for W, whereas for Mo, it increases from about 30°K. In Fig. 41, the amount of fractional recovery below 90°K after low temperature irradiation, are plotted against doping irradiation time. In the figure, a similar results on Mo are shown for a comparison purpose. Resistivity increase and the fractional amount of recovery in stage I for specimens of the (a) annealed, (b) radiation doped and (c) radiation doped followed by aging are shown in Table V. We summarize the main results of the doping experiments as follows.

(1) The amount of recovery is enhanced by doping throughout stage I and former part of stage II.

(2) The enhancement tends to saturate as the doping dose increases. (Fig. 41).

(3) The effect of doping does not vanish when the doped specimen is annealed at 400°C, where stage III is considered to be completed. But when the doped specimen is annealed at 890°C, the effect of doping vanishes almost completely.

(4) The temperatures of recovery peaks in stage I do not seem to shift by the doping.

(5) Damage rate of resistivity at low temperature is little influenced by the doping.

The observation (5) excludes the enhanced production of stage I defects due to dynamical events, for example, decrease of threshold energy for the production of close pairs near the defects induced by doping. From (4), the recovery of stage I is considered to be of 1-st order kinetics. The observation (3) shows that the enhancement is not associated with the stage III defects but with the defects which annealed out above stage III. For Mo, a similar result with W, except the observation (3), are found, as is shown in the previous section. The effect of doping on Mo vanishes when the doped specimen are annealed at 400°C, where stage III is completed. When the doped specimen is annealed at 200°C, a half of the doping effect vanishes in Mo. This suggests that the enhancement of stage I is associated with the stage III defects for Mo but not for W.

e. Fe

Figure 42 shows the isochronal curves and the differential isochronal curves of annealed and as-received specimens. The as-received specimen is annealed for 10 min at 150°C before irradiation. The main results in Fig. 42 are as follows.

(a) Stage I divide into two substages centered at 95° and 110°K. The substage at 66°K found in electron irradiation does not appear.

(b) Recovery curves in the temperature range between 140°K and 300°K (stage II) in annealed specimen is different from that of as-received one. In the annealed specimen, there are the recovery peaks at 165° and 190°K, but in the as-received at 165° and 220°K.

(c) In stage III above 300°K, the large recovery stage at 340°K occur in the annealed specimen, but this recovery stage in the as-received one is very small.

3.6 The change in the resistivity versus the applied magnetic field curves for V specimens by annealing after deformation

In Fig. 43, the resistivity (R) vs. the applied magnetic field (H) for specimen deformed at 4.2°K is shown. The H-R curve of specimen annealed at room temperature after deformation at 4.2°K is nearly the same as that of as-annealed specimen. In Fig. 44, the voltage (V) vs. H curves for specimens deformed at various temperatures, namely 4.2°, 54° and 74°K, are shown for two different current densities, 240 A/cm^2 and 40 A/cm^2. The H-V curves are different between the cases deformed at 54° and 74°K and those when deformed at 4.2°K and annealed at 54°K or 74°K. This suggests that specimens deformed at 54° and 74°K have different distribution of dislocations from the one deformed at 4.2°K.

4. Discussions

4. 1. Recovery of f.c.c. metals after deformation at 4.2°K.

The stage I recovery of deformed polycrystalline f.c.c. metals is generally less than 5%. The recovery of the open metals as Al and Pt is about twice greater than that of the more close packed metals as Cu and Au according to recent experiments.[45] In our experiments, the stage I after deformation is below 110°K for Au, below 90°K for Cu and below 50°K for Al.

For the fully annealed specimen, the resistivity show continuous decrease up to 120°K in Au. For the specimen with the largest initial dislocation density, the initial continuous recovery is observed with a much larger slope. It can be seen from the results of Schumacher et al.[38] that the percent recovery up to 120°K remain almost the same for different degrees of deformation at 4.2°K. Present results show that the increase in dislocation density before deformation at 4.2°K increase this percent recovery up to 120°K. This suggests that the dislocation rearrangement may be associated with this recovery because a larger dislocation rearrangement could be expected for the specimen with a larger dislocation density. This cannot be expected by the annihilation of correlated interstitial-vacancy pairs suggested by Schumacher et al.[38] The expected number of the Frenkel pairs would also be too small to account for the observed amount of the recovery. If we assume one half of the resistivity increase $\Delta\rho$ by deformation is due to dislocations, the resistivity due to dislocation ρ_D recover less than 2% up to 120°K. Therefore, even if we assume that the recovery in these temperatures would have been solely due to the reduction of the dislocation density, the dislocation density would have decreased by less than several percent which would not be unreasonable. In the internal

friction experiments, it is observed that the specimen deformed by torsion at 4.2°K in one direction, untwist continuously in another direction during warm-up through these temperatures (see Fig. 45). This would provide a direct evidence for the dislocation rearrangement. Further, the additional deformation increases the amount of stage I, as shown in Fig. 5. This enhancement is too large to be explained by the increased concentration of close pairs produced by the additional deformation. The present interpretation can also be applied to stage I of Cu and Al. The recovery rate in stage I of Cu does not appear to be influenced by the impurity concentration (Fig. 6). The amount of stage I recovery in Al is large, compared to Au and Cu, as shown in Fig. 9. This may be explained by more piled-up dislocations in deformed Al than Au and Cu due to a strong oxide film on the surface of Al.

Therefore, the initial continuous recovery observed in f.c.c. metals deformed at 4.2°K could best be explained by the dislocation rearrangement. Recently, Swanson[45] discussed on the stage I recovery of deformed metals. He observed the structure in the stage I recovery of Pt. The most prominent Frenkel pair substages in electron irradiated specimen, at 20° and 23°K, are notably absent in the deformed one. This behaviour is expected that the probability of overlap of vacancy and interstitial strings is small. The enhancement in the stage I recovery caused by a prior deformation and low temperature anneal is explained by defect rearrangement. Since neither substitutional impurities nor quenched-in vacancies affected the stage I recovery of Al, he suggested a short range process of defects. According to Swanson,[46] since the substage of Zr deformed occurred only in the presence of oxygen impurity atoms, its stage is due to a close defect-oxygen

atom interaction. For stage II, the detailed mechanism of recovery is not understood yet. For the reverse annealing in Au, Schumacher et al.[38] observed a resistivity increase in the isochronal recovery with a maximum at 150°K. They suggested that the increase was due to the partial decomposition of interstitial clusters. Dawson[39] obtained different experimental results, and he considered that the rising portion of reverse annealing was obscured in the specimen with less impurity content. Swanson[40] did not observe such a reverse annealing. In our experiments, the amount of reverse annealing appear to vary for differently-treated specimens. The impurity effect seems to be important for the appearance of a reverse annealing. In Cu, no reverse annealing was observed in our experiments. However, Dawson[39] observed a complicated reverse annealing in Cu. The difference still remains unexplained at present.

The following interpretations of the stage II recovery in deformed metals have been proposed :[47] (1) Release of impurity trapped interstitials. It has been ascribed to release of interstitials trapped by impurities since this stage in irradiated metals is impurity sensitive. However, in heavily deformed metals the concentrations of point defect are of the order of 10^{-4}, to be compared with impurity concentration of 10^{-5}. The stage II in deformed metals is at least partially due to intrinsic defects. (2) Recombination of close interstitial-vacancy pairs. This would mean that attraction of these pairs should not be negligible at distances as large as 30 $\sim$ 40 atomic distances. This seems to be improbable. Stage II should increase in the fractional recovery with increasing degree of deformation, which is not observed. (3) Annealing of di-vacancies or larger vacancy clusters. It can be ruled out because the migration energy of

di-vacancy are too large for stage II. (4) Rearrangements of dislocations. A resistivity stage II is not accompanied by the plastic after effect. (5) Rearrangements within point defect strings. This interpretation is contrary to the following experimental results : Prequenched specimen shows to influence the stage II annealing and the stage II defects arrive at the dislocations as is shown by the internal friction experiments. (6) Migration or dissociation of di-interstitials or larger interstitial clusters. (7) Attraction of the stage III defects by dislocations. This is not in agreement with the present experimental results as will be shown later. The terms (6) is most probable, it will be discussed in the followings in more detail.

As to the recovery of interstitial type defects in f. c. c metals, the recovery stage is still in controversy. The main problem is whether the interstitials migrate in stage I or stage III. One school considers that the close pairs and crowdions move in stage I, normal interstitials in stage III and vacancies in stage IV (model 1).[48] Another school considers that normal interstitials move in stage I and vacancies in stage III (model 2).[49] In the following, we will discuss how the present results can be explained on the two models.

Stage III in deformed specimens can hardly be ascribed to the free migration of interstitials, because it was observed by Dawson[50] in the recovery of ordered alloys that the recovery process in stage II was due to the migration of interstitial-type defects at least and in stage III to divacancies and single vacancies. The internal friction and dynamic modulus[51,52] of Cu and Au deformed at low temperature also showed that possibly interstitials arrived at dislocation lines in stage II and impeded their motion by pinning. On the basis of model 1, if the migration

energy of free interstitials in cold worked Au were 0.71 ev[53] the same as that obtained for irradiated Au, free interstitials could not possibly migrate at all in the temperature range of stage II. Therefore, if interstitials migrate in stage II, the attraction due to the stress field of dislocations might play an important role in this recovery stage. However, the temperature range of stage II of Cu and Al is too low to be explained by the stage III defects. The recovery peak at 130°K in Cu does not shift in temperature for different degrees of deformation (Fig.6). Another possibility is that di-interstitials or interstitial clusters produced by deformation dissociate to single interstitials or become mobile in stage II. The former process, proposed by Schumacher et al.,[38] assumes that single interstitials move in stage III. However, as mentioned before, Dawson's results[39] seemed to show that the stage III defects in deformation were of the vacancy type. Also, the resistivity measurements of Au deformed after quench by Sakairi et al.[54] seem to support this view. Therefore, the last possibility for model 1 is that interstitial clusters become mobile in stage II.

In model 2, free interstitials move in stage I. Corbett et al.[56] proposed that some interstitials, mobile in stage I, would form di-interstitials, for electron-irradiated Cu, which became mobile in stages II or III. Theoretical calculation by Johnson[55] showed that the migration energy of interstitial and di-interstitial in Cu were 0.05 and 0.08 ev, respectively. He also calculated for Ni that the migration energy of interstitial and di-interstitial were 0.15 ev and 0.29 ev.[56] Both results showed that the migration energy of di-interstitial was larger than that of single interstitial. For Al, also, Swanson[40] observed that stage II (peak at 80°K) was due to

the migration of di-interstitials. According to Bauer et al.[57], the migration or breaking up of any di-interstitials occurs neither in stage II nor III for electron-irradiated Cu. However, the migration or breaking up of interstitial clusters could be a possible process in recovery in cold worked specimens. Van den Beukel[58] pointed out that since the defect concentration in this stage after large deformation was several times larger than the impurity concentration, stage II was associated with the dissociation of interstitial clusters and liberation of impurity-trapped interstitials, followed by annihilation at sinks. Our results, however, show a somewhat different details of the spectrum to Van den Beukel's results.[58] Van den Beukel's stage at about 125°K is small compared with stage at about 140°K. He explained that this was possibly due to the conversion of the weakly bound pairs of the early stage(125°K) to the more strongly-bound configuration dissociated in the later stage (140°K). In contrast to his results, our recovery peak at 130°K is larger than the one at 150°K. (The peak temperatures, in our experiments, shift to somewhat higher temperatures, as compared to the Van den Beukel's results, because of the three times larger heating rate in our experiments.) Therefore, the above explanation by Van den Beukel for their two peaks appears not to be justified. Finally, it should be pointed out that this model 2 should, however, assume that the interstitials produced by deformation are mostly in the form of a cluster of string, because there is no pronounced stage I recovery in deformed specimens.

4.2. Recovery of b.c.c. metals after deformation at 4.2°K.

In the present experiment for vanadium, stages I, II and III are below 60°K, 350°K and above 350°K, respectively.

The continuous recovery below around 60°K, is considered to be due to dislocation rearrangement as in the case of f.c.c. metals (Cu, Au and Al).

From comparison with f.c.c metals, it seems that the recovery at 80°K in V is possibly associated with the interstitial clusters induced by deformation. However, the slightly deformed specimen exhibits a large recovery below 300°K (∿ 50%) (Fig. 9). Such a behaviour cannot be observed in deformed f.c.c metals except Al. Swanson [46] observed large recovery (∿ 80%) below 370°K for Zr. He suggested that the resistivity increase is mostly caused by vacancies, interstitials and dislocations produced by deformation, but certain part is also due to a close defect-oxygen atom interaction. For the deformed vanadium, therefore, impurities may also be associated with the recovery in stages I and II, as in Zr.

There are two opinions concerning the defects which move in stage III ; first, intrinsic defects, and second impurities. According to Köthe et al.[25], stage III in vanadium is due to the migration of interstitial oxygen and nitrogen; whereas, Perepezko et al.[59] reported that stage III was probably due to the annihilation of intrinsic point defects. It cannot be determined whether the stage III recovery in the present experiments is due to intrinsic defects or interstitial impurities.

For Fe, it seems not probable to consider in general that about 90% of the defects induced by deformation at 4.2°K recovered below 300°K. Therefore, this recovery is considered mostly to be due to the magnetic effect.

The fact that the remarkable variation of resistivity occurs at the temperature around 200°K suggests that the stage at 200°K is associated with the migration of defects. As seen in Fig. 12, Fe specimen deformed at

79°K has a recovery stage at about 200°K. This stage of recovery is similar to that observed by Cuddy.[60] For this recovery, he attributed the annihilation of a vacancy-type defects to dislocations. However, the migration of vacancies is considered to occur at above 300°K, since the recovery in the specimen quenched in liquid helium was observed at above 300°K by Glaeser et al..[61] On the other hand, the migration of interstitials is considered to occur at 130°K.[62] Therefore, the recovery stage at 200°K is considered to be associated with the migration or dissociation of interstitial clusters.

4.3 Recovery of Cu and Au after neutron irradiation at low temperature.

4.3.1 Damage rates

Blewitt et al.[63] observed 10% enhancement in damage rate for Cu deformed before irradiation and attributed it to the defocusing of focusons at stacking faults.[11] Swanson et al.[64] also observed that the damage rate of deformed Cu was approximately 10% greater than that of annealed one in agreement with the results of Blewitt et al.. The enhancement of damage rate of 13 ∿ 14% in our experiments is in rough agreement with the results of Blewitt et al. and Swanson et al..

For Au, Swanson et al.[64,65] observed that the damage rate was considerably enhanced by cold work and impurity doping after low dose neutron irradiation. Herschbach et al.[66] observed 8 ∿ 20% enhancement of damage rate by cold work after 10 MeV and 20 MeV deuteron irradiation. Bauer[67] also observed an increase of the damage rate for impure specimens after 2 MeV electron irradiation. The enhanced damage rate in cold worked specimens for low

dose neutron irradiation was explained by Swanson et al. as due to the defocusing of collision chains at dislocations. On the contrary, in our experiments, the damage rate of Au is reduced by the similar amount of cold work and also by the addition of impurity. One possibility is that a decreased damage rate for cold worked specimens in our experiments may be due to the enhanced recovery at lower temperature not covered in our measurements.

4.3.2 Recovery of Cu

The recovery below 60°K in our experiments decreases by deformation. Blewitt et al. also observed a decrease of the stage I_E recovery for deformed specimen after 8 x 10^{17} n/cm^2 fast neutron irradiation. In the case of electron irradiation, a suppression of the latter part of stage I by deformation has been reported by Meechan et al..[68] This suppression can be explained in two ways : (1) crowdions are converted to normal interstitials at dislocations and the converted crowdions remain up to stage III.[68] (2) some of normal interstitials moving in stage I are trapped at dislocations and they are released at higher temperature.[69] Contrasting with these results, Swanson et al.[64] observed that the recovery below 100°K for Al and Cu was slightly enhanced by deformation at low neutron dose. They explained that extra close pairs are expected to be created when high energy collision chains defocused at dislocations, so that more stage I recovery would result. However, the suppression of stage I in the high dose such as in our experiment and in Blewitt's experiment cannot be explained by their explanation. Thus, the experimental results seem to show that the behaviour of stage I is altered by the irradiation dose.

The recovery peak at 225°K seems to be characterized by low number of jumps, since the temperature shift of this peak is not observed for cold worked specimens. A possible model for this peak would be the release of interstitials from impurities. Martin observed the recovery peaks at 133°, 193° and 215°K after electron irradiation[70] and fast neutron irradiation[71] which he considered to be associated with the release of interstitials from impurities. The following model seems, however, more plausible than the above one: The recovery peak at 300°K seems to shift toward a lower temperature in the cold worked specimens. The recovery peaks at 225° and 300°K are considered to correspond with stages III_1 and III_2, which Burger et al.[72] found after neutron irradiation. According to them, these peaks are associated with the annihilation of interstitials moving inside cascade zones and outside cascade zones to vacancies, respectively. Because of the difference in the range of migration, the dislocation density would have rather large influence on stage III_2, but not on stage III_1. The similar phenomenon can be observed in Au, in which the two peaks are at 230° and 310°K. When increasing radiation dose, the similar behaviour can be observed as that in deformation. In low dose neutron irradiation in Al, the recovery peaks at 190° and 240°K can also be observed and with increasing radiation dose, the second peak shifts but not the first one. The interpretation for these peaks by Burger et al. seems to be correct since the migration energies of these two recovery peaks are the same. However, the recovery peak at 240°K in Al agrees with the migration energy of vacancies in quenching experiments. Therefore, in Al, the former peak is considered to be associated with interstitial clusters, the latter peak with vacancies.

4. 3. 3. Recovery of Au

Bauer et al.[73] reported that the recovery below 50°K after electron

irradiation was slightly enhanced by cold work. Swanson et al. also observed the enhancement by cold work of recovery below 100°K after neutron irradiation. Herschbach et al.[74] observed, however, that the recovery below 40°K after deuteron irradiation was reduced and recovery above 40°K was enhanced in the cold worked specimens. Herschbach's results are somewhat similar to ours which show that the recovery below ∿28°K seem to be reduced by cold work, but enhancement is observed above 50°K up to 315°K. Thus, similar to that of Cu the behaviour of stage I might be dose dependent. Bauer[67] reported that in impure specimens the suppression of recovery below 70°K could be explained by interstitial-impurity interaction and that the amount of stage II recovery was larger than that in the pure specimens. Herschbach et al.[74] observed also that alloying suppressed the stage I recovery. The suppression of recovery below 70°K is also observed in our results on the alloyed specimens but no enhancement in stage II is observed. It is noted that the effect of cold work on the recovery above ∿28°K in Au is similar to that above 120°K in Cu. The recovery behaviour of Au at low temperature is different from the other f.c.c. metals. The amount of recovery in stage I is extremely small compared with other metals. To account for the small recovery in stage I one can assume that the reaction radius for interstitial-interstitial trapping is large compared with that for recombination at vacancies and also a separation of interstitial and vacancy which could be produced by focussing collisions is large. For the stage I recovery of Au, it seems most plausible to speculate that the most prominent low temperature stage around 19°K is the equivalent to stage I_D in the other f.c.c. metals although no direct experimental proof has yet been given.

The recovery peak at 320°K in the annealed specimen shifts by about

30°K toward the lower temperature by cold work. Therefore, the long range migration of some defects is likely associated with this stage. The mean distance between zones expected from the present neutron dose is 10^2 atomic distances. Then, if 10^4 jumps are assumed in this recovery stage, the activation energy associated with this stage would be at most 0.8 eV. In the 38% drawn specimen, the resistivity increase is 1.5×10^{-8} Ωcm and this increase corresponds to the dislocation density of 4×10^{10} Ωcm^{-2} with 3.5×10^{-19} Ωcm^3/dislocation.[75] If the defects annihilate at dislocations, their jump number should be about 10^4 which is comparable to that in the annealed specimen. With an activation energy of 0.8 eV, the defects could make only about 10^3 jumps in the cold worked specimens. Therefore, some accerelation due to dislocations are suggested for the annihilation of the defects.

4. 4. Effect of deformation on the recovery of f.c.c. metals after neutron irradiation.

The main experimental results for the three metals, Cu, Al and Au, are as follows.

(a) The large reduction (about 20%) of the amount of stage I recovery occurs in irradiated and deformed Cu specimen by small deformation of a few percent surface shear strain after irradiation. A similar but much smaller reduction of the amount of possible stage I occurs in Au. On the other hand, no reduction of this kind is found in Al.

(b) The Cu specimen, which is deformed at room temperature and irradiated at low temperature, shows a small reduction in the amount of the fractional recovery below about 43°K, which is the same temperature as the temperature in (a).

(c) If we assume that the disapperance of a certain fraction of the defects by deformation can be neglected, the amount of recovery in stages II and III increases in the irradiated and deformed specimen of all three metals. Therefore, this enhancement does not necessarily seem to be associated with the reduction of stage I.

The reduction in the amount of stage I recovery by deformation could occur by the following mechanisms:

(1) Partial recovery or micro-recrystallization in depleted zones by near by sweeping dislocations. The amount of deformation is 5% surface shear strain or on the average about 2% of shear strain. This means that only about 2% of the atomic planes are swept out by dislocations. If we assume that the size of the zones is 20b and recovery occurs when the zones are cut by moving dislocations, this might be a possible mechanism. However, the recovery mechanism in depleted zones is not known in detail.

(2) Recombination due to the heat generated on the slip plane by moving dislocations or due to kinetic energy transferred from moving dislocations. If the dislocation velocity is 10% of the sound velocity, the duration of the temperature increase at 5 atomic distances away from the slip plane will be too short for any recovery to occur. Momentum transferred to interstitials is also too small for any recovery to occur. Therefore, the amount of recovery due to these mechanisms is not large enough to explain the results.

(3) Recombination of close pairs which are brought into unstable configuration by slip. When an interstitial is brought into a recombination volume by dislocations cutting that close pair, it will spontaneously recombine. To obtain the large amount of recovery in this way, however, we have to assume a rather artificial configuration and recombination volume for close pairs. Therefore, the next case would be more probable.

(4) In the close pairs with interstitials of crowdion type, a crowdion could not recombine easily with a vacancy after they were cut by dislocations.
(5) Conversion of crowdions into split interstitials by either strain field or kinetic energy of moving dislocations. The amount of momentum transfer to crowdions at 5 atomic distance from the slip plane from moving dislocations would be too small for the conversion to occur as in (2), but the strain field of moving dislocations might be possible to convert crowdions. In the case of (4) and (5), since the transformed stage I defects should recover in stages II and III, but not in the case of (1), (2) and (3). To make distinction between the cases (1), (2) and (3), and (4) and (5), the relative amount of the reduction of stage I and the enhancement of stages II and III should be examined. If their relative amounts are comparable, the cases (4) and (5) are more probable. This is the case in Cu, however, in Au, the reduction of stage I is much smaller than the enhancement of stages II and III. Even more, in Al, no reduction of stage I is observed but the enhancement of stages II and III is still observed. To reconcile this observation with the case (4) and (5) models, it must be assumed that in Al, the distance between the interstitial and vacancy in a close pair is so small or crowdion is so stable that they could not be transformed by moving dislocations.

On the other hand, if one assumes that the deformation at 4.2°K would produce more defects of stages II and III in an irradiated specimen than in an as-annealed one, the cases (1), (2) and (3) would explain the present results, at least qualitatively: In Al, no stage I reduction is observed since no depleted zones are formed in Al.[76] In Cu and Au, the stage I reduction could be due to the recovery in depleted zones. The above experimental results seem to be in favour of the case (1), qualitatively.

4. 5. Recovery of b.c.c. metals after neutron irradiation at low temperature.

4. 5. 1. Mo

The retardation of the recovery amount with increasing impurity content in the 60°K stage is analogous with the impurity dependence of stage I_E in Cu,[56] which is interpreted as a long range migration of interstitials. The internal friction measurement of electron irradiated Mo by Lomer et al.[77] indicated that the pinning of dislocation by point defects took place between 50° and 70°K, which is usually observed when defects perform a long range migration.

As a consequence of the assignment of the free interstitial migration to the 60°K stage, the 42°K peak, the major peak in stage I, is considered to correspond to the correlated annihilation of interstitials with their own vacancies as inferred from the recovery model of stage I of Cu. The 28°K peak is considered to be a close pair recovery, which is also inferred from the stage I model of Cu.

Annealing peak at 28°K in deformed specimen are retarded with respect to that in the annealed one. Since the annihilation of the closest Frenkel pairs is not considered to be affected by deformation, we have to consider that the mode of damage production is altered by the presence of high density of dislocations. The amount of stage I in the specimen, whose ratio of electrical resistivity at 4.2°K and room temperature is 5, is comparable to that of the specimen of resistivity ratio 1000 and the amount of recovery at 28° and 42°K in the impure specimen is a little larger than the pure one. This results appears to be in contrast to Hemmerich's result,[78] where stage I in oxygen doped specimen is markedly retarded. Most of substages in stage II are not reproducible in specimens with different purities. This

indicates that impurities are involved in the recovery processes in stage II. Therefore, stage II is interpreted as the annihilation of interstitials detrapped from impurities.

For the stage III recovery, this stage is explained in terms of interstitial impurities which have a migration energy equal to the observed stage III activation energy. Nb[24] and Ta[78] doped with oxygen atoms show a large stage III recovery but undoped specimens show no stage III recovery. It is believed that interstitial impurities play an important role. However, the following results suggests that the stage III defects are intrinsic one: The stage III recovery appears in high purity W specimen after deformation and irradiation,[27] stage III is of the second order of reaction and the electron microscopic study shows that intrinsic defects are present. The defect doping at room temperature affects on annealing behaviour of defects introduced by low temperature irradiation. This may give some clues to determine the species of defects responsible for stage III. The resistivity change ($\Delta\rho$) due to migration of defects are given by

$$I + V = 0 \qquad \Delta\rho = \Delta\rho_I + \Delta\rho_V \qquad (a)$$

$$I + I = \text{cluster} \qquad \Delta\rho = 0 \qquad (b)$$

where $\Delta\rho_I$ and $\Delta\rho_V$ are the resistivity due to an interstitial and a vacancy, respectively. It is assumed that the resistivity of an interstitial is not altered upon the formation of a cluster. As an evidence of the process (b), we may count the fact that the resistivity remaining in the only low temperature irradiated specimen after the completion of stages I and II is much higher than the resistivity increase due to room temperature irradiation of the same dose. In the latter case, the instantaneous concentration

of interstitials is low, so that the process (b) does not take place appreciably. If additional defects are introduced by the doping treatment prior to low temperature irradiation, they can act as sinks for interstitials and some fraction of the interstitials, which would form clusters during the stages I and II recovery in a only low temperature irradiated specimen, annihilate to these sinks in the doped specimen. The additional resistivity recovery is observed as the enhancement. The most probable defects induced by the doping, which can act as sinks for interstitials, are vacancies. The other conceivable defects may be interstitial clusters which grow around impurity atoms during doping irradiation. The large clusters may be considered as dislocation loops and hence can absorb interstitials. However, if one compares the concentration of the interstitial clusters with that of vacancies, one cannot consider the interstitial clusters as the dominant sinks to give rise to the enhancement. Suppose that the average cluster consists of n interstitial atoms. Then, the concentration of the clusters is 1/n of that of the corresponding vacancies, because vacancies and intersitials are produced in an equal number during the doping irradiation. Hence, in the process of the enhancement, the probability of an interstitial to collide with the doped vacancies should be much higher than that with the clusters.

In the following, we will discuss the experimental results (1) ∿ (4) in terms of the vacancy sink model and neglects the effect due to the clusters.

If the vacancy sink model of the enhancement is correct, the probability of an interstitial atom to meet the additional vacancies should be proportional to the concentration of the additional vacancies introduced by the doping. The resistivity increase during doping is 7.5×10^{-9} Ω·cm

for the 22 hr doping and 12 x 10^{-9} Ω cm for the 64 hr doping. On the other hand, the enhancement is 12% or 1.4 x 10^{-9} Ω cm for the 22 hr doping and 19% or 2.2 x 10^{-9} Ω cm for the 64 hr doping at 308°K (end of stage II). The ratio of the enhanced resistivity to the doping induced resistivity is about 0.18 regardless the time of the doping irradiation (see Table II). This result seems to support the idea that the enhancement is proportional to the vacancy concentration. The production rate of resistivity at room temperature tends to saturate with increasing dose due to radiation annealing. Hence, the observation (2) is due to the saturation tendency of vacancy concentration with dose during doping irradiation. The observation (3) show that vacancies annihilate during the annealing at 400°C. The annihilation can take place by either (i) the migration of vacancies in stage III or (ii) the migration of defects other than vacancies and their recombination with vacancies. The observation (4) is important to distinguish these two cases. The recovery amount in the stage corresponding to the vacancy annealing should be reduced by the increased amount in stages I and II in the doped and low temperature irradiated specimen. However, the present result of the stage III measurement on the doped specimen does not show the decrease. On the other hand, the effect of doping treatment is almost lost if the doped specimen is annealed at 400°C prior to the low temperature irradiation. This observation shows that vacancies annihilate during the annealing at 400°C. These results could be explained by migration of two kinds of defects in stage III. Recently, Kissinger et al.[79] examined the stage III recovery by simultaneous lattice parameter and length change measurements, together with stored energy release measurements of single crystal and polycrystals. They reported that stage III may consist of both reactions of defects,

vacancies and interstitials.

4. 5. 2. W

In the internal friction and electrical resistivity measurements on electron irradiated W, DiCarlo et al.[80] found many recovery peaks below 45°K which were ascribed to close pair recovery. They suggested that long range migration of interstitials did not occur up to 45°K. Sinha et al.[81] have given direct evidence of interstitial migration in the temperature range 50° ~ 90°K by means of field ion microscope observations. It is noteworthy that stage I of neutron irradiated W consists of well defined at least five peaks. In the present experiments, however, no peak shift being observed for these peaks by doping, long range migration stage can not be assigned to any of these peaks. Stage I in W will be below 100°K from the analogy with the recovery of stage I in Cu. It should be noted here, that no enhancement of stage I recovery is observed for low temperature irradiation of even 30 hr. Therefore, during the low temperature irradiation without doping irradiation, the increase in the number of stage I defects does not seem to occur at least within the doses of 30 hr. This may suggest a characteristic distribution of interstitials and vacancies in a cascade zone. For the stage III recovery, a number of investigators assign stage III to the migration of intrinsic defects, vacancies or interstitials. On the other hand, sometimes, as in Mo, this stage is explained in terms of interstitial impurities which have a migration energy equal to the observed stage III activation energy.[82]

The effect of doping does not vanish when doped specimen is annealed at 400°C. But the effect of doping vanishes almost when doped specimen is annealed at 890°C. Therefore, the enhancement is not associated with the

stage III defects, but with defects above stage III. In our experiments, the stage III vacancy model does not seem probable. Either interstitials or interstitial impurities seem to be responsible as the stage III defects. It is noted, here, that experiments on high purity specimen by Kuhlmann et al.[27] and also recent reviews by Schultz and Nihoul[82] suggested that the stage III defects were intrinsic ones. On quenching experiments in liquid helium, the large recovery stage was found at about 700°C.[83] From the quenching experiments on W, Schultz[84] obtained 3.3 eV for the formation energy of vacancies. Combined with the self diffusion energy of 6.1 eV,[85] the most recent value, the migration energy of vacancy in W is estimated to be 2.8 eV. This energy also suggests that vacancies would migrate in stage IV.

As it was mentioned above, the effect of doping in Mo vanishes after stage III annealing. Therefore, the so-called stage III defects of W are probably of different type from those of Mo.

4. 5. 3. Fe

Recovery in Fe after irradiation is usually divided into following stages: from the lowest temperature, stage I is below 140°K, stage II_A from 140° to 180°K, stage II_B from 180° to 300°K and stage III from 300° to 400°K.

Recently, Neely et al.[86] found that stage I consisted of six substages between 33° and 150°K in 1.3 MeV electron irradiated Fe. From the dose dependence, they attributed stage I_E (120° to 150°K) to the long range migration of interstitials. The other substages in stage I are considered to be associated with recombination of close pairs by analogy with the f.c.c. metals.[15] Disappearrance of 66°K peaks after neutron irradiation seems to be consistent with this explanation because the higher energy collisions would reduce the relative concentration of the closest pairs. Cassayre[87]

also pointed out the decrease of 66°K peak height with increasing electron energy. The recovery peaks at 95° and 110°K in the present result would correspond to 87° and 100°K peaks after electron irradiation.

Detailed investigations in low temperature range are performed on Fe which is based on measurements of magnetic after effect, internal friction and electrical resistivity.[20] The measurement of after effect shows that stage I_E is due to a defect having <110> symmetry. Therefore, crowdion seems to be excluded as a possible configuration in stage I.

For stage II_A, Cassayre[87] observed that this stage is highly sensitive to the energy of incident electrons and impurities diminish this stage a little. He considered this stage is due to the migration of crowdions. On the other hand, from its dose dependence Neely et al.[86] considered that this stage is associated with the release of interstitials from impurity traps. In our experiments, only a slight temperature shift of this peak between the cold worked and the annealed specimen is observed. This result, little effect of dislocation doping on this recovery stage, seems to be in agreement with the release of interstitials from impurity traps.

Stage II_B is quite different between the as-received and the annealed specimen: Recovery peaks at 220°K for the former and 190°K for the latter. As will be discussed below, some interstitial impurities seem to be absorbed in the specimen during the annealing treatment. Therefore, this difference could be attributed to these impurities. Furthermore, this may suggest that 190°K peak would correspond with the release of interstitials from interstitial impurity traps. Although not shown in the figures, it should be noted that some specimens annealed in the different run showed almost no stage III recovery and in that case, stage II_B appeared at 220°K.

Stage III lies between 300° and 400°K. According to Fujita et al.,[88] this stage corresponds to trapping of carbon atoms by vacancies. In Nb[24] and Ta, oxygen atoms migrate to elementary defects in stage III. In our experiments, the annealed specimens show a large stage III recovery but the as-received one shows no stage III recovery. Therefore, it is believed that interstitial impurities are absorbed in the specimens during the annealing treatments.

4. 6. The identification of defects in the recovery stages

At the present time, two main models for the radiation damage in f.c.c. metals are being discussed, namely: (1) The one-interstitial model and (2) the converstion two-interstitial model. In electron irradiation experiments the interstitials migrating freely in stage III are generated by the conversion from the stage I_E interstitials and not directly produced during the displacement process. Experiments confirming the two-interstitial model are the followings: (a) The reaction order has been shown to range from three to two in the two-interstitial model.[48] Experimentally, the reaction order of stage I_E in Ni are three, which may be explained in terms of one-dimensional migration of crowdins and their annihilation at randomly distributed vacancies. (b) Observation of transmission electron microscopy showed that Ni foils annealed at 100°C after irradiation leads to an increases of the density of the loop.[89,90] This is understood in terms of interstitial migration in stage III. (c) The investigation of the magnetic after effect on electron irradiated Ni have showed that the defect annealed out in stage III has <100> symmetry.[91] Internal friction experiments[92] led to the same conclusion. (d) The modulus defect of electron irradiated Cu is reduced

during room temperature annealing.[93] (e) The internal friction studies of γ irradiated Cu by Thompson and Buck[94] indicated that thermal conversion took place at 180°K. This experiments following γ irradiation indicate that the instantaneous concentration of defects was so low as 10^{-10} that clustering of defects could be discarded. (f) The discrepancy between the activation energy for vacancy migration and the migration energy of stage III for Cu, Ag and Ni is large.

On the other hand, the one interstitial model works well for Al and Pt. The activation energies for single vacancies deduced from quenching experiments are the same as that of stage III. Objections for the two interstitial model are as follows: (a) It seems to be difficult to draw conclusions from the experiment of the small I_E bump on the high temperature side of the large stage I_D. The reaction order of stage I_E for Cu was two.[56] (b) Observation of interstitial clusters in stage III may be due to the dissociation of small clusters following the association of large clusters by released interstitials.[95] (c) The magnetic after effect due to defects annealing out in stage I_E after irradiation can be ascribed to the split interstitials in the <100> direction.[19] The after effect in stage III may be due to impurity trapped interstitials. (d) The activation energy for a reorientation and the activation energy for the stage III recovery in Cu are identical.[92] This implies that in Cu the reorientation of the stage III defects is coupled with its migration. The activation energy for a reorientation and the migration energy of di-vacancy is identical. (e) Schilling et al.[96] reported that the predictions of the crowdion model are by orders of magnitude in disagreement with the experimental results of Thompson et al..[94] A direct proof for the vacancy model for

Al is the observation of formation of GP zones during stage III in irradiated dilute alloys.[97] For Cu, Ag and Ni the activation energies observed for stage III are too low to be compatible with the values for the migration of single vacancies. Koehler[98] assigned stage III to di-vacancy from the view that in the beginning of annealing vacancies start to move at a reduced activation energy in the strain field of interstitial clusters and associate into divacancies. Van den Beukel[99] suggested that since the defect concentration is an order of 10^{-6} in the electron irradiation, divacancies can be neither produced during irradiation nor formed by migration of single vacancies.

However, divacancies could be produced directly if the initial direction of knock-on is suitable. The atomic displacement processes due to the irradiation depends on the initial direction of motion and the kinetic energy of the knock-on atoms. Suzuki[100] discussed the direct formation process of divacancies in collision processes and estimated that the probability of formation of di-vacancies seems to be of the order of 10 percent of single vacancies under the irradiation of about 1 MeV electrons.

For b.c.c metals, Nb and Fe exhibit no intrinsic stage III recovery, since the absence of a pronounced stage III recovery in neutron irradiated Nb[24] and in deformed α-Fe[26], Ta and Nb[25] was reported in very pure specimens. On the other hand, an experiments by Kuhlmann et al.[27] demonstrated that the stage III recovery occurs after neutron irradiation in the decarburized high purity W. Furthermore, the magnitude of the stage III recovery in heavily deformed specimen also suggests to be due to an intrinsic effect. Therefore, the question arises whether stage III in b.c.c. metals is

an intrinsic effect or an impurity effect.

Several investigators interpretated that the stage III recovery is due to interstitial migration from the following reasons.

(1) Direct evidence for interstitial observations after neutron irradiation by field ion microscopy on W.[101]

(2) The migration energies of vacancies, derived from self-diffusion energies and activation energies for vacancy formaiton, is higher than the observed activation energies in stage III.[82]

(3) The bi-molecular kinetics is observed for stage III.[37]

Youngs modulus is about three times lower for Nb and Ta than for the VI_a metal, Mo and W.[82] The difference in elastic properties between the two groups of b.c.c. metals may be the origin of different recovery behaviours. Schultz and Nihoul[82] discussed that b.c.c. metals consisted of two groups if it is accepted that the stage III recovery in W and Mo is of the intrinsic character. The one group, Mo and W, may have two types of interstitials, one migrates at low temperature and is of crowdion type having direction of <111>, and another migrates at stage III and is of split type having direction of <110> or <100>. The other group, V, Nb, Ta and Fe, has only a low temperature interstitials. However, it seems not reasonable to interprete stage III as interstitial migration from the following observations.

(a) DiCarls et al.[79] indicated that the defects have either <100> or <110> orientation in the range of close pair annihilation between 20° and 45°K by internal friction experiment of single crystal of W.

(b) Magnetic after effect and internal friction experiments by the Grenoble group showed that stage I_E is ascribed to an interstitial with <110> symmetry.[20]

(c) Since the difference in elastic modulus probably reflect on the different

recovery temperatures alone, it might not be reasonable to assign the different recovery models to V_a group and VI_a group.

(d) Electron microscopic observation showed that interstitial clusters are present after room temperature neutron irradiation for Mo, which suggests that one kind of interstitials are mobile below room temperature.[102]

4. 7. The change in superconductive property of V by annealing after deformation

V is a type-II superconductor. Many workers have studied the effects of mechanical deformation on the property of type-II superconductors, in terms of the interaction of Abrikosov vortices or flux lines in the mixed state with dislocations. One explanation of the flux line pinning is based on the change of flux line energy which is a local variation of Ginzburg-Landau parameter with the variation of electron mean free path[103]. In dislocated regions, the mean free path is smaller than that in the undislocated regions so that the flux line energy is smaller. Or, alternatively, pinning is due to the modification of elastic constants when the material changes from the normal into the superconducting state where flux lines are treated as normal cylinders in superconducting matrix[104]. The movement of a flux line occurs when Lorentz force due to a transport current becomes greater than pinning force. When the flux line is pinned at the pinning center, it becomes difficult for the neighbouring lines to move because of their interaction with the pinned line. The flux lines are bound together by the elasticity of the flux line lattice. These bundled flux lines stop at pinning center; the configuration may be such as shown in Fig. 46. Then, due to the local deformation of the flux line lattice, a force appears at the deformed flux lattice

site, possibly due to the elastic energy in the flux line lattice. If the interaction energy between two flux lines is U(r), when one of the flux lines is given the displacement δ, the total increase in energy of the flux line is[105]

$$\Delta V = \frac{1}{2}\sum_i [U'\cos\theta_i/\delta + U''\cos^2\theta_i + (U'/r)\sin\theta_i]_{r_0}\cdot\delta^2 \equiv \frac{1}{2}k\delta^2$$

where θ is the angle between the line joining the two "vortices" and the direction of the displacement of one of the vortices, r_0 is the inter-flux line spacing and k is the effective spring constant of the flux line lattice. The first term is considered to be neglected since it is a deviation from the stable position. The interaction energy between two flux lines may be expressed by[106]

$$U(r) = 2(\phi_0/4\pi\lambda)^2 K_0(r/\lambda)$$

where K_0 is the modified Hankel function of zero order, λ the penetration depth and ϕ_0 is the one quantum of a flux line. The inter-flux line spacing, r_0, is related to the magnetic induction, by

$$B = N\phi_0 = (2/\sqrt{3})(\phi_0/r_0^2)$$

where N is the number of flux lines per unit area. Nabarro et al.[107] calculated a restoring force for a flux line when it is displaced a small distance δ from its equilibrium position in the flux line lattice. A restoring force, f, is

$$f = \frac{3\phi_0^2}{16\pi^2\lambda^3}\left[K_0\left(\frac{\beta^{\frac{1}{2}}}{B^{\frac{1}{2}}}\right) + K_2\left(\frac{\beta^{\frac{1}{2}}}{B^{\frac{1}{2}}}\right)\right]\cdot\delta \equiv k\cdot\delta$$

where $\beta = 2\phi_0/3^{\frac{1}{2}}\lambda^2$.

In the following calculation, the deformation of flux lines between the two pinning centers is assumed to be similar to that of a flexible string with a spring constant kr_0. When the string, which is fixed at the two ends, a distance L_p apart, is subjected to uniform transverse force distributed along its length, the shape is parabolic. However, the string could be approximated by circular arc if the deformation of the string is small. Then, the relative increase in length of the string is $L_p^2/24R^2$ under the external force, where L_p is a separation between the pinning centers and $1/R$ the curvature of the flexible string. Therefore, a tension T is

$$T \sim (kr_0)\frac{\delta}{r_0} \sim \frac{kr_0}{24}\left(\frac{L_p}{R}\right)^2$$

$$T/R = F_a$$

where F_a is the applied force or the Lorentz force ($F_a = B \cdot I$). Above a certain critical magnetic field, the flux lines around the pinning centers could flow by shear of the flux line lattice. The presence of dislocations as flux line lattice defects, such as observed by Essmann et al.[35] could make easy for flux lines to flow. When the deflection angle of the flux line lattice at a pinning center reaches the critical angle, θ_c, flux flow could occur between the pinning centers. Since $2R\sin\theta_c = L_p$,

$$T/R_c = 2T\sin\theta_c/L_p \sim \phi_0^{\frac{1}{6}} \cdot k^{\frac{1}{3}} \cdot B^{\frac{1}{2}} \cdot I^{\frac{2}{3}} \sin\theta_c / L_p^{\frac{1}{3}}$$

where I is electrical current. T/R_c increases rapidly with increasing B. If the applied force exceeds the force T/R_c, the flux lines can move through the medium. On the other hand, if θ_p is the critical angle at a pinning center as shown in Fig. 46, above which the trapped flux lines are liberated from

the pinning center, then

$$2T\sin\theta_p = F_p \qquad (1)$$

where T is a tension of string and F_p a pinning force. The following relations are obtained at the critical state

$$2R\sin\theta_p = L_p \qquad (2)$$

$$T/R = F_a \qquad (3)$$

where 1/R is the curvature of the deformed flux line lattice. From the eqs. (1), (2) and (3),

$$F_p/L_p = F_a \qquad (4)$$

If a separation between the pinning points, L_p, is 10 μm, and the pinning force is $F_p \sim 10^{-4}$ dyne, F_p/L_p would become comparative to the Lorentz force of current density 10^2 A/cm^2 and magnetic field 10^3 gauss. When the applied force exceeds F_p/L_p, the flux lines can move. F_a is considered to increase linearly with the magnetic induction since F_a is the Lorentz force. T/R_c is proportional to a certain power of the magnetic induction and so the relation among F_a, F_p/L_p and T/R_c would be as shown in Fig. 48 (a).

The equation for the force balance in a flux line flow is written as follows.

In the region I, in Fig. 47 (b), $F_a - T/R_c \geq F_v$ where F_v is the resistive force acting on a flux line. The average velocity of flux lines v_L is $v_L = (F_a - T/R_c)/D$ where D is the damping coefficient. The voltage induced in the mixed stage, V, is produced by flux line motion, and given by $B \times v_L$.

The maximum and minimum

voltages are found in a limited magnetic field range on the deformed specimen. The voltage maximum and minimum are known as a peak effect. The peak effect would appear as shown in Fig. 47 (b), in the region I. On the other hand, the relation between B and H is given as $B = H + 4\pi M$. According to Silcox et al.[108], the magnetization, M, depends on the density of the pinning centers and the values of a lower critical field, H_{c1}, and an upper critical field, H_{c2}. It is, therefore, considered that the magnetization and hence the shape of H-V curve could change during annealing the specimen. The peak effect can be shown in H-V curve as in B-V curve. In the present experiments the peak effect is observed in deformed specimens, as shown in Fig. 43. The explanation of the peak effect, by Anderson et al.[109] is as follows: As the magnetic field approaches H_{c2}, or the two flux lines get very close together, the force between the flux lines is no longer electromagnetic, but is the more steeply varying force. By this hard core intraction, the flux bundles cannot move independently past each other and the peak effect occurs. In general, it is observed that the peak effect does not occur when a pinning space is too small or a pinning force is too weak.[103] Based on the present explanation, if the inter-pin spacing were small, the peak effect would not appear since the curves of F_a and T/R_c cannot cross each other before they cross with F_p/L_p. Furthermore, it is seen from the figure that materials with weak pinning show no peak effect.

There are various dissipative mechanisms that are proposed to account for the damping of the flux lines.[110] The predominant mechanism is that due to the normal eddy current. The additional dissipative mechanisms are due to the intrinsic relaxation associated with a moving flux line and the cycloid damping. The damping coefficient D in the clean material has been

given by Kim et al.[110]

In the dirty state i.e. with defects, additional mechanisms could be considered from the analogy of the damping of dislocations.[111] Therefore, in the present case, the further additional damping mechanisms are considered to exit which are a) the dissipation of energy, which is caused by a small fluctuation in the velocity of flux line as it moves through the pinning centers, b) the deformation of a wave function of electrons due to the strain field, and c) the scattering of electrons.

The first mechanism arises from the reason that the interaction between flux line and dislocation causes a flux line to accelerate and retard as it moves through the obstacle. It radiates energy in the form of wave. The latter two energy dissipations occur by the relative motion of dislocations and normal electrons as a result of the electron viscosity and scattering of the electrons by the strain field of dislocations.

According to the theory for the dragging of electrons by dislocation.[112,113] The damping coefficient increases linearly with the concentration of normal conduction electrons. If the electron drag coefficient for dislocation movement, η, is $\sim 10^{-5}$ dyne.sec.cm^{-1}, the damping coefficient, D, is given as $C_D \cdot \eta \cdot B/H_{c2} \approx 10^5$ dyne.sec.cm^{-3}, provided that the damping coefficient increases linearly with the concentration of conduction electrons and the density of dislocations C_D is 10^{10} cm^{-2}. To obtain the value of D in a dirty superconductor, therefore, the contribution from these dampings cannot be neglected.

Since not only the values of F_p and L_p but also D would vary during annealing, the change in behavior of the H-R curve during annealing could occur rather rapidly comparing with the recovery of the defects.

The H-R curve of a specimen deformed at 4.2°K in Fig. 43 returns nearly to that of an as-annealed one, when the temperature is increased to room temperature. However, the defect produced by deformation cannot recover completely by annealing at room temperature. Since dislocations are not completely annealed at room temperature, if pinning center is assumed to be dislocations, these observation is difficult to be explained. However, if pinning centers are assumed to be point defects, it is also difficult to interpret the results, since there is no corresponding recovery stage in the electrical resistivity. Therefore, at present, it seems hard to understand the remarkable change of the H-R curve during this low temperature annealing.

5. Conclusions

The recovery after cold work at 4.2°K of Au, Cu and Al (f.c.c. metals) and V and Fe (b.c.c. metals) was investigated by electrical resistivity measurements and the recovery structure was determined from 4.2°K to above 400°K.

The fast neutron irradiation of Au, Cu and Al (f.c.c. metals) and Mo and W (b.c.c. metals) were performed at about 5°K in LHTL of JRR-3. The recovery of the electrical resistivity for metals with various treatments has been studied and the recovery structure was discussed, from 4.2°K to about 400°K.

(1) The Stage I recovery in cold worked Au, Cu and Al (f.c.c. metals) and V and Fe (b.c.c. metals) was considered to be due to the rearrangement of dislocations rather than the annihilation of correlated Frenkel pairs or the migration of crowdions.

(2) The reverse annealing was observed in Au but not in Cu and Al. The impurity effect seemed to be important for its appearance.

(3) The stage II recovery in cold worked Au, Cu and Al (f.c.c. metals) and V and Fe (b.c.c. metals) could be ascribed to the migration or dissociation of interstitial clusters. One has to assume that deformation mainly gives rise to the formation of interstitials in the clustered form.

(4) The damage production rate after fast neutron irradiation at liquid helium temperature was decreased by cold work and by alloying in Au, but it was increased by cold work in Cu. Cold work enhanced the recovery above 150°K in Cu and above 50°K in Au. In Au and Cu, the stage III recovery shifted by about 30°K toward lower temperature in cold worked specimens.

(5) The recovery after fast neutron irradiation at liquid helium temperature of Mo and W was investigated. Radiation doping at room temperature enhanced

the amount of recovery in stages I and II.

In Mo, the effect of doping vanished when the doped specimen was annealed at 400°C, where stage III was completed. The enhancement phenomenon was discussed in conjunction with the stage III recovery study.

Stage I below 90°K of W consisted of at least five substages. The effect of doping did not vanish when the doped specimen was annealed at 400°K, where stage III was completed. This is in contrast with Mo.

(6) The effect of deformation after irradiation on the recovery spectra of fast neutron irradiated metals below 10°K was studied on Cu, Al and Au.

The reduction of the stage I recovery due to the deformation was observed in Cu and Au but not in Al. On the other hand, the enhancement of the stages II and III recovery was observed on all metals studied. The results were discussed in relation with the two possible cases, nemely (1) recovery or disappearance of stage I defects and (2) transformation of stage I defects through interactions with moving dislocations. The experimental results seemed to be in favor of the case (1).

The deformation after annealing above stage I after low temperature irradiation increased a little the amount of stage I recovery in Cu but not in Al. For Cu, this could be associated with the destruction of interstitial clusters during the deformation.

(7) The motion of flux lines in the medium containing defects, i.e. pinning centers, was considered in some detail. The various mechanisms were discussed, i.e. the relation among Lorentz force, pinning force and tension, the peak effect, and the damping mechanism in the medium with pinning centers.

(8) The applied magnetic field (H) versus the resistance (R) of a specimen of V deformed at 4.2°K returned nearly to that of an as-annealed one, when the temperature was increased to room temperature. It seemed hard to understand

the remarkable change of the H-R curve during low temperature annealing from the simple recovery process of point defects or dislocation rearrangement.

Acknowledgements

The author would like to thank Dr. S. Okuda for his guidance and Drs. K. Kubo, Y. Obata and Prof. H. Kimura for their encouragement throughout this work. Invaluable cooperations given by Drs. H. Maeta and R. Hanada and technical assistance given by Messrs. M. Watanabe and T. Kato are gratefully appreciated. The author is also grateful to the members of JRR-3 for their helpful support during the irradiation work.

References

1) E. P. Wigner : J. appl. Phys. 17 (1946) 857.

2) T. Broom : Adv. Phys. 3 (1954) 26.

3) A. C. Damask and G. J. Dienes : Point Defects in Metals (Gordon and Breach, New York, 1963)

4) F. Seitz : Adv. Phys. 1 (1952) 43.

5) N. F. Mott : Phil. Mag. 43 (1952) 1151.

6) A. Seeger : Proc. 2nd U. N. Int. Conf. on the peaceful Uses of Atomic Energy (Geneva, 1958) Vol. 6, P. 260.

7) N. F. Mott : Dislocations and Mechanical Properties of crystals ed. J. C. Fisher, (Wiley, New York, 1957) p. 458.

8) G. H. Kinchin and R. S. Pease : Reports on Progress in Physics No. 18 (1955) p. 1.

9) A. Seeger : Proc. Symp. on Radiation Damage and Reactor Materials IAEA. Paper SM-25/41 (1963).

10) R. H. Silsbee : J. appl. Phys. 28 (1957) 1246.

11) G. Leibfried : J. appl. Phys. 31 (1960) 117.

12) M. T. Robinson and O. S. Oen : Appl. Phys. Letters 2 (1963) 30.

13) O. S. Oen and M. T. Robinson : Appl. Phys. Letters 2 (1963) 83.

14) H. G. Cooper, J. S. Koehler and J. M. Marx : Phys. Rev. 97 (1955) 599.

15) J. W. Corbett, R. B. Smith and R. M. Walker : Phys. Rev. 114 (1959) 1452.

16) G. W. Iseler, H. I. Dawson and J. W. Kanffman, Lattice Defects and Their Interactions, ed. R. R. Hasiguti (Gordon and Breach, New York, 1967) p. 654.

17) R. A. Johnson and E. Brown : Phys. Rev. 127 (1962) 446.

18) R. A. Johnson : Phys. Rev. 134 (1964) A1329.

19) G. de Keating-hert, R. Cope, C. Minier and P. Moser: Report of the Intern. Conf. on Vacancies and Interstitials in Metals (Jul, 1968) Vol. I, p. 327.

20) H. Bilger, V. Hivert, J. Verdone, J. L. Leveque and J. C. Soulie : Report of the Intern. Conf. on Vacancies and Interstitials in Metals (Jul, 1968) Vol. II, p. 751.

21) D. E. Peacock and A. A. Johnson : Phil. Mag. 8 (1963) 563.

22) J. Nihoul : Radiation Damage in Solids, (IAEA, Vienna, 1962) Vol. I, 309.

23) A. R. Rosenfield : Acta metallurgica 12 (1964) 119.

24) J. M. Williams, J. T. Stanley and W. E. Brundage : ORNL Report No. 4097 (1967) p. 30.

25) A. Kothe and F. Schlat : J. Mater. Sci. 2 (1967) 201.

26) L. J. Cuddy : Phil. Mag. 12 (1965) 855.

27) H. H. Kuhlmann and H. Schultz : Acta metallurgica 14 (1966) 798.

28) A. H. Cottrell and B. A. Bilby : Proc. Phys. Soc. 62A, (1949) 49.

29) A. H. Cottrell, S. C. Hunter and F. R. N. Nabarro : Phil. Mag. 44 (1953) 1964.

30) J. Friedel : Dislocations (Pergamon, Oxford, 1964) p. 363.

31) C. J. Meechan A. Sosin and J. A. Brinkman : Phys. Rev. 120 (1960) 411.

32) T. H. Blewitt, R. R. Coltman, C. E. Klabunde, D. K. Holmes and J. K. Redman : ORNL, Report No. 2614 (1958) p. 67.

33) A. Sosin : Bull. Am. Phys. Soc. 6 (1961) 151.

34) A. A. Abrikosov : Soviet Phys. JETP, 5 (1957) 1174.

35) U. Essmann and H. Trauble : Phys. Letters 24A (1967) 526.

36) A. A. Gerristsen : Hundbuch der Physik ed. S. Flugge (Springer, Berlin, 1956) Vol. 19, 156.

37) M. DeJong and H. B. Afman : Acta metallurgica 15 (1967) 1.

38) D. Schumacher and A. Seeger : Phys. Letters 15 (1963) 184.

39) H. I. Dawson : Physica 31 (1965) 1046).

40) M. L. Swanson : Canad. J. Phys. 42 (1964) 1890.

41) L. J. Cuddy : Acta metallurgica 16 (1968) 23.

42) O. Dimitrov and C. Dimitrov-Frois : Report of the Intern. Conf. on Vacancies and Interstitials in Metals, (Julich, 1968) Vol. I, p. 304.

43) R. R. Coltman, C. E. Klabunde and J. K. Redman : Phys. Rev. 156 (1967) 715.

44) G. Burger, K. Isebeck, R. Kerler, J. Volkl, H. Wenzl, H. H. Kuhlmann and H. Schultz : Phys. Letters 20 (1966) 470.

45) M. L. Swanson : Phys. Status Solidi (a) 3 (1970) 551.

46) M. L. Swanson : Canad. J. Phys. 44 (1966) 3241.

47) Van den Beukel : Vacancies and Interstitials in Metals ed. Seeger et al. (North-Holland, Amstrerdom, 1970) p. 427.

48) W. Frank and A. Seeger : Radiation Effects 1 (1969) 117.

49) J. W. Corbeet : Solid State Physics Suppl 7 (1966).

50) H. I. Dawson : Acta metallurgica 13 (1965) 453.

51) S. Okuda and R. R. Hasiguchi : Acta metallurgica 11 (1963) 257.
S. Okuda : Sci. Pap. Inst. Phys. Chem. Res. Tokyo 57 (1963) 116.

52) W. Schule, A. Seeger, D. Schumacher and K. King : Phys. Status. Solidi. 2 (1962) 1199.

54) H. Sakairi, T. Sugai and R. R. Hasiguchi : to be published.

55) R. A. Johnson : J. Phys. Chem. Solids 26 (1965) 75.

56) J. W. Corbett, R. R. Smith and R. M. Walker : Phys. Rev. 114 (1959) 1460.

57) W. Bauer and A. Sosin : Phys. Letters 24A (1967) 193.

58) A. Van den Beukel : Acta metallurgica 11 (1963) 97.

59) J. H. Perepezko, R. F. Murphy and A. A. Johnson : Phil. Mag. 19 (1969) 1.

60) L. J. Cuddy : Acta metallurgica 16 (1968) 23.

61) W. Glaeser and H. Wever : Phys. Stat. Sol. 35 (1969) 367.

62) H. H. Neely and D. W. Keefer : Phys. Stat. Sol. 24 (1967) 217.

63) T. H. Blewitt : ORNL, Report No. 2614 (1958) 67.

64) M. L. Swanson and G. R. Piercy : Canad. J. Phys. 42 (1964) 1605.

65) M. L. Swanson, G. R. Piercy and D. J. Mackinnon : Phys. Rev. Letters 9 (1962) 418.

66) K. Herschbach and J. J. Jackson : Phys. Rev. 153 (1967) 689.

67) W. Bauer : Phys. Letters 19 (1965) 180.

68) C. J. Meechan, A. Sosin and J. A. Brinkman : Phys. Rev. 120 (1960) 411.

69) D. K. Holmes : The Interaction of Radiation with Solids ed. R. Strumance et al. (North-Holland, Amsterdam, 1964) p. 147.

70) D. G. Martin : Phil. Mag. 6 (1961) 839.

71) D. G. Martin : Phil. Mag. 7 (1962) 803.

72) G. Burger, K. Isebeck, J. Volkl, W. Schilling,and H. Wenzl : Z. angew. Phys. 22 (1967) 452.

73) W. Bauer and A. Sosin : Phys. Rev. 136 (1964) A474.

74) K. Herschbach and J. J. Jackson : Phys. Rev. 153 (1967) 694.

75) J. Friedel : Dislocations (Pergamon, London, 1964) p. 426.

76) G. Burger, H. Meissner and W. Schilling : Phys. Status Solidi 4 (1964) 267.

77) N. J. Lomer and R. J. Taylow : Phil. Mag. 19 (1969) 437.

78) H. Hemmerich, D. Meissner, H. Schultz and F. Walz : Report of the Intern. Conf. on Vacancies and Interstitials in Metals (Jul, 1968) Vol. II, p. 724.

79) H. E. Kissinger, J. L. Brimhall, B. Mastel and T. K. Bierlein : Report of the Intern. Conf. on Vacancies and Interstitials in Metals (Jul, 1968) Vol. II, p. 681.

80) J. A. DiCarlo, C. L. Sneed, Jr., and A. N. Goland : Phys. Rev. 178 (1969) 1059.

81) M. K. Sinha and E. W. Muller : J. appl. Phys. 36 (1964) 1256.

82) Review : H. Schultz : Materials Scl. Eng. 3 (1968/69) 189.

83) R. J. Gripshover, M. Khoshnevisan, J. S. Zetts and J. Bass : Phil. Mag. 22 (1970) 757.

84) H. Schultz : Acta metallurgica 12 (1964) 761.

85) R. E. Pawel and T. S. Lundy : Acta metallurgica 17 (1969) 979.

86) H. H. Neely and D. W. Keefer : Phys. Status Solidi 24 (1967) 217.

87) C. Minier Cassayre : ORNL-tr report No. 668 (1965)
C. Minier Cassayre and M. D. Dantreppe : Academie des Sciences 11 (1963) 2368.

88) F. E. Fujita and A. C. Damask : Acta metallurgica 12 (1964) 331.

89) A. Bourret : Report of the Intern. Conf. on Vacancies and Interstitials in Metals (Jul, 1968) Vol. I, p. 3-7.

90) A. Bourret and D. Dantreppe : Phys. Statue Solidi 29 (1968) 283.

91) H. Kronmuller, H. E. Schaefer and H. Rieger : Phys. Status Solidi 9 (1965) 863.

92) A. Seeger and F. J. Wagner : Phys. Status Solidi 9 (1965) 583.

93) D. W. Keefer, J. C. Robinson and A. Sosin : Acta metallurgica 13 (1965) 1135.

94) D. O. Thompson and O. Buck : Phys. Status Solidi 37 (1970) 53.

95) W. Schilling, G. Burger, K. Isebeck and H. Wenzl : Vacancies and interstitials in Metals (North-Holland, Amsterdom, 1969) p. 255.

96) W. Schilling, K. Schroeder and H. Wollenberger : Phys. Status Solidi 38 (1970) 245.

97) K. R. Garr and A. Sosin : Phys. Rev. 162 (1967) 681.

98) J. S. Koehler : Vacancies and Interstitials in Metals (North-Holland, Amsterdom, 1969) p. 1020.

99) A. van den Beukel : Vacancies and Interstitials in Metals (North-Holland, Amsterdom, 1969) p. 1020.

100) H. Suzuki : Proc. Intern. Conf. on Crystal Lattice Defects, J. Phys. Soc. Japan 18, Supplement III (1963) 299.

101) M. J. Attardo, J. M. Galligan and J. G. Chow : Phys. Rev. Letters 19 (1967) 75.

102) M. E. Downey and B. L. Eyre : Phil. Mag. II (1965) 53.

103) G. J. Van Gurp : Philips Res. Repts 22 (1967) 10.

104) W. W. Webb: Phys. Rev. Letters 11 (1963) 191.

105) H. B. Huntington, G. A. Shirn and E. S. Wajda : Phys. Rev. 99 (1955) 1085.

106) P. G. de Gennes : Superconductivity of Metals and Alloys, P. A. Pincus Transl. (W. A. Benjamin, Inc., New York, 1966).

107) F. R. N. Nabarro and A. T. Quintanita : Mat. Res. Bull. 5 (1970) 669.

108) J. Silcox and R. W. Rollins : Appl. Phys. Letters 2 (1963) 231.

109) P. W. Anderson and Y. B. Kim : Rev. Mod. Phys. 36 (1964) 39.

110) Y. B. Kim, C. F. Hempstead and A. R. Strnad : Phys. Rev. 13 (1965) A1163.

111) F. R. N. Nabarro : Theory of Crystal Dislocations (Clarendon Press, Oxford, 1967) p. 505.

112) V. Ya Kravchenko : Soviet Physics-Solid State 8 (1966) 740.

113) C. P. Huffman and N. P. Lovat : Phys. Rev. 176 (1968) 773.

Table I. Neutron irradiation damage rates and resistivity recovered in moderate temperature ranges of Cu, Al and Au specimens.

neutron dose (>0.1 MeV) (hr)	resistivity increase by irradiation ($\times 10^{-9}$ Ωcm)	resistivity increase by deformation ($\times 10^{-9}$ Ωcm)	resistivity annealed in each temperature range ($\times 10^{-9}$ Ωcm)		pre-irradiation treatment
Cu			below 43°K	55°∿308°K	
30	7.1	2.1	1.40	4.40	treatment 3
	7.4	1.7	1.48	3.92	"
	7.4	0	1.75	3.37	treatment 4
	6.8	0	1.67	2.90	treatment 1
10	2.5	0	0.58	1.03	"
	2.6	3.7	0.45	2.73	treatment 3
	0	7.1	0.04	2.75	treatment 2
Au			below 30°K	30°∿279.5°K	
10	1.65	2.36	0.08	1.47	treatment 3
	1.58	1.02	0.09	0.98	"
	1.65	0	0.10	0.77	treatment 1
	1.43	0	0.10	0.78	treatment 4
	0	0.86	0.003	0.15	treatment 2
	0	0.87	0.008	0.43	"
Al			below 60°K	60°∿279.5°K	
10	Run I 0.78	0	0.38	0.39	treatment 1
	Run I 0.81	0	0.41	0.38	treatment 4
	Run I 0.77	1.03	0.43	0.94	treatment 3
	Run II 0.80	0	0.36	0.43	treatment 1
	Run II 0.73	1.28	0.44	1.05	treatment 3
	0	0.16	0.0046	0.05	treatment 2
	0	0.52	0.022	0.27	"

Table II Summary of the stages I and II enhancement due to the doping. The amount of the enhancement at the end of stage II (308°K) ($\Delta\rho_E$) is given in terms of (%) and (Ω-cm). $\Delta\rho_D$ gives the resistivity increase during doping irradiation. The ratio $\Delta\rho_E/\Delta\rho_D$ is almost constant regardless the amount of the doping dose. This fact indicates that the enhancement is proportional to the concentration of defects introduced by the doping

Dope (hr)	$\Delta\rho_D$*	Recovery (% at 308°K)	$\Delta\rho_E$ (%)	$\Delta\rho_E$* (Ω-cm)	$\Delta\rho_E/\Delta\rho_D$
0	-	48	0	-	-
12	4.3	54	6	0.7**	0.17
22	7.5	60	12	1.4**	0.18
64	12.0	67	19	2.2**	0.18

* In unit of 10^{-9} Ω-cm ** Normalized to 10 hr low temp. irrad.

Table III Summary of the stage III recovery in the only doped and the doped and low temperature irradiated specimen. The value $\Delta\rho'(III)-\Delta\rho_D(III)$ should be compared with $\Delta\rho_{L.I.}(III)$ to see that the stage III defects is not being lost during the process of the enhancement in stages I and II.

	Dope (hr)	L.I. (hr)	$\Delta\rho_D(III)$	$\Delta\rho'$**(III)	$\Delta\rho'(III)-\Delta\rho_D(III)$	$\Delta\rho_{L.I.}(III)$
Sp. 3	0	18.7	—	—	—	2.76±0.1
Sp. 1	27.5	0	2.76*±0.1	—	2.70±0.2	
Sp. 2	27.5	18.7	—	5.46***±0.1		
Sp. 1	54.0	0	4.06 ±0.1	—	2.98±0.2	
Sp. 2	54.0	18.7	—	7.04***±0.1		

* In unit of (10^{-9} Ω-cm) ** $\Delta\rho'(III) = \Delta\rho_D'(III)+\Delta\rho'_{L.I.}(III)$

*** Average of two measurements

Table IV Neutron-irradiation damage rates of Mo
fast neutron flux = 1 x 10^{12} neutrons/cm^2·sec
(>0.1 MeV)

	Resistivity ratio $\rho_{300°K}/\rho_{4.2°K}$	Damage rate (10^{-9} Ωcm/hr)
Annealed	5.7	1.36
Cold worked	5.6	1.37
As-received	5.6	1.32

Table V The resistivity increase and the fractional amount of recovery in stage I of W.

W irrad time (hr)	the resistivity increase after low temperature irradiation (Ωcm)	the fractional amount of recovery in stage I (below 90°K) (%)	pre-irradiation treatment before low. temp. irradiation
6	7.1×10^{-9}	27	as annealed
	6.8×10^{-9}	43	64 hr doping
	6.8×10^{-9}	43	64 hr doping then annealed at 400°C
	7.2×10^{-9}	35	22 hr doping
6	7.7×10^{-9}	27	as annealed
	7.0×10^{-9}	51	112 hr doping
	7.5×10^{-9}	29	112 hr doping then annealed at 890°C
	7.4×10^{-9}	33	12 hr doping
30	47.7×10^{-9}	26	as annealed

Fig. 1. Schematic drawing of liquid helium temperature loop

Fig. 2. Cryostat used in the experiments for deformation at 4.2°K.

Fig. 3. The improved apparatus for resistivity measurements for deformation

Fig. 4. Isochronal recovery curves of 99.999% Au cold worked at 4.2°K. Resistivity is measured at 4.2°K after each pulse annealing (6 minutes). Total resistivity increase ($\Delta\rho$), ratio of resistivity at room temperature $\rho_{R.T}$ and at 4.2°K $\rho_{4.2}$ before deformation at 4.2°K ($\rho_{R.T}/\rho_{4.2}$) and elongation (ε) are indicated. Pre-deformation states of the specimens are as follows: as-received wire is 1, annealed 890°C x 100 min. (△), 2, annealed 980°C x 50 hr. (▲), 3, annealed 900°C x 80 min. (●), 4, annealed 600°C x 2 hr (○), 5 and 6, annealed 600°C x 2 hr, cold drawn 19% (reduction of area) and then annealed 100°C x 2 hr (▽, □).

Fig. 5. Fractional isochronal recovery curves of cold worked Au. Treatments of the specimens are as follows: 1, as-received wire is annealed 900°C x 80 min., cold worked 10% at 4.2°K and isochronally annealed up to 235°K (×), 2, this specimen is given a further additional deformation of about 2% (+), 3, as-received wire is annealed 600°C x 120 min., cold worked 9.4% at 4.2°K and isochronally annealed up to 200°K (○), 4, this specimen is given a further additional deformation of about 0.5% (◉), 5 and 6, same as the specimen 5 and 6 of Fig. 4. (▽, □).

Fig. 6. Isochronal recovery curves of 99.999% Cu cold worked at 4.2°K. As-received wires is annealed 900°C x 70 min. and cold worked at 4.2°K.

Fig. 7. Isochronal recovery curves of 99.999% Al deformed at 4.2°K. As received cold drawn wires is annealed at 4.2°K. As received cold drawn wires is annealed 350°C x 120 min. $\rho_{R.T}/\rho_{4.2}$ are 3350.

Fig. 8. Fractional isochronal recovery curves of cold worked Au, Cu and Al.

Fig. 9. Fractional isochronal recovery curves for V specimens deformed at 4.2°K. Treatment of the specimens are as follows: 1, as-annealed specimen is deformed about 3% and the amount of resistivity increase after deformation at 4.2°K ($\Delta\rho$) is 4.5×10^{-8} Ωcm. (○), 2, specimen deformed at 4.2°K after deformation of about 3% at room temperature and the amount of resistivity increase after deformation at 4.2°K ($\Delta\rho$) is 2.9×10^{-8} Ωcm. (△), 3, treatment of the specimen is the same as the specimen 2 and ($\Delta\rho$) is 1.5×10^{-8} Ωcm. (□), 4, as-annealed specimen is deformed at 4.2°K and ($\Delta\rho$) = 0.7×10^{-8} Ωcm. (●)

Fig. 10 The differential isochronal curves calculated from Fig. 9, except for the specimen 4 of Fig. 9.

Fig. 11 Resistivity of Fe in an applied magnetic field at 4.2°K. Curves of specimen before deformation (○) and after deformation (×).

Fig. 12 The isochronal recovery curves for Fe specimens deformed at 4.2°K (○) and deformed at 79°K (△) are measured at 4.2°K under a magnetic field of 140 Oe. The increase of resistivities due to deformation are 2×10^{-9} Ωcm and 10^{-9} Ωcm. respectively.

Fig. 13 Fractional isochronal recovery curves for 6 minutes pulse annealings at each temperature for fast neutron irradiated Cu.

Fig. 14 Differential isochronal recovery curves of Fig. 13.

Fig. 15 The difference of resistivity not recovered in the cold worked specimen and the annealed specimen, are plotted against annealing temperatures.

Fig. 16 Fractional isochronal recovery curves for 6 minutes pulse annealings at each temperature for fast neutron irradiated Au.

Fig. 17 Differential isochronal recovery curves of Fig. 16.

Fig. 18 The difference of resistivity not recovered in the cold worked or 0.1% alloyed specimen and the annealed specimen, are plotted against annealing temperatures.

Fig. 19 The isochronal recovery curves for Cu specimens of three different treatments: 30 hr irradiation at low temperature of as-annealed specimen (treatment 1) (x), as-annealed specimen is first irradiated for 30 hr then deformed by twisting at 4.2°K (treatment 3) (initial resistivity increase is normalized to that of treatment 1) (o), specimen deformed at 4.2°K without irradiation (treatment 2) (Δ).

Fig. 20 The difference between the isochronal recovery curves of treatments 1 and 3 specimens with 30 hr irradiation $\Delta\rho_{I+D}-\Delta\rho_I$ (O), the isochronal recovery curve of the only deformed specimen, where $\Delta\rho_D$ is normalized to the amount of the resistivity increase after deformation in treatment 3 specimen (Δ), and the difference between the isochronal curves between the specimens of treatment 4 and 1. $\Delta\rho_{D+I}$ is normalized to $\Delta\rho_I$ of treatment 1 (x).

Fig. 21 The differential curve of the difference $\Delta\rho_{I+D}-\Delta\rho_I$ between treatments 3 and 1 (o). The differential isochronal curves of the

resistivity increase $(\Delta\rho_D)'_2$ (Δ), and of the treatment 1 specimen after 30 hr irradiation (x).

Fig. 22 The isochronal recovery curves for Al specimens of three different treatment, treatment 1 (x), treatment 2 (Δ) and treatment 3 (o).

Fig. 23 The difference between the isochronal recovery curves of treatments 3 and 1 $\Delta\rho_{I+D}-\Delta\rho_I$ (o), the isochronal recovery curve of the only deformed specimen $(\Delta\rho_D)'_2$ (Δ), and the difference between the isochronal curves of treatments 4 and 1, where $\Delta\rho_{D+I}$ is normalized to $\Delta\rho_I$ of treatment 1 (x).

Fig. 24 The differential curve of the difference $\Delta\rho_{I+D}-\Delta\rho_I$ between the specimens of treatments 3 and 1 (o), the differential isochronal curves of the resistivity increase $(\Delta\rho_D)'_2$ (Δ) and of the treatment 1 specimen after 10 hr irradiation (x).

Fig. 25 The isochronal recovery curves for Au specimens of three different treatments; treatment 1 (x), treatment 2 (Δ) and treatment 3 (o).

Fig. 26 The difference of the isochronal recovery curves between treatments 1 and 3 specimens $\Delta\rho_{I+D}-\Delta\rho_I$ (o) and the isochronal recovery curve of the only deformed specimen $(\Delta\rho_D)'_2$ (Δ).

Fig. 27 The differential curve of the difference $\Delta\rho_{I+D}-\Delta\rho_I$ between treatments 3 and 1 (o), the differential isochronal curves of the resistivity increase $(\Delta\rho_D)'_2$ (Δ) and of the treatment 1 specimen after 10 hr irradiation (x).

Fig. 28. The difference between the isochronal recovery curves of treatments 5 and 1 for Cu.; in treatment 5, two specimens are annealed at 30°K and at 40°K respectively after irradiation then deformed at 4.2°K.

Fig. 29 The fractional recovery curves of the treatment 5 specimens of Cu; in treatment 5, three specimens are annealed at 125° (Δ) 253° (x) and 293°K (●), respectively after irradiation then deformed at 4.2°K. The initial resistivity increase after deformation $(\Delta\rho_D)_5$ is taken as 100%.

Fig. 30 Recovery structures in 10 hr fast neutron irradiated Mo specimens. Three curves correspond to three different purity specimens (resistivity ratio 520, 320, 20). Note that the 60°K substage shows systematic retardation with impurity contents.

Fig. 31 Recovery structures in the radiation doped Mo specimens. (Δ) shows the recovery of the 64 hr doped specimen, whereas (□) shows the recovery of the doped and subsequently annealed at 400°C specimen. The recovery of the as-annealed specimen (○) is also shown for comparison.

Fig. 32 $(\Delta\rho(\%)/\Delta T_i)_{Doped}/\ (\Delta\rho(\%)/\Delta T_i)_{As\text{-}Anneal}$ is plotted against the annealing temperature to show the enhancement more clearly. The same curve for W is also shown.

Fig. 33 The differential recovery curves of stage III in the only doped (B) and the doped and low temperature irradiated (A) specimens. Fig. 33 (a) shows the results of 27.5 hr doping, Fig. 33 (b) is for 54.0 hr doping time. Low temperature irradiation time was 18.7 hr in both case. The dashed lines show the difference (A - B) in order to compare the results with the only low temperature irradiated specimen. (see Fig. 34).

Fig. 34 The comparison of the (A - B) curves in Fig. 33 with the stage III recovery in the only low temperature irradiated specimens.

Note that the amount of recovery (A - B) is almost comparable with that of the only low-temperature irradiated specimen. Also see Text and Table III).

Fig. 35 Fractional isochronal recovery curves for 6 minutes pulse annealings at each temperature for fast neutron irradiated Mo.

Fig. 36 The differences in fractional recovery, i.e., the percentage of not recovered resistivity in cold worked or as-received specimen minus that in the annealed specimen are plotted against annealing temperatures.

Fig. 37 Fractional isochronal recovery curves after fast neutron irradiation for specimens (1) as-annealed, (2) 64 hr doped, (3) 64 hr doped and subsequently annealed at 400°C (4) 22 hr doped.

Fig. 38 Differential isochronal recovery curves of Fig. 37. (22 hr doped specimen is not included).

Fig. 39 Fractional isochronal recovery curves after fast neutron irradiation for 6 hr specimens of (1) as-annealed, (2) 112 hr doped. The recovery curves after 30 hr low temperature irradiation of as-annealed specimen is also included for comparison purpose.

Fig. 40 Differential recovery curves of specimens (1) as-annealed, (2) 112 hr doped, (3) 112 hr doped and then annealed at 890°C.

Fig. 41 The amount of fractional recovery below 90°K after low temperature irradiation are plotted against doping irradiation time.

Fig. 42 Fractional isochronal recovery curves for Fe and their differential curves for 6 minutes pulse annealing at each temperature.

Fig. 43 Resistivity of deformed V in an increasing magnetic field for the current density of 240 A/cm^2. For as-annealed specimen (●) and specimen after deformation at 4.2°K (○) and specimen annealed at 2 25° (△), 40° (□), 55° (▽), 70° (•), 110° (▲), 413° (■) and 442°K (×) after deformation at 4.2°K.

Fig. 44 Voltage versus the applied magnetic field for V specimens after deformation at 4.2° (○), 54° (△) and 74°K (□) for two different current densities, (a) 240 A/cm^2 and (b) 40 A/cm^2. Voltage versus an increasing magnetic field of as-annealed specimen before deformation at 4.2° (●), 54° (▲) and 74° (■) are given. The plot H-V relation of specimen annealed at 54° (×) and 74°K (+) after deformation at 4.2°K are also shown for comperison.

Fig. 45 The magnitudes of the plastic after effects of Au specimens. The apparatus used is similar in shape to the inverted torsion pendulum. Specimen with fixed lower end is suspended over a pulley by a counterweight with tungsten wire. The recovered angle is measured by means of optical lever. Treatments of the specimens as follows: as received wire are annealed 950°C, deformed by torsion at 4.2°K in one direction, untwisted in another direction during warm-up; ○, annealed wire are deformed by torsion at 78°K in one direction, untwisted during warming-up; △, the isochronal recovery curve (□) deformed at 4.2°K is measured by electrical resistivity.

Fig. 46 The configuration in the flux line lattice. The flux lines are considered to be arranged in a triangular lattice. The flux line

lattice deform at pinning center under Lorentz force. The angle deviated from the normal state of lattice is given by θ_p.

Fig. 47 The relation among Lorentz force on the flux line lattice, F_a, pinning force, F_p/L_p, and the force from the tension of flux line lattice, T/R_c are shown in (a). (b) If Lorentz force exceed the force, T/R_c, the flux line lattice can move until $F_a = T/R_c$ (region I). When Lorentz force, F_a exceeds pinning force, F_p/L_p, the flux line lattice can move again (region II).

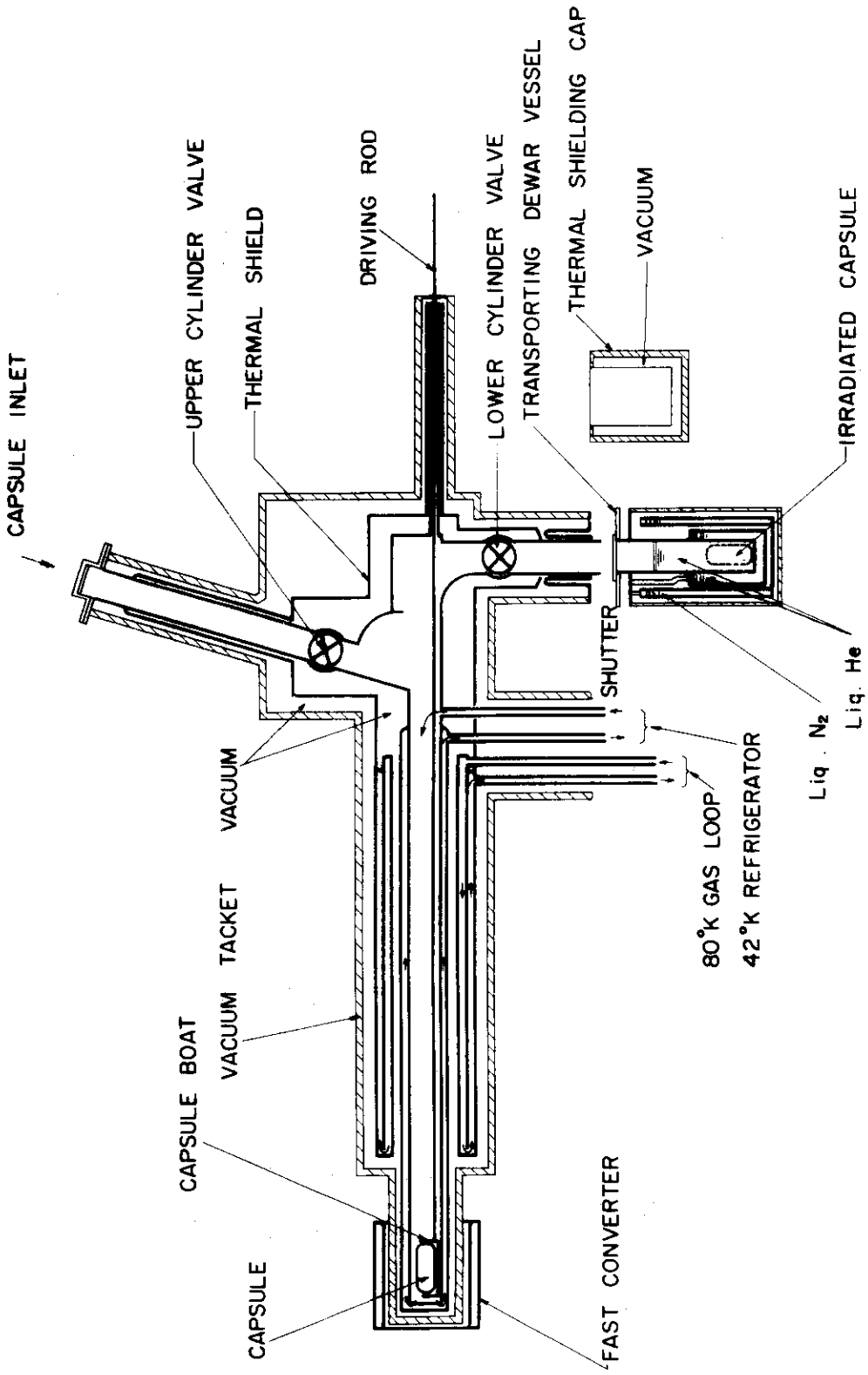
CAPSULE INLET
UPPER CYLINDER VALVE
THERMAL SHIELD
DRIVING ROD
LOWER CYLINDER VALVE
TRANSPORTING DEWAR VESSEL
THERMAL SHIELDING CAP
VACUUM
IRRADIATED CAPSULE
SHUTTER
Liq. He
Liq. N2
80°K GAS LOOP
42°K REFRIGERATOR
VACUUM
TACKET
VACUUM
CAPSULE BOAT
CAPSULE
FAST CONVERTER

Fig. 1

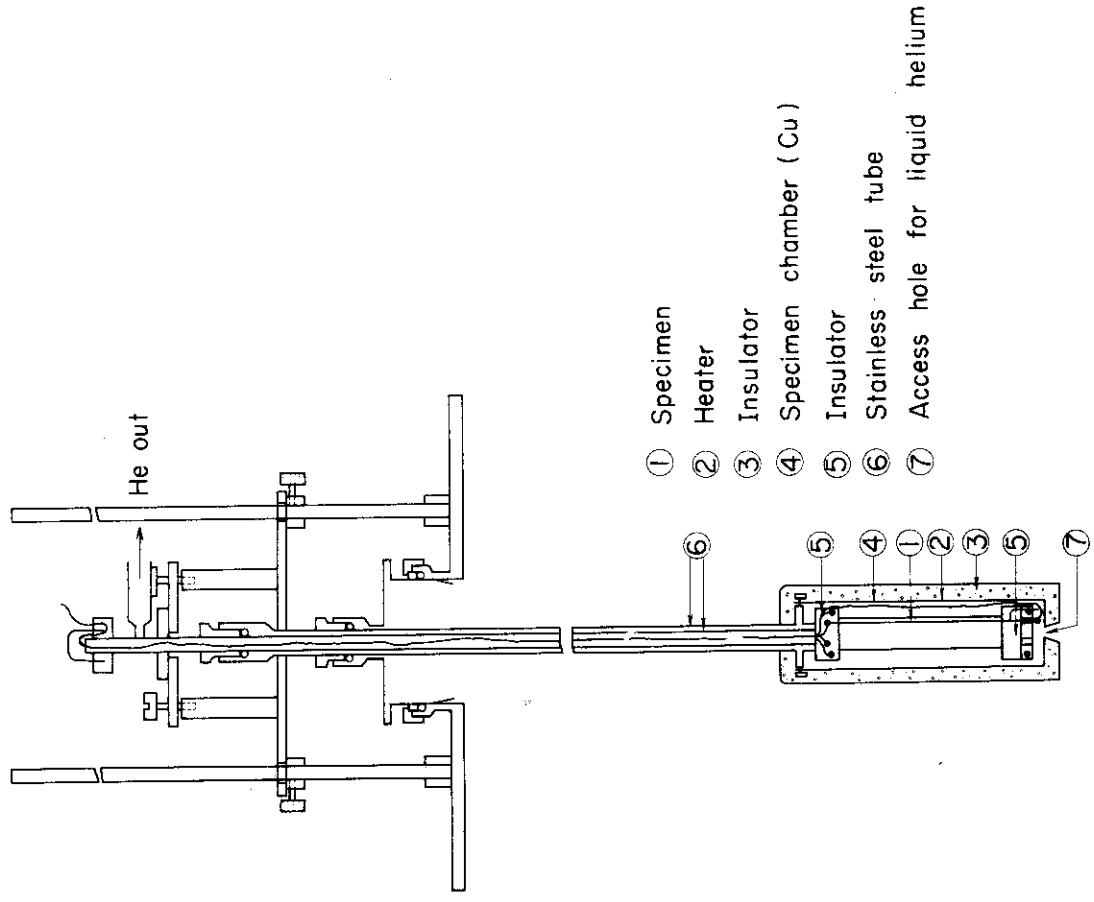
He out
① Specimen
② Heater
③ Insulator
④ Specimen chamber (Cu)
⑤ Insulator
⑥ Stainless steel tube
⑦ Access hole for liquid helium

Fig. 3

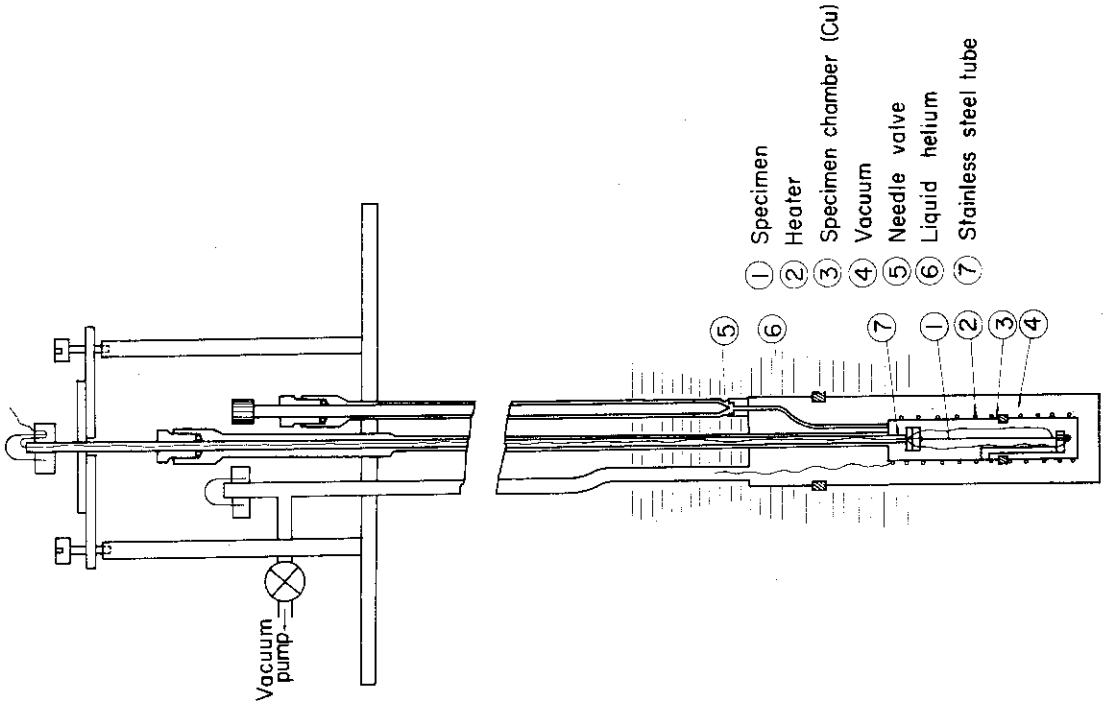
Vacuum pump
① Specimen
② Heater
③ Specimen chamber (Cu)
④ Vacuum
⑤ Needle valve
⑥ Liquid helium
⑦ Stainless steel tube

Fig. 2

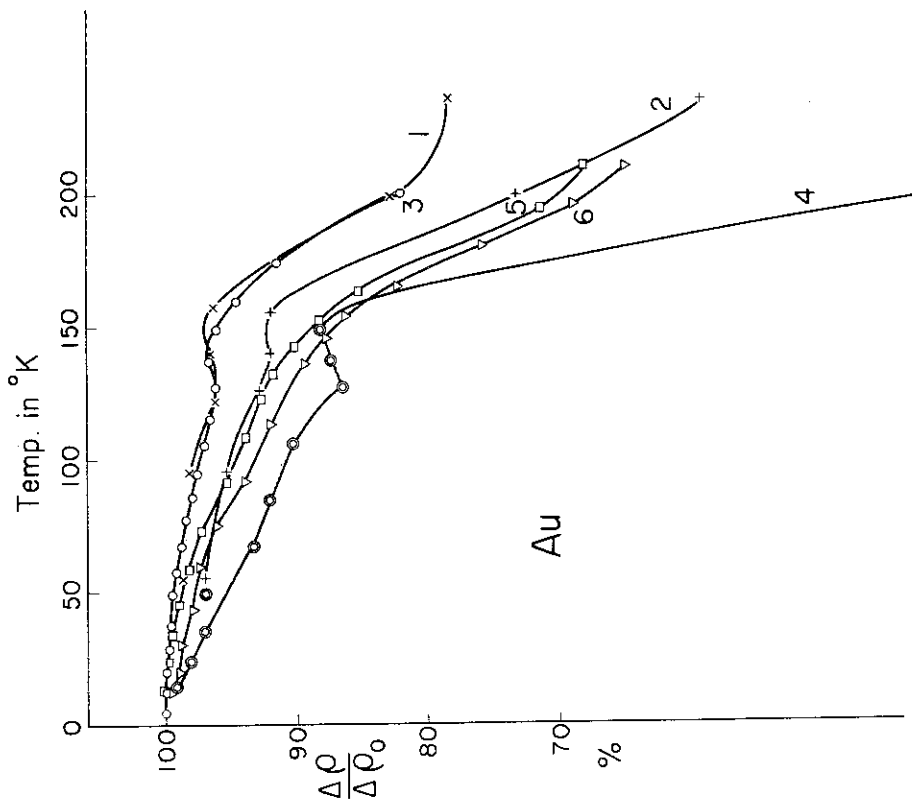
Temp. in °K
0
50
100
150
200
1
2
3
4
5
6
Au
100
90
80
70
%
$\frac{\Delta\rho}{\Delta\rho_0}$

Fig. 3

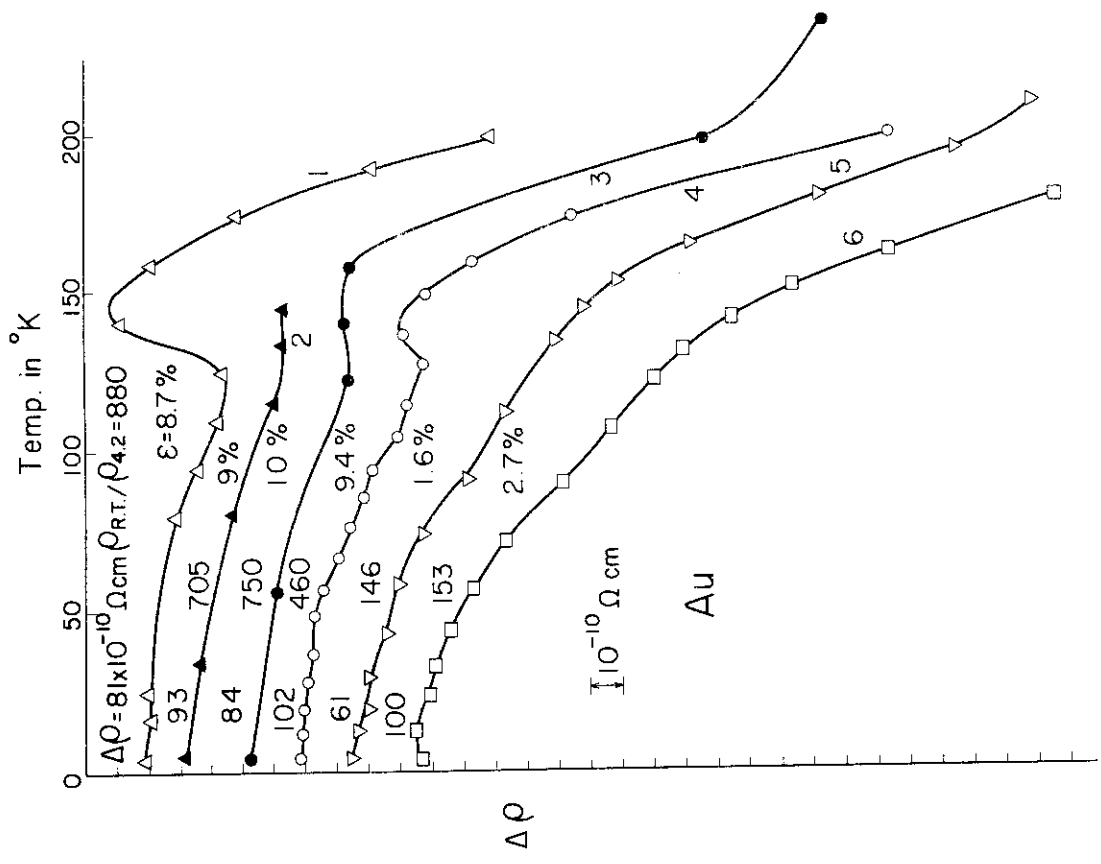
Temp. in °K
0
50
100
150
200
$\Delta\rho = 81\times10^{-10}\,\Omega cm\,\rho_{R.T.}/\rho_{4.2} = 880$
ε=8.7%
9%
10%
9.4%
1.6%
2.7%
93
705
84
750
102
460
61
146
100
153
1
2
3
4
5
6
$\pm 10^{-10}\,\Omega\,cm$
Au
$\Delta\rho$

Fig. 4

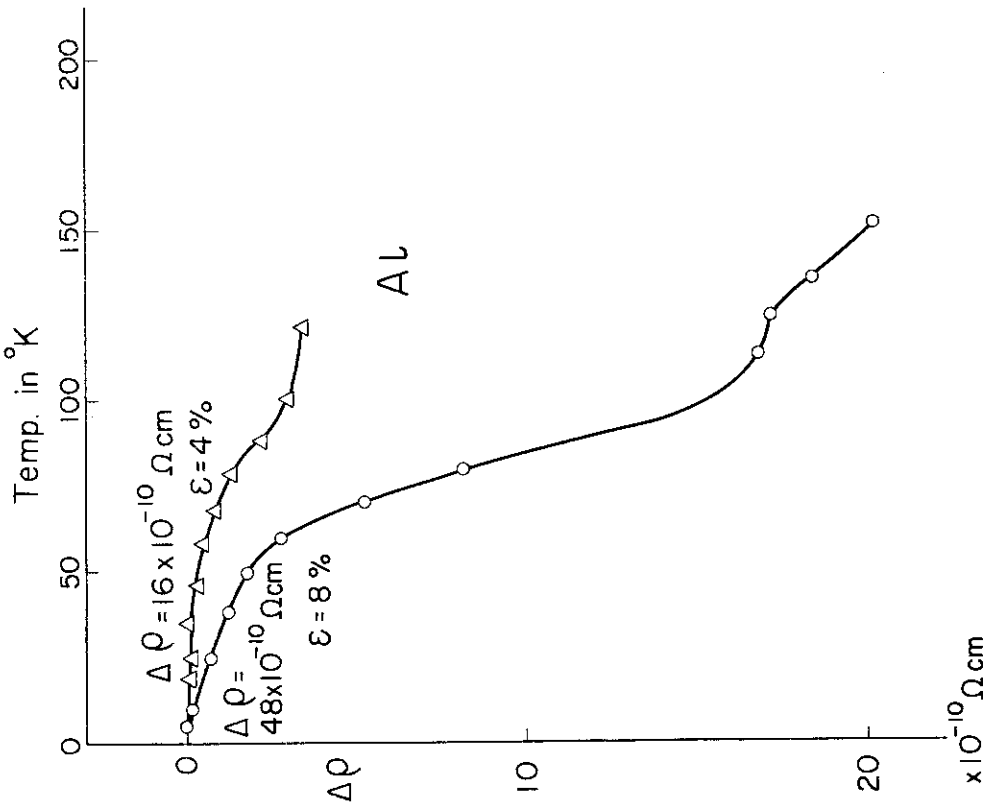
Temp. in °K
0
50
100
150
200
Δρ=16×10⁻¹⁰ Ωcm
ε=4%
Δρ=
48×10⁻¹⁰Ωcm
ε=8%
Al
Δρ
0
10
20
×10⁻¹⁰Ωcm

Fig. 7

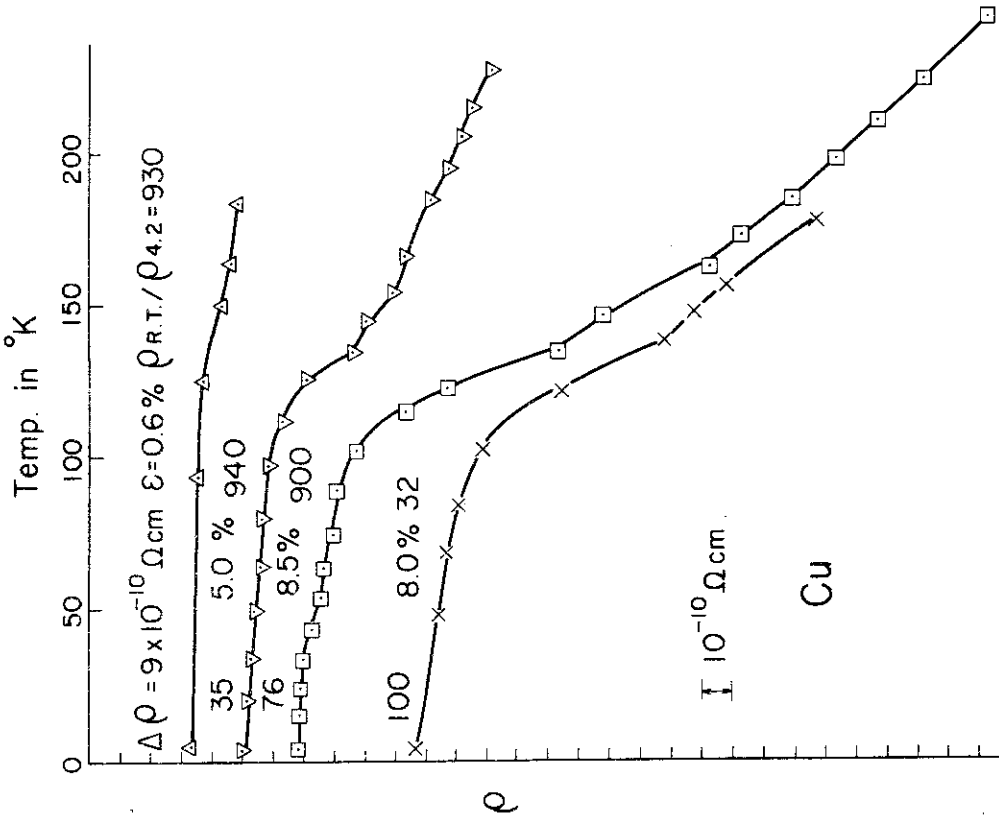
Temp. in °K
0
50
100
150
200
Δρ=9×10⁻¹⁰Ωcm ε=0.6% ρR.T./ρ4.2=930
35
5.0 % 940
76
8.5% 900
100
8.0% 32
1×10⁻¹⁰Ωcm
Cu
Δρ

Fig. 8

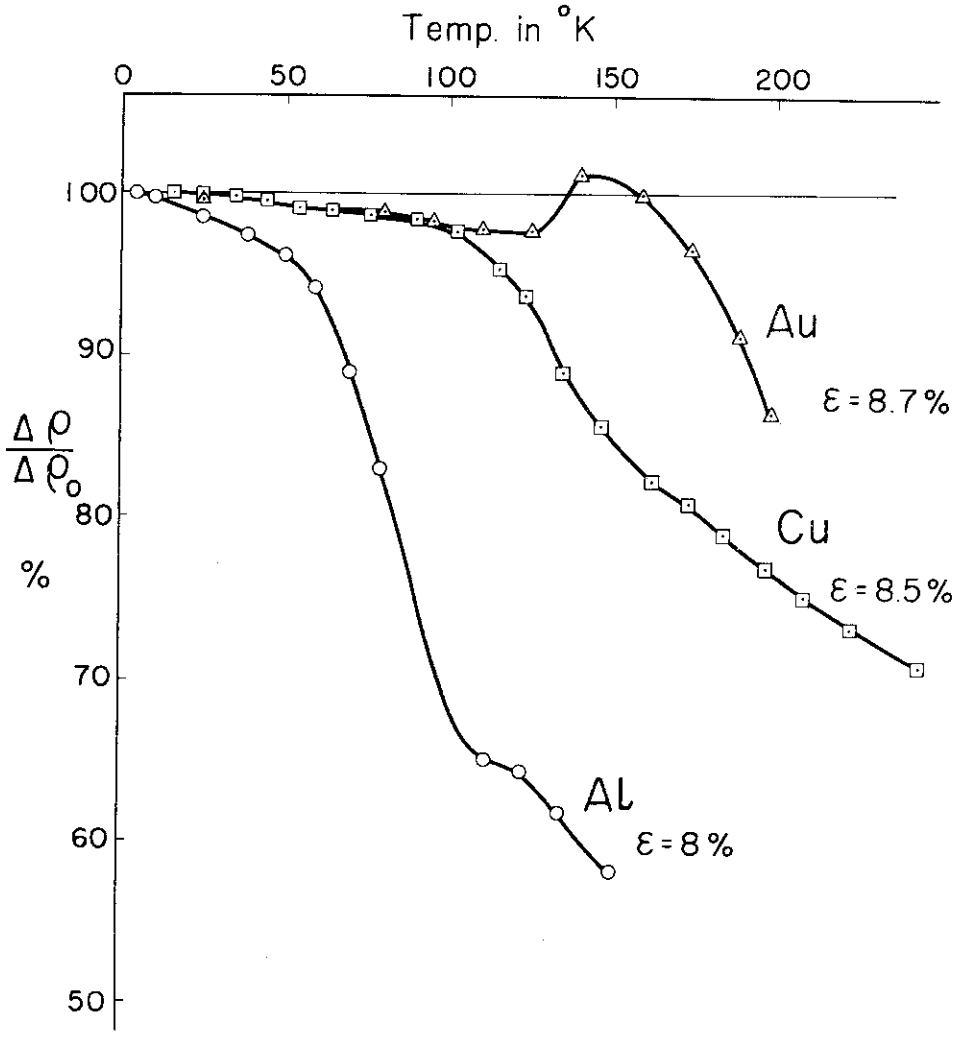
Temp. in °K
0
50
100
150
200
100
90
80
70
60
50
Δρ/Δρ₀
%
Au
ε = 8.7%
Cu
ε = 8.5%
Al
ε = 8%

Fig. 8

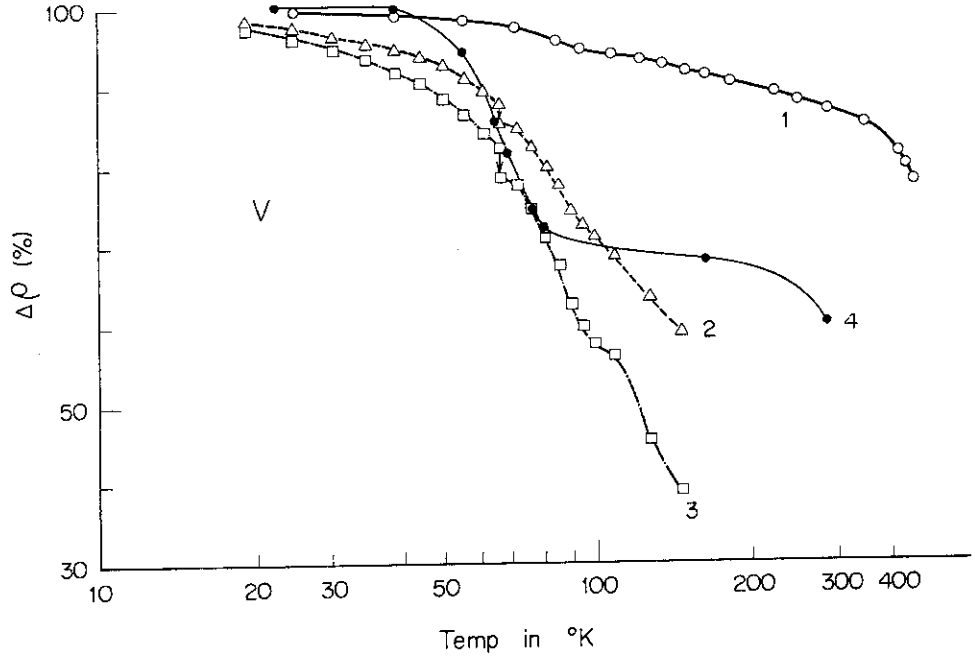
100
50
30
10
20
30
50
100
200
300
400
V
Δρ (%)
Temp in °K
1
2
3
4

Fig. 9

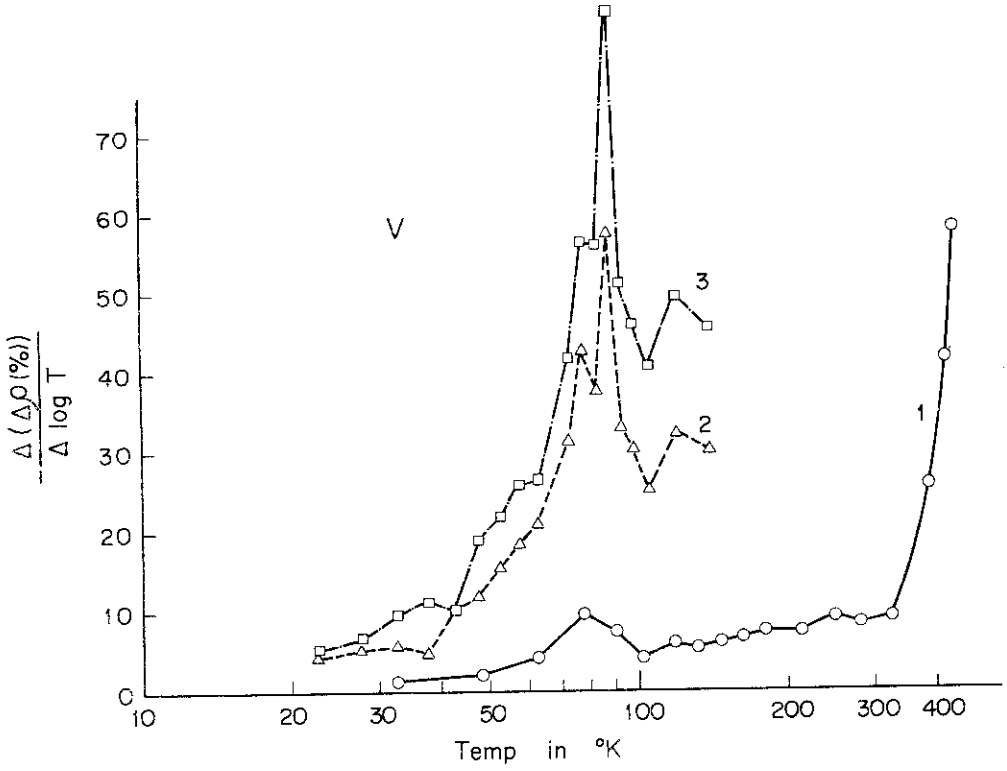
70
60
50
40
30
20
10
0
10
20
30
50
100
200
300
400
V
Δ(Δρ(%))/Δ log T
Temp in °K
1
2
3

Fig. 10

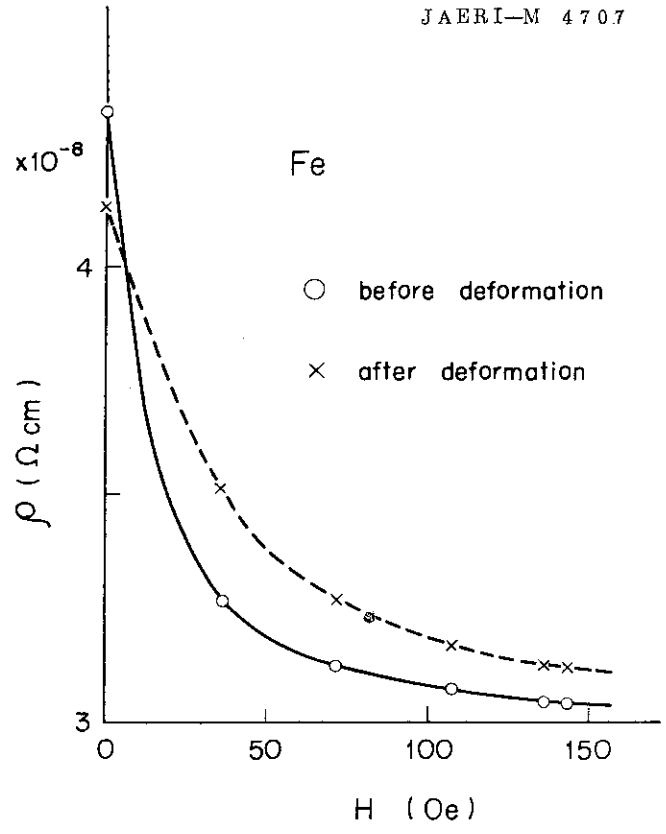
x10⁻⁸
Fe
○ before deformation
× after deformation
ρ (Ω cm)
4
3
0
50
100
150
H (Oe)

Fig. 11

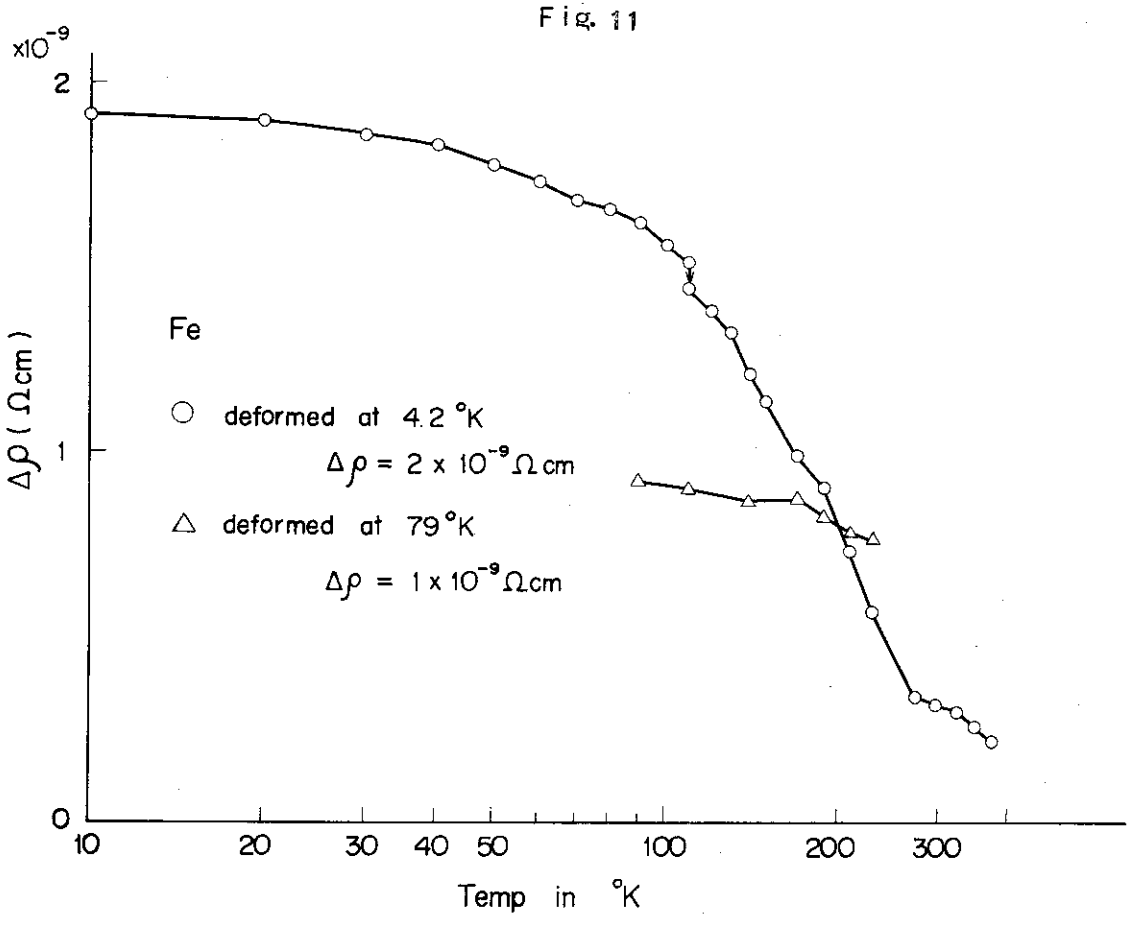
x10⁻⁹
2
1
0
Δρ (Ω cm)
Fe
○ deformed at 4.2 °K
Δρ = 2 x 10⁻⁹ Ω cm
△ deformed at 79 °K
Δρ = 1 x 10⁻⁹ Ω cm
10
20
30
40
50
100
200
300
Temp in °K

Fig. 12

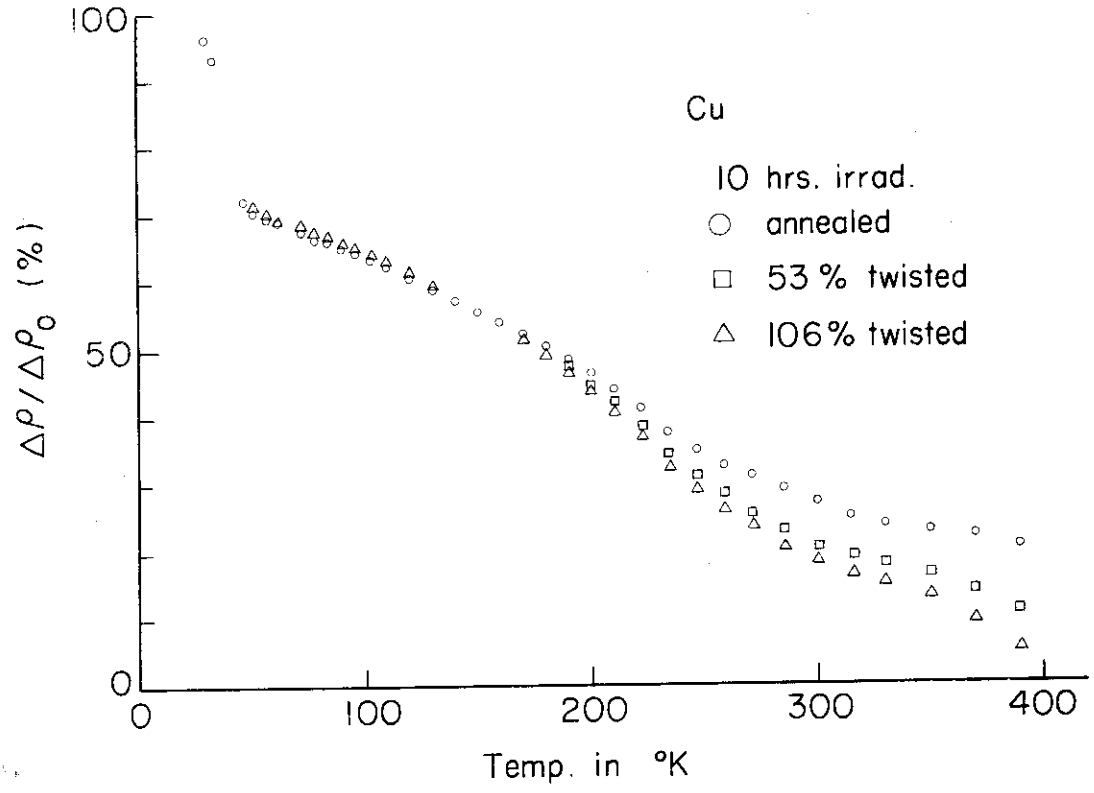
100
50
0
0
100
200
300
400
Cu
10 hrs. irrad.
annealed
53 % twisted
106 % twisted
Δρ/Δρ0 (%)
Temp. in °K

Fig. 13

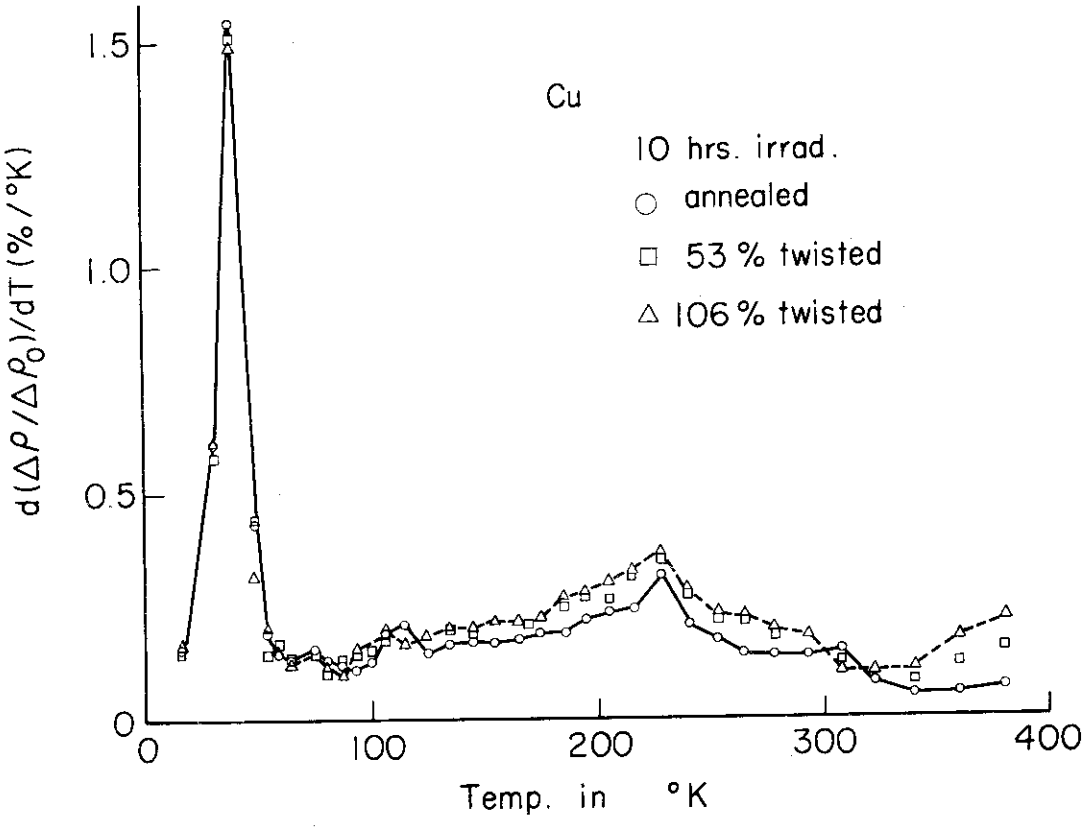
1.5
1.0
0.5
0
0
100
200
300
400
Cu
10 hrs. irrad.
annealed
53 % twisted
106 % twisted
d(Δρ/Δρ0)/dT (%/°K)
Temp. in °K

Fig. 14

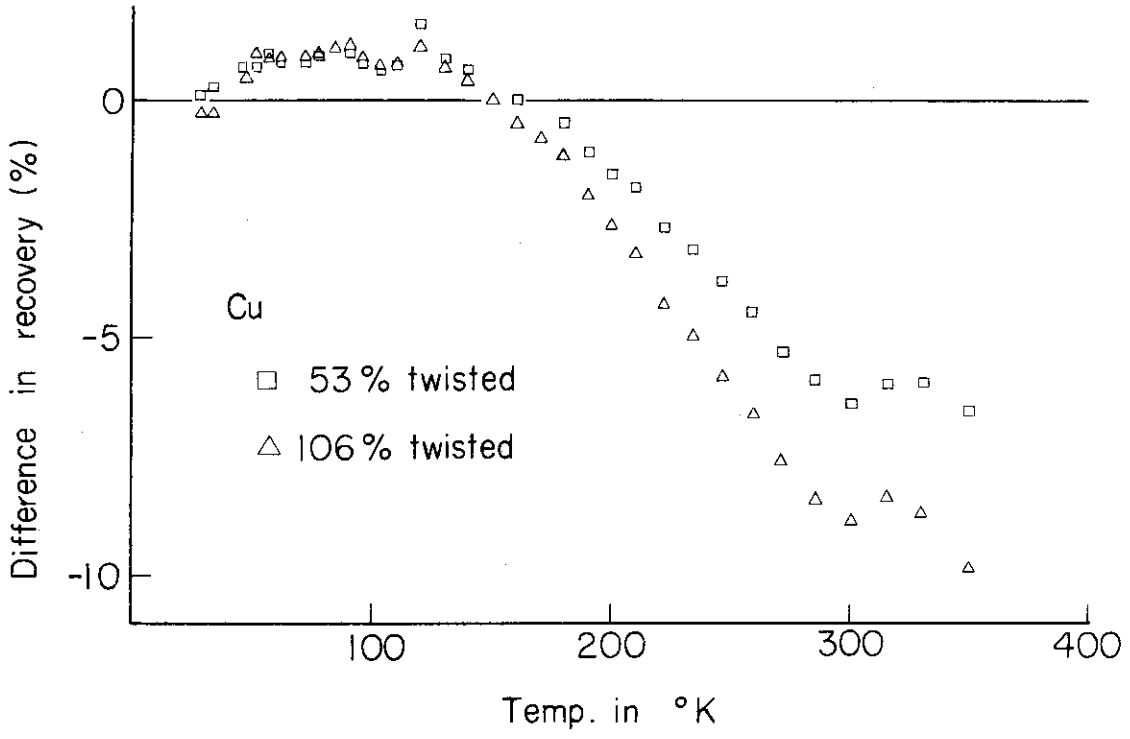
0
-5
-10
Difference in recovery (%)
Cu
□ 53 % twisted
△ 106 % twisted
100
200
300
400
Temp. in °K

Fig. 15

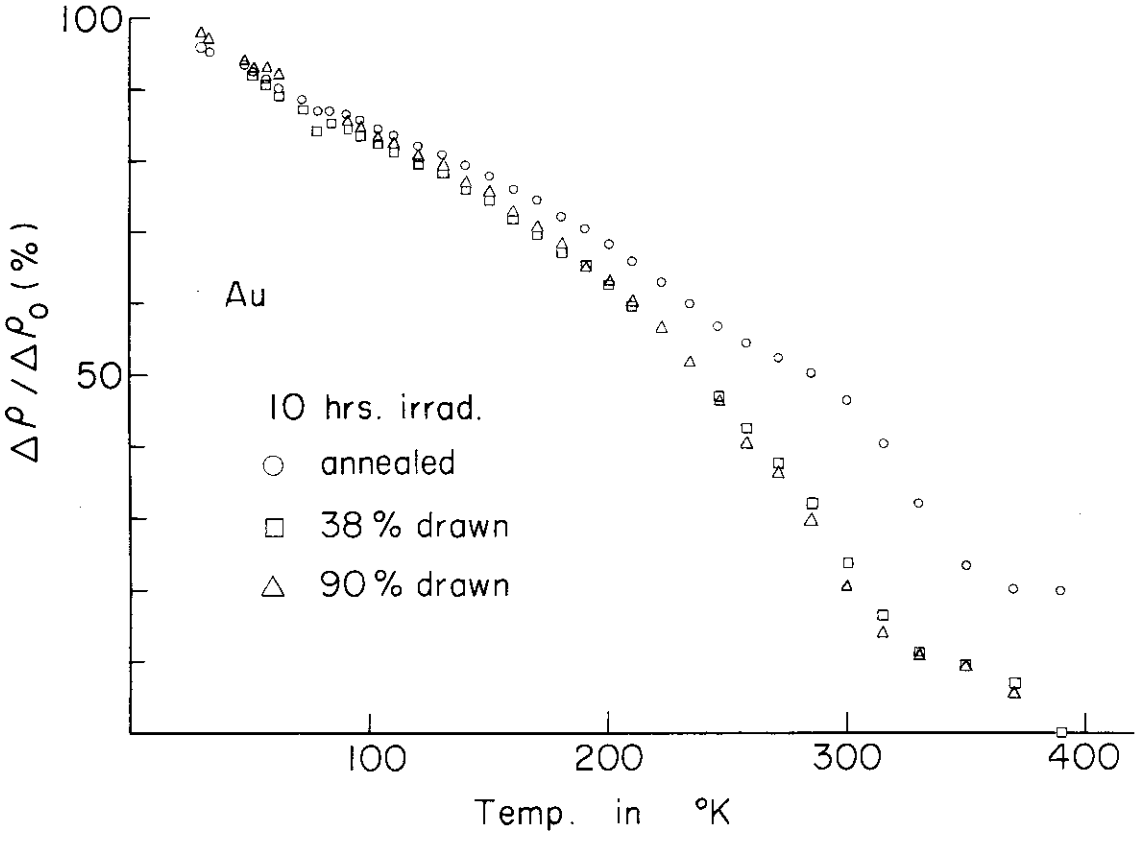
100
50
Δρ / Δρ0 (%)
Au
10 hrs. irrad.
○ annealed
□ 38 % drawn
△ 90 % drawn
100
200
300
400
Temp. in °K

Fig. 16

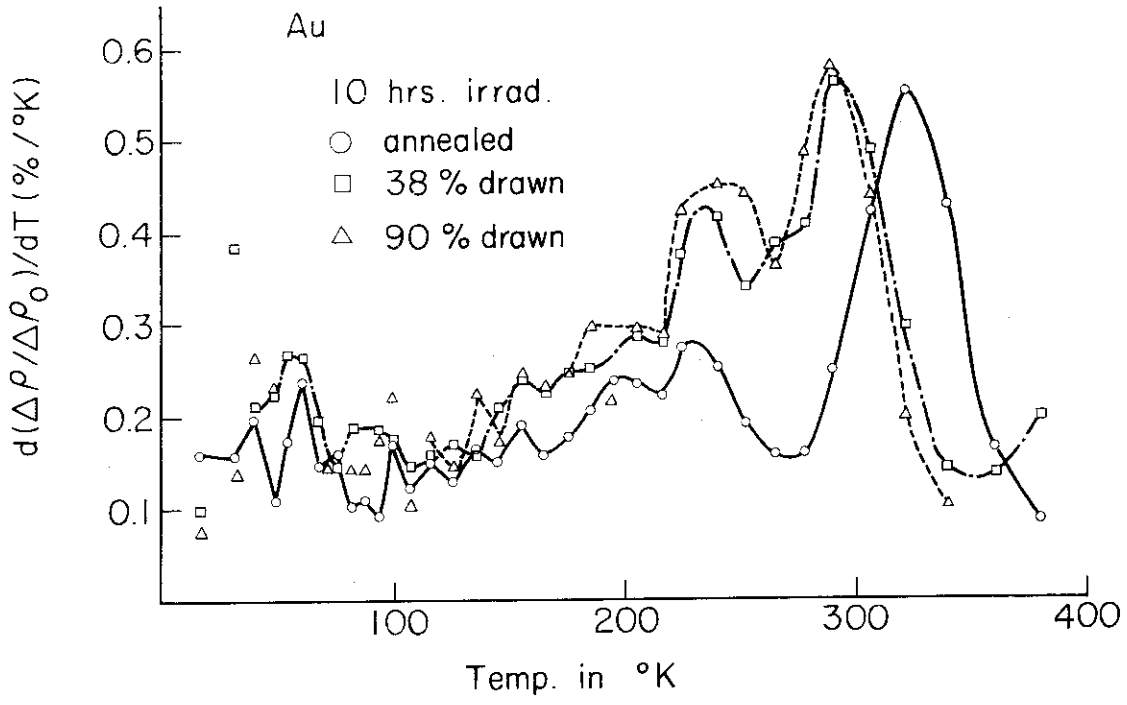
Au
10 hrs. irrad.
○ annealed
□ 38 % drawn
△ 90 % drawn
d(Δρ/Δρ0)/dT (%/°K)
0.6
0.5
0.4
0.3
0.2
0.1
100
200
300
400
Temp. in °K

Fig. 17

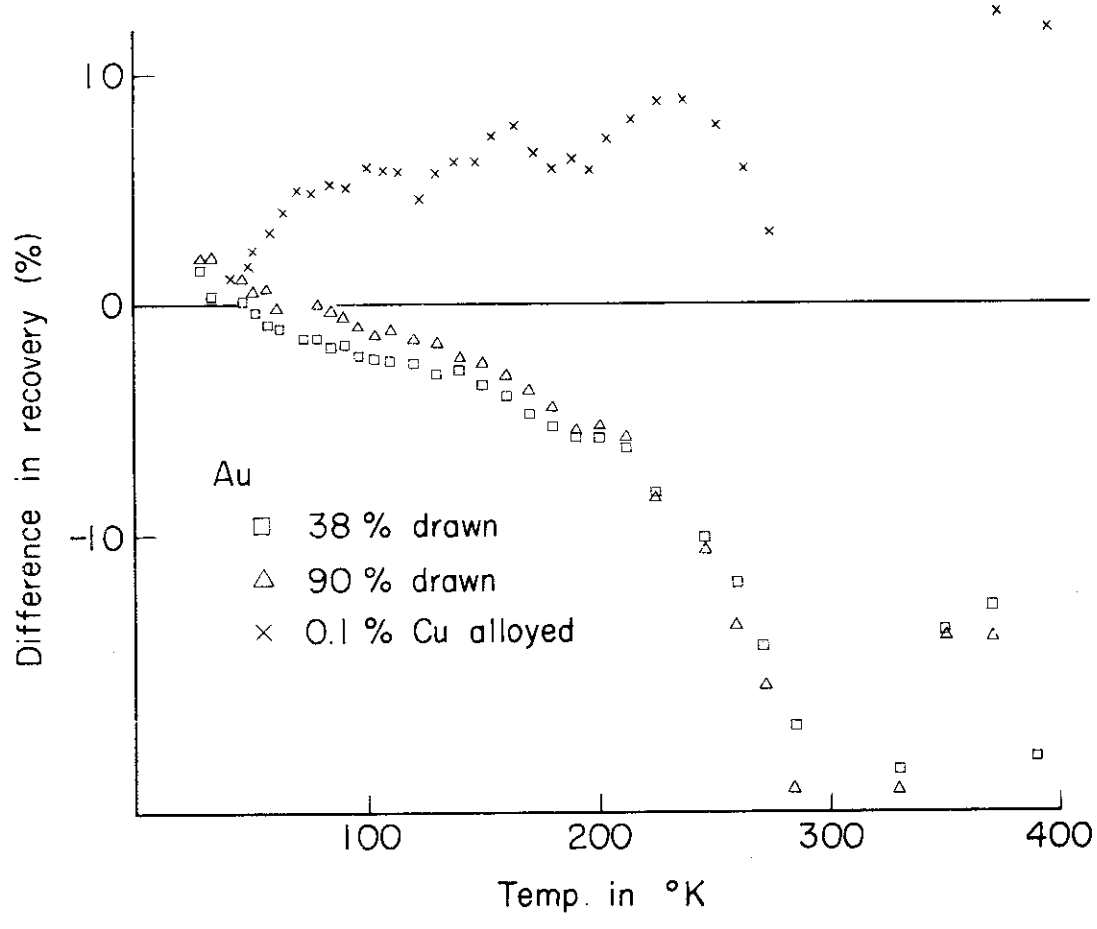
Difference in recovery (%)
10
0
-10
Au
□ 38 % drawn
△ 90 % drawn
× 0.1 % Cu alloyed
100
200
300
400
Temp. in °K

Fig. 18

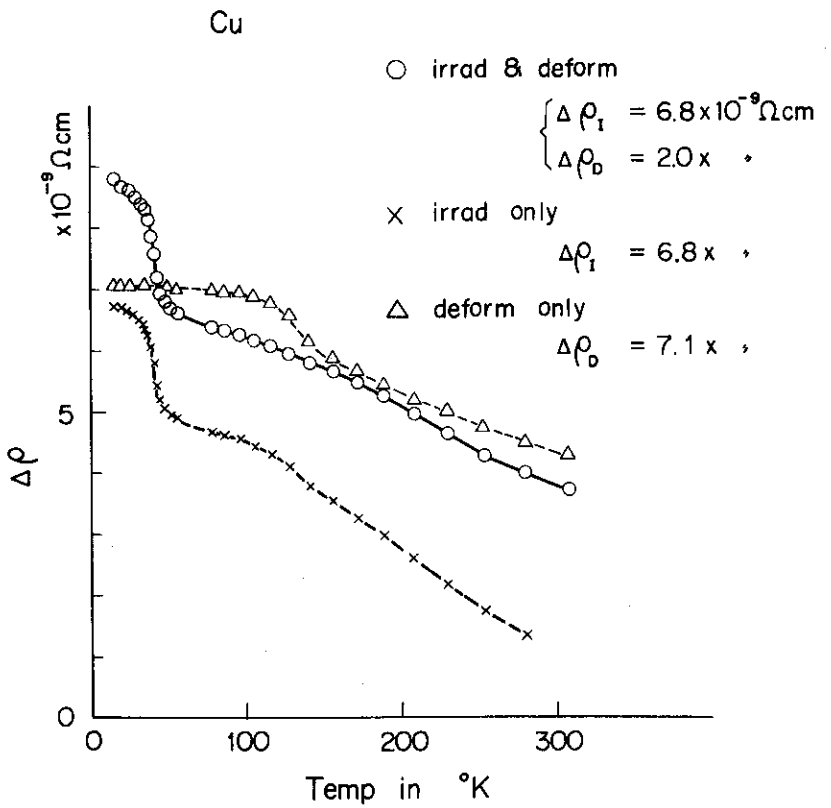
Cu
○ irrad & deform
Δρ_I = 6.8 x 10^-9 Ωcm
Δρ_D = 2.0 x ,
× irrad only
Δρ_I = 6.8 x ,
△ deform only
Δρ_D = 7.1 x ,
Δρ x10^-9 Ωcm
0
5
0
100
200
300
Temp in °K

Fig. 19

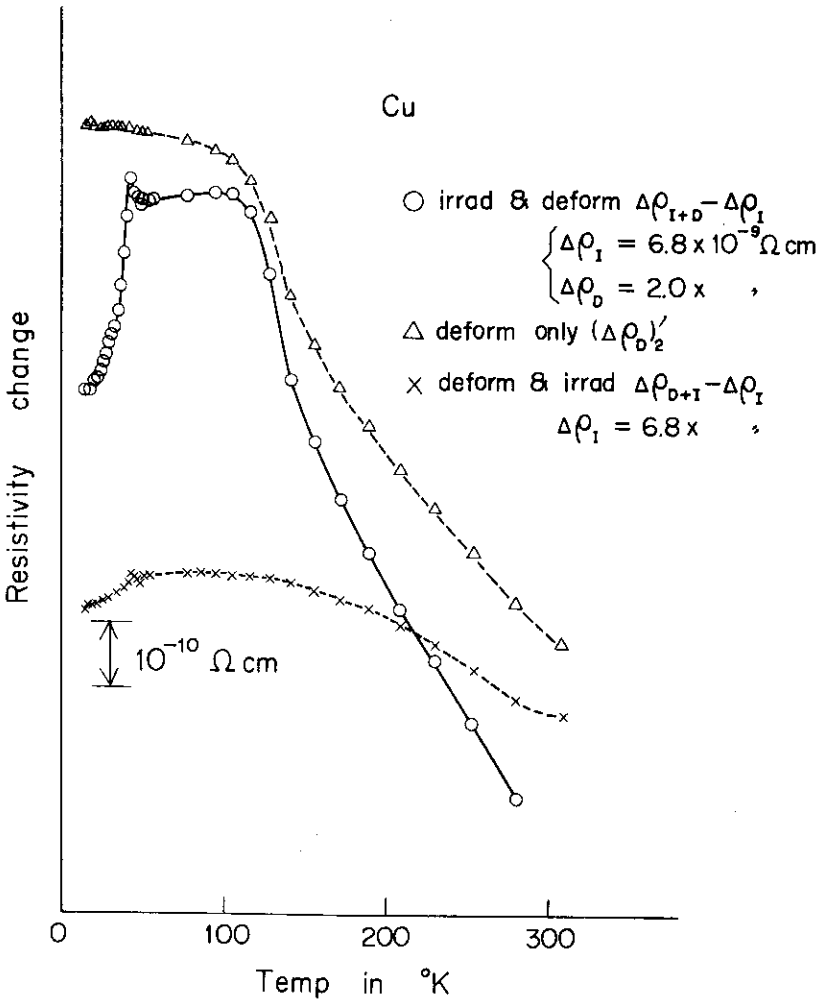
Cu
○ irrad & deform Δρ_I+D − Δρ_I
Δρ_I = 6.8 x 10^-9 Ωcm
Δρ_D = 2.0 x ,
△ deform only (Δρ_D)'_2
× deform & irrad Δρ_D+I − Δρ_I
Δρ_I = 6.8 x ,
Resistivity change
10^-10 Ωcm
0
100
200
300
Temp in °K

Fig. 20

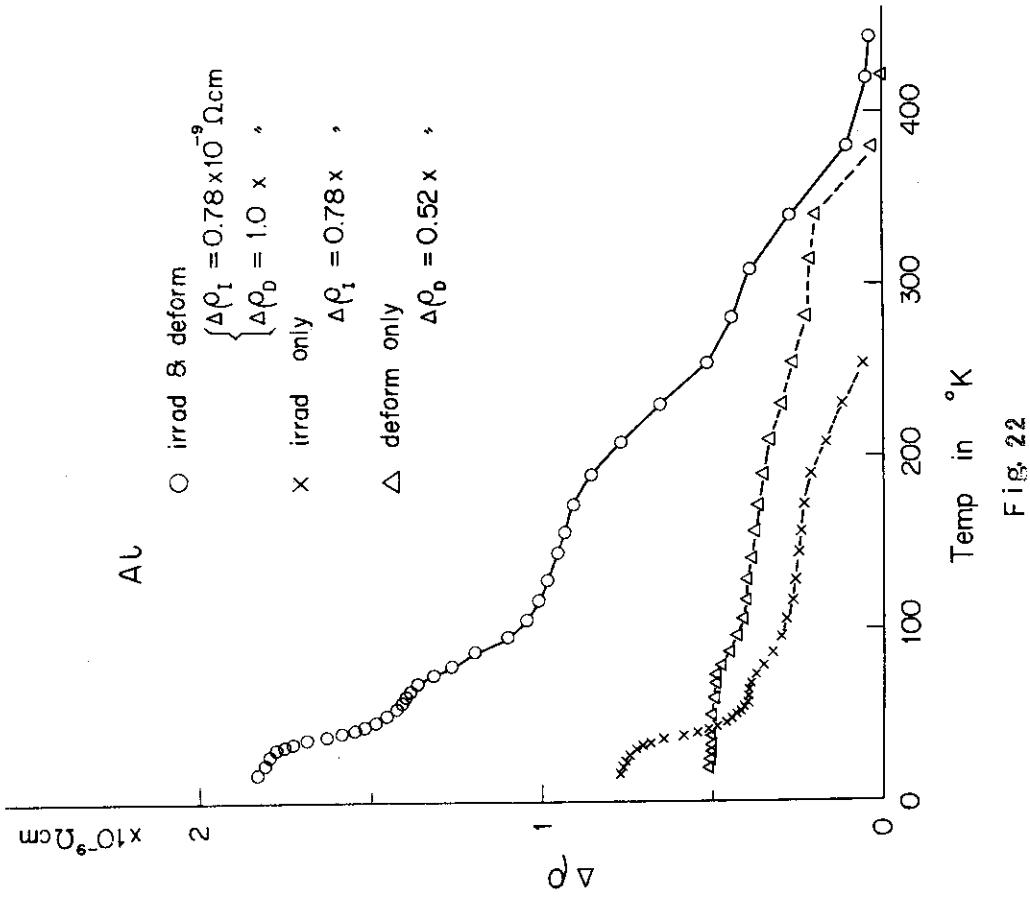
Al
○ irrad & deform
Δρ_I = 0.78×10⁻⁹ Ωcm
Δρ_D = 1.0 × "
× irrad only
Δρ_I = 0.78 × "
△ deform only
Δρ_D = 0.52 × "
Δρ
×10⁻⁹Ωcm
Temp in °K

Fig. 22

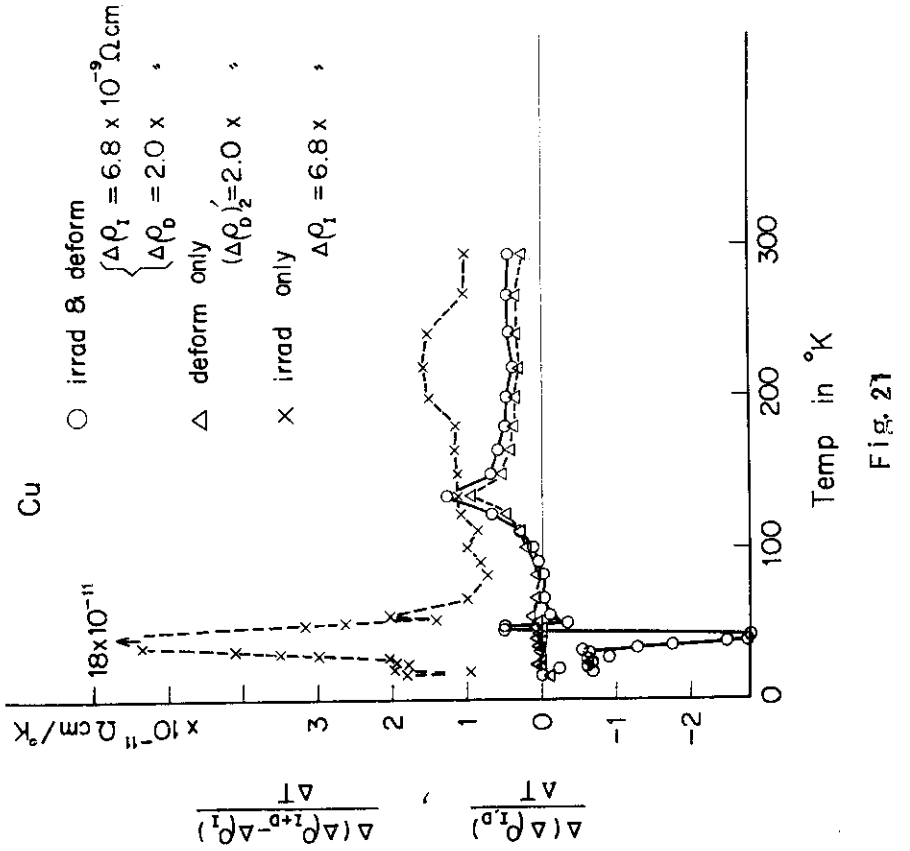
Cu
○ irrad & deform
Δρ_I = 6.8 × 10⁻⁹ Ωcm
Δρ_D = 2.0 × "
△ deform only
(Δρ_D)'_2 = 2.0 × "
× irrad only
Δρ_I = 6.8 × "
18×10⁻¹¹
×10⁻¹¹ Ωcm/°K
Δ(Δρ_I,D)/ΔT
Δ(Δρ_I+D − Δρ_I)/ΔT
Temp in °K

Fig. 21

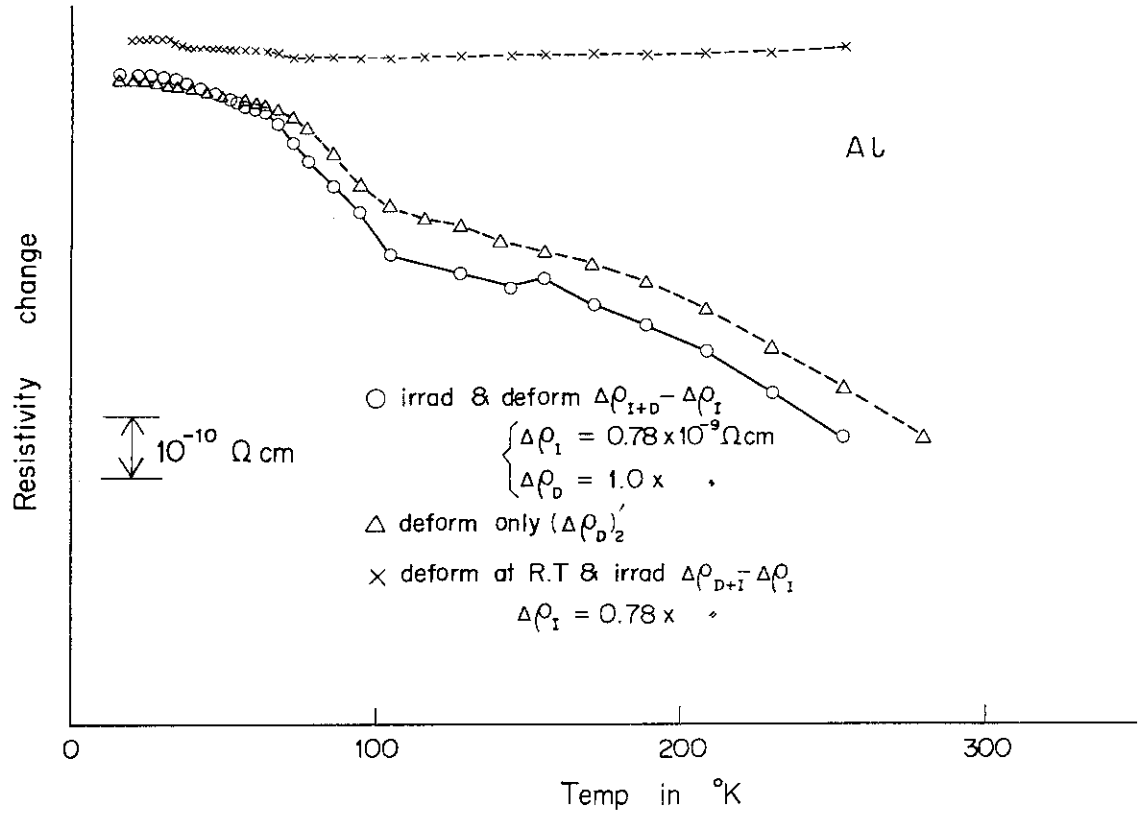
Al
Resistivity change
○ irrad & deform $\Delta\rho_{I+D}-\Delta\rho_I$
$\Delta\rho_I = 0.78\times10^{-9}\,\Omega$cm
$\Delta\rho_D = 1.0\times$
△ deform only $(\Delta\rho_D)'_2$
× deform at R.T & irrad $\Delta\rho_{D+I}-\Delta\rho_I$
$\Delta\rho_I = 0.78\times$
$10^{-10}\,\Omega$ cm
0
100
200
300
Temp in °K

Fig. 23

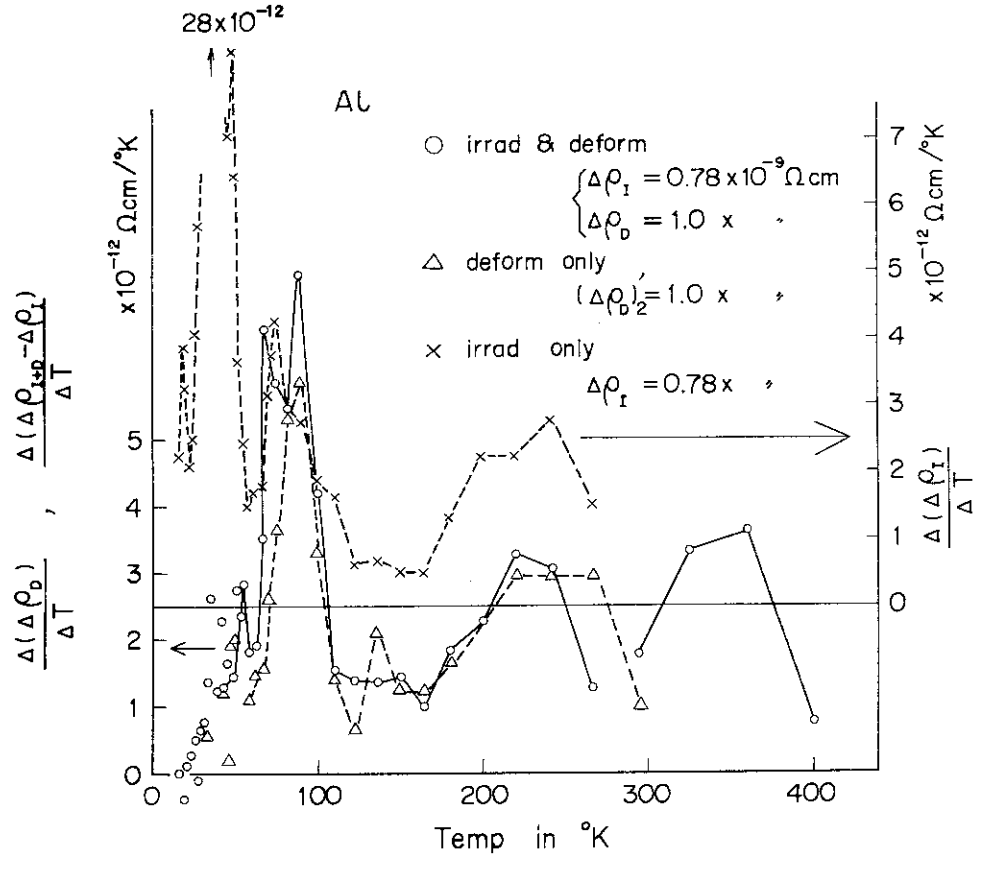
28×10^{-12}
Al
○ irrad & deform
$\Delta\rho_I = 0.78\times10^{-9}\,\Omega$cm
$\Delta\rho_D = 1.0\times$
△ deform only
$(\Delta\rho_D)'_2 = 1.0\times$
× irrad only
$\Delta\rho_I = 0.78\times$
$\frac{\Delta(\Delta\rho_D)}{\Delta T}$, $\frac{\Delta(\Delta\rho_{I+D}-\Delta\rho_I)}{\Delta T}$
$\times10^{-12}\,\Omega$cm/°K
$\frac{\Delta(\Delta\rho_I)}{\Delta T}$
$\times10^{-12}\,\Omega$cm/°K
0
100
200
300
400
Temp in °K

Fig. 24

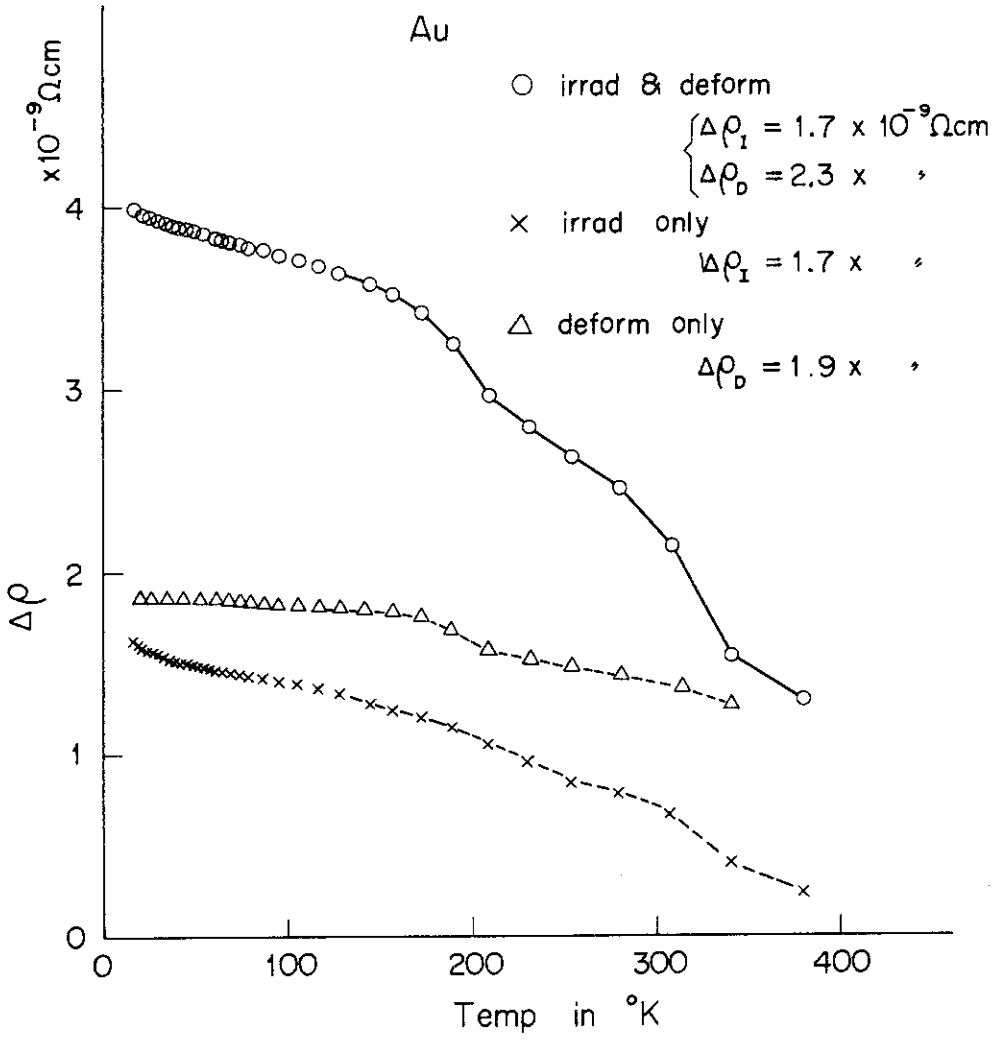
Au
○ irrad & deform
Δρ_I = 1.7 x 10⁻⁹Ωcm
Δρ_D = 2.3 x "
× irrad only
Δρ_I = 1.7 x "
△ deform only
Δρ_D = 1.9 x "
Δρ
x10⁻⁹Ωcm
0
1
2
3
4
0
100
200
300
400
Temp in °K

Fig. 25

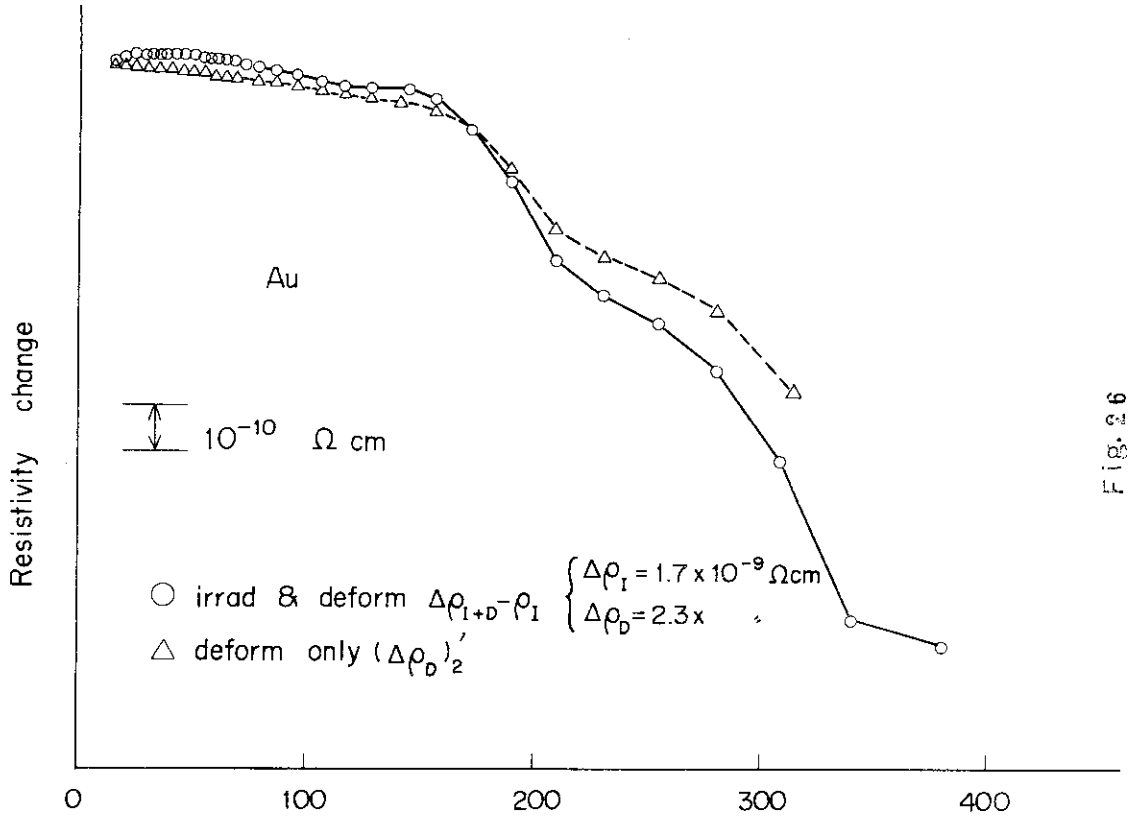
Au
Resistivity change
10^{-10} Ω cm
○ irrad & deform $\Delta\rho_{I+D}-\rho_I$ $\Delta\rho_I = 1.7\times10^{-9}$ Ωcm
△ deform only $(\Delta\rho_D)_2'$ $\Delta\rho_D = 2.3\times$
0
100
200
300
400
Temp in °K

Fig. 26

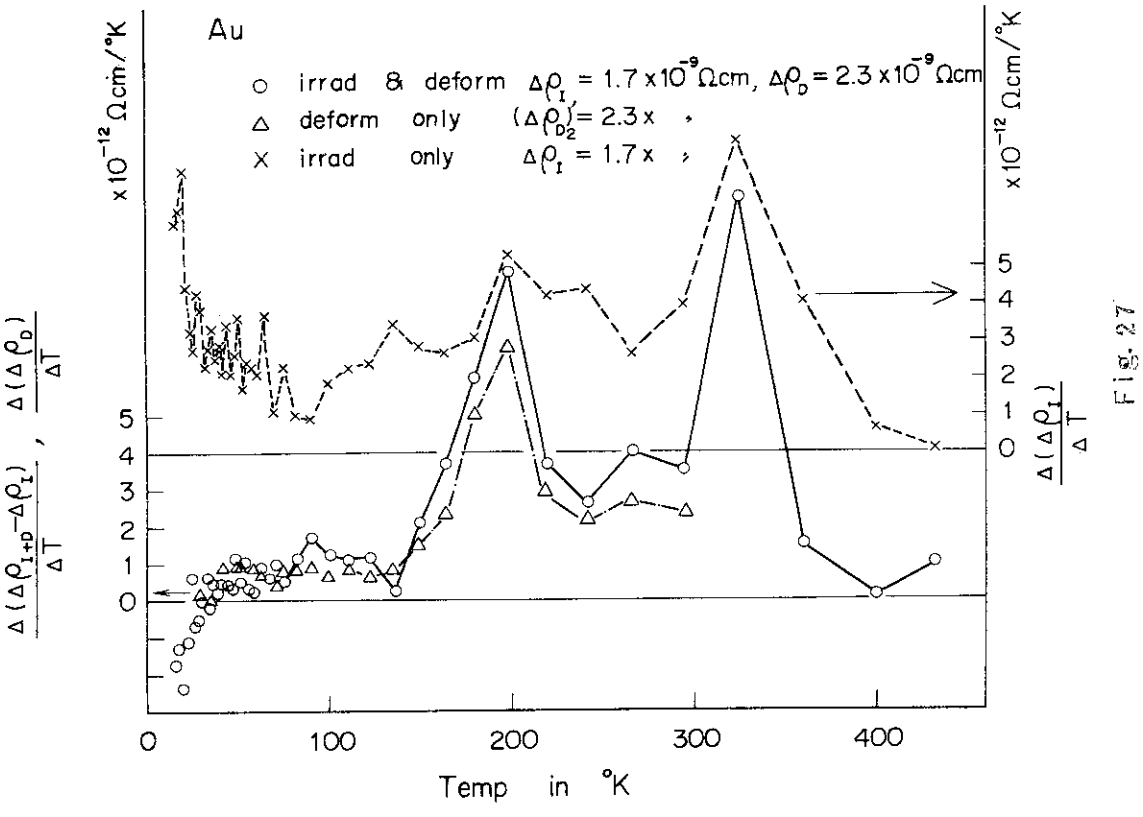
Au
○ irrad & deform $\Delta\rho_I = 1.7\times10^{-9}$Ωcm, $\Delta\rho_D = 2.3\times10^{-9}$Ωcm
△ deform only $(\Delta\rho_D)_2 = 2.3\times$
× irrad only $\Delta\rho_I = 1.7\times$
$\times10^{-12}$ Ωcm/°K
$\frac{\Delta(\Delta\rho_{I+D}-\Delta\rho_I)}{\Delta T}$, $\frac{\Delta(\Delta\rho_D)}{\Delta T}$
$\frac{\Delta(\Delta\rho_I)}{\Delta T}$
0 1 2 3 4 5
0
100
200
300
400
Temp in °K

Fig. 27

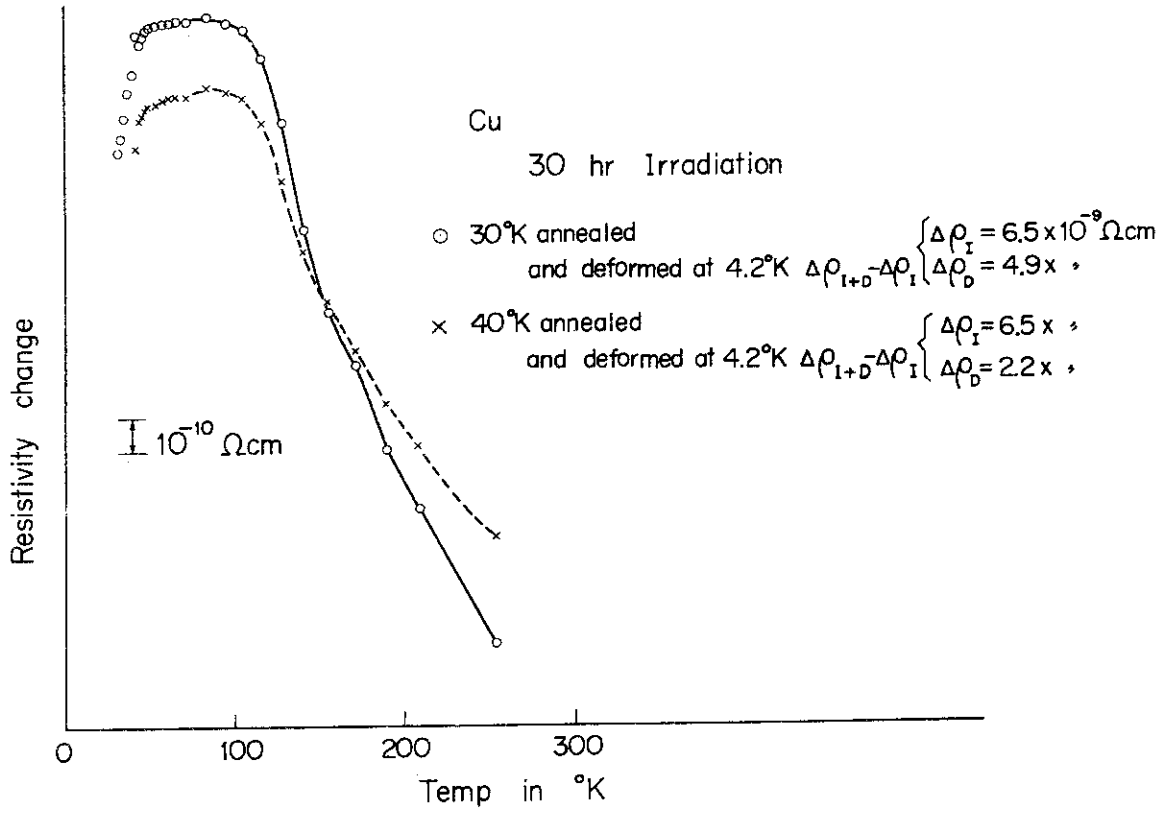
Cu
30 hr Irradiation
○ 30°K annealed
and deformed at 4.2°K Δρ_{I+D}-Δρ_I { Δρ_I = 6.5×10^-9 Ωcm, Δρ_D = 4.9× "
× 40°K annealed
and deformed at 4.2°K Δρ_{I+D}-Δρ_I { Δρ_I = 6.5× ", Δρ_D = 2.2× "
I 10^-10 Ωcm
Resistivity change
0
100
200
300
Temp in °K

Fig. 28

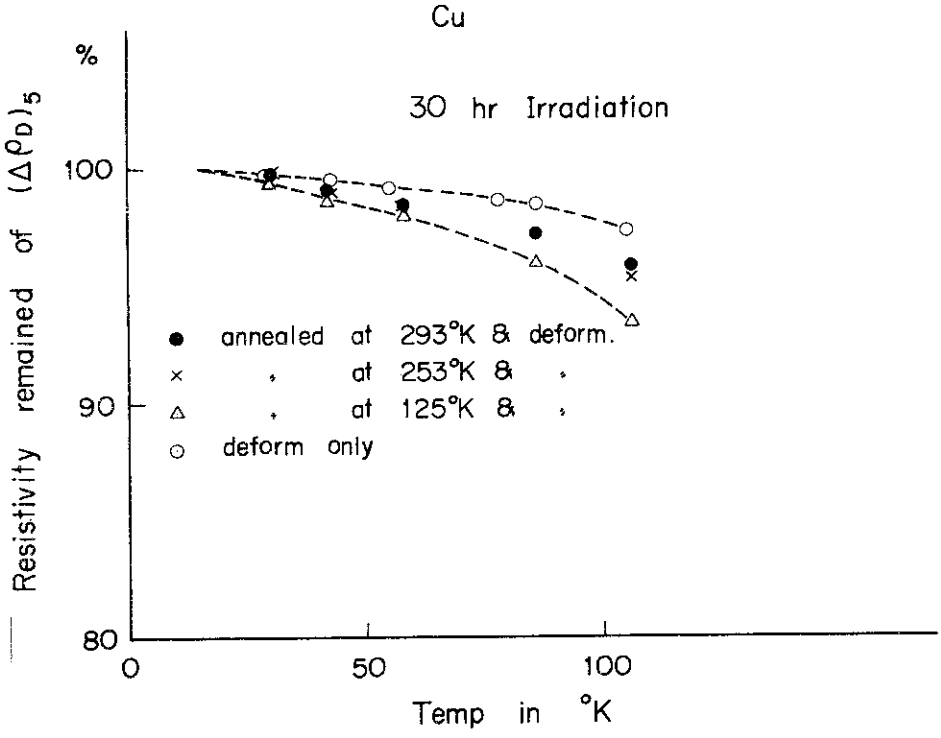
Cu
30 hr Irradiation
% Resistivity remained of (Δρ_D)_5
100
90
80
● annealed at 293°K & deform.
× " at 253°K & "
△ " at 125°K & "
○ deform only
0
50
100
Temp in °K

Fig. 29

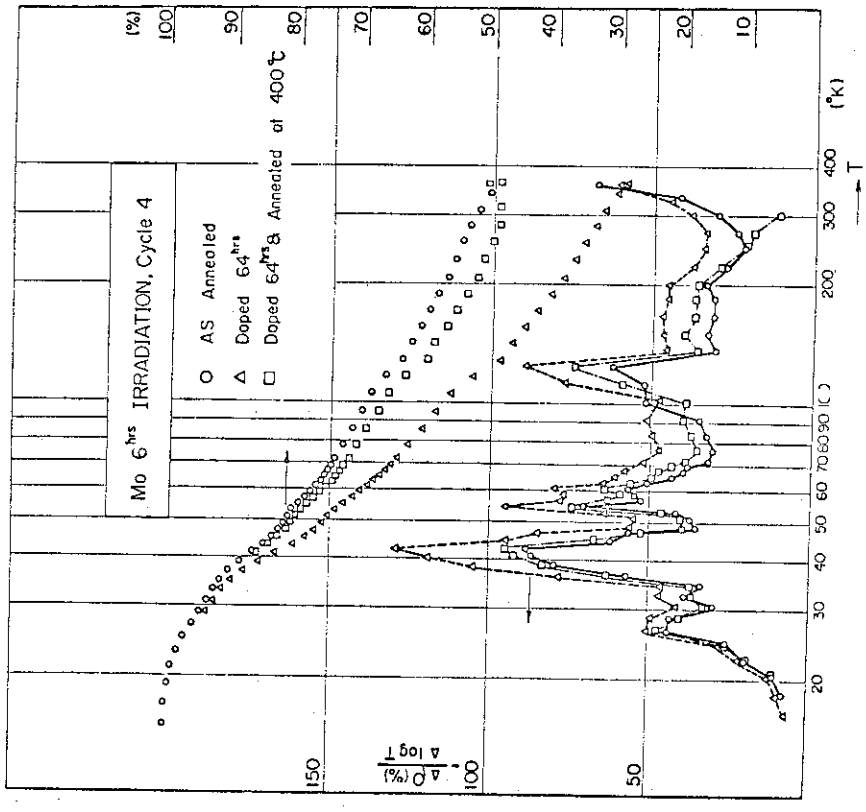
Mo 6hrs IRRADIATION, Cycle 4
○ AS Annealed
△ Doped 64hrs
□ Doped 64hrs & Annealed at 400℃
(%)
(°K)
T

Fig. 31

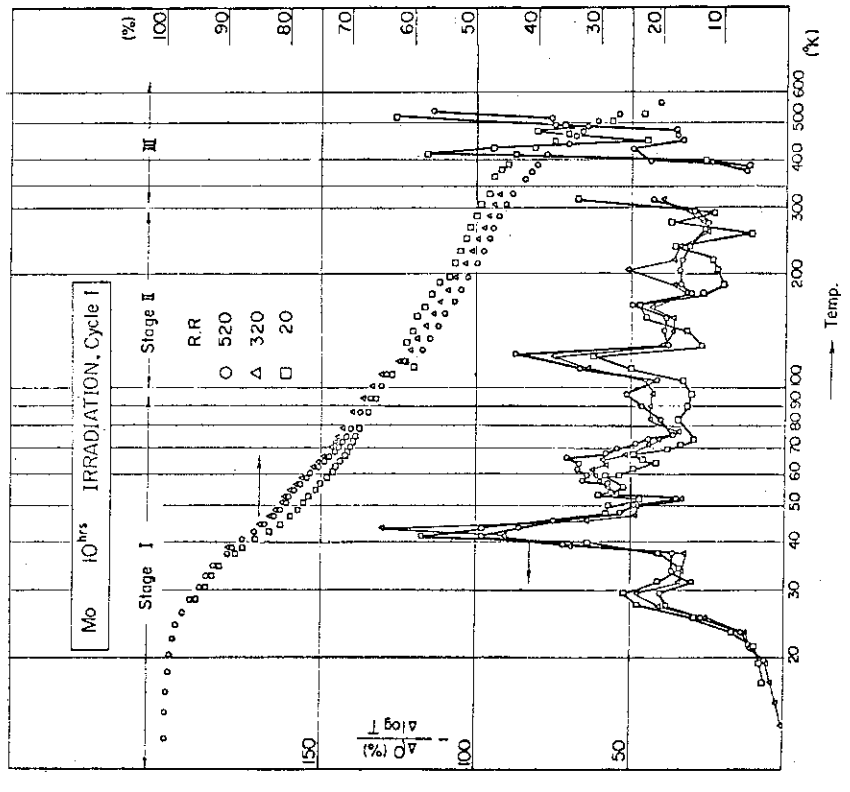
Mo 10hrs IRRADIATION, Cycle 1
Stage I
Stage II
III
R.R
○ 520
△ 320
□ 20
(%)
(°K)
Temp.

Fig. 30

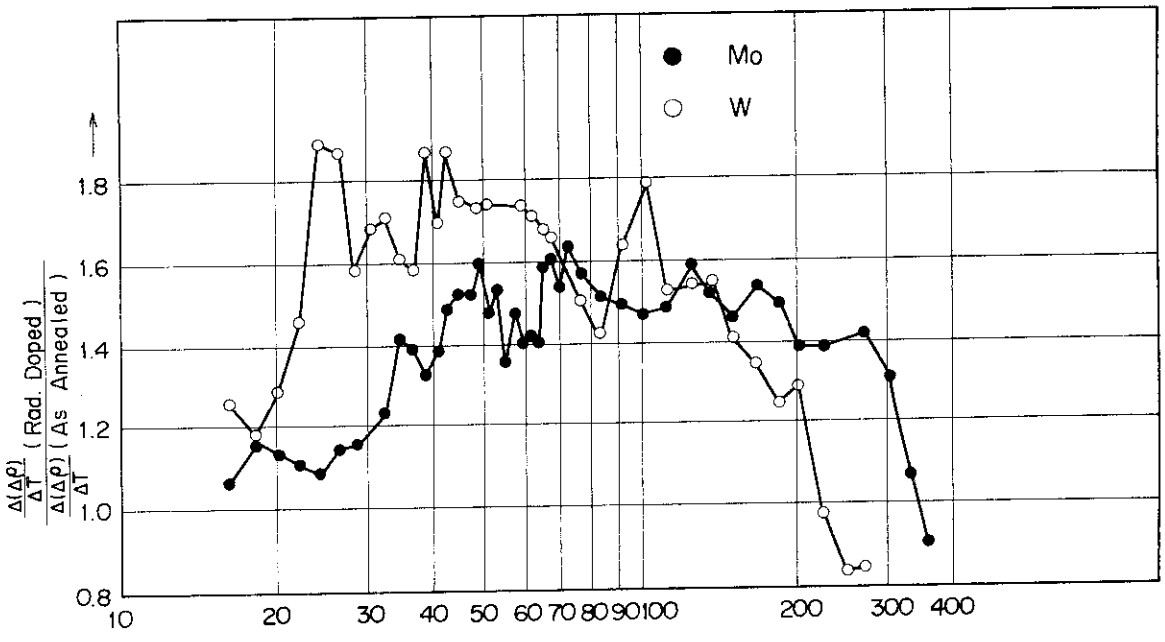
Mo
W
1.8
1.6
1.4
1.2
1.0
0.8
10
20
30
40
50
60
70
80
90
100
200
300
400

Fig. 32

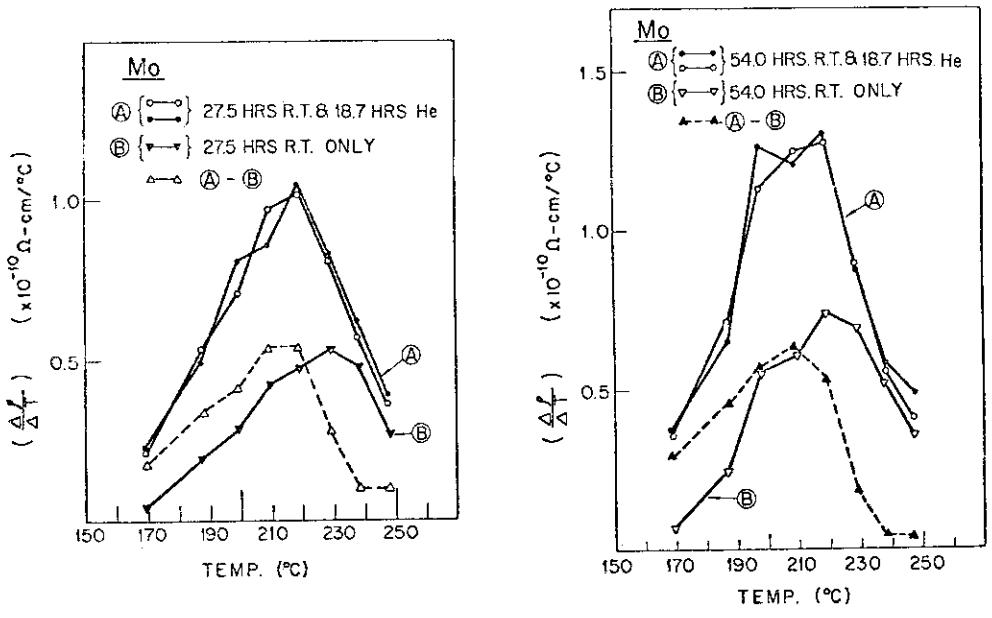
Mo
Ⓐ 27.5 HRS R.T. & 18.7 HRS He
Ⓑ 27.5 HRS R.T. ONLY
Ⓐ - Ⓑ
1.0
0.5
150
170
190
210
230
250
TEMP. (°C)
Mo
Ⓐ 54.0 HRS. R.T. & 18.7 HRS. He
Ⓑ 54.0 HRS. R.T. ONLY
Ⓐ - Ⓑ
1.5
1.0
0.5
150
170
190
210
230
250
TEMP. (°C)

Fig. 33

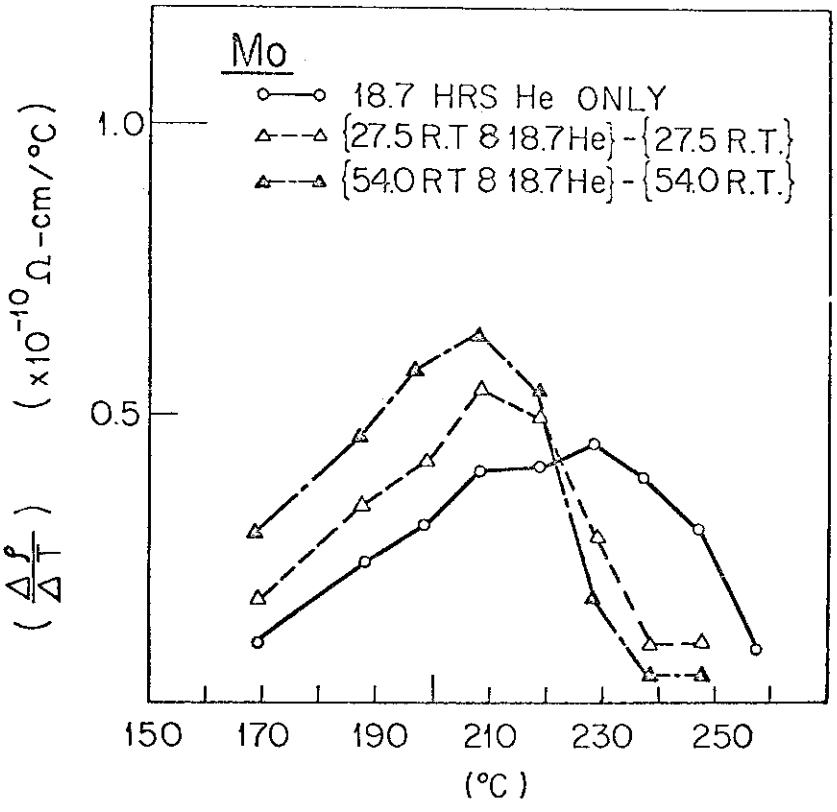
Mo
18.7 HRS He ONLY
{27.5 R.T & 18.7 He} - {27.5 R.T.}
{54.0 R.T & 18.7 He} - {54.0 R.T.}
1.0
0.5
$(\frac{\Delta\rho}{\Delta T})$ $(\times 10^{-10}\ \Omega\text{-cm}/°C)$
150
170
190
210
230
250
(°C)

Fig. 34

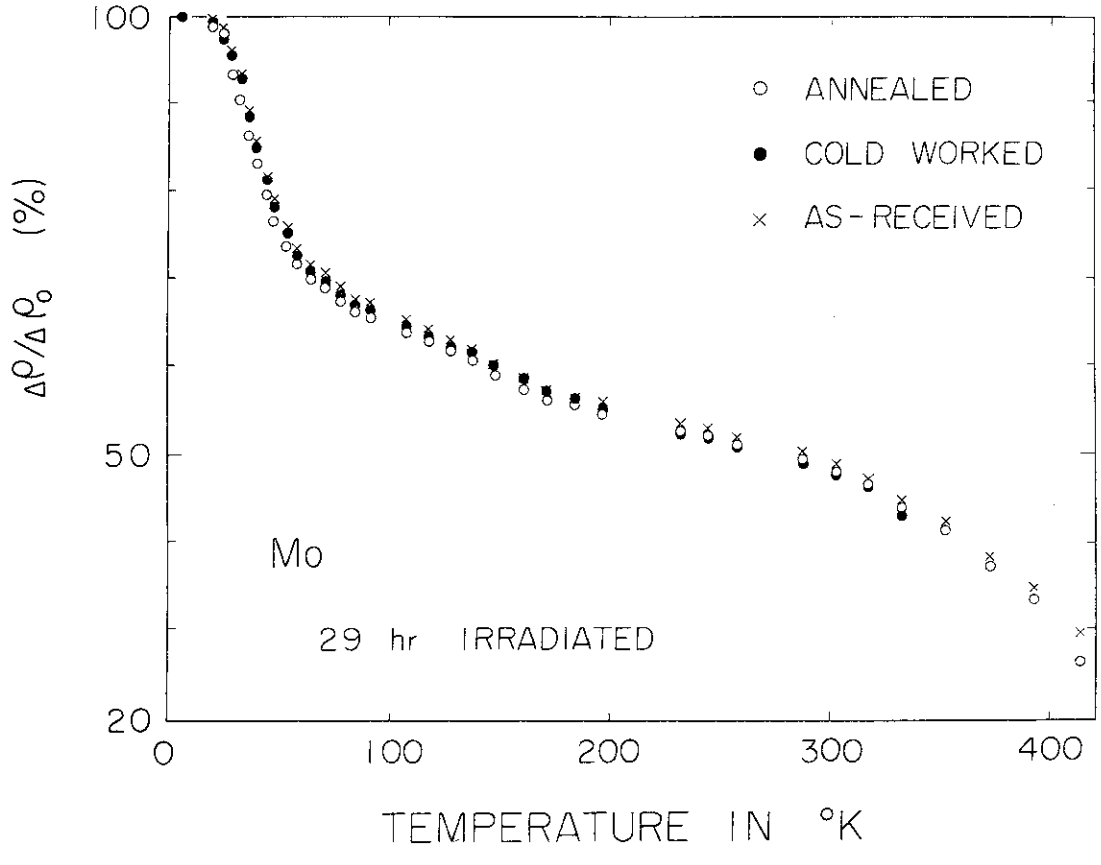
100
50
20
$\Delta\rho/\Delta\rho_0$ (%)
ANNEALED
COLD WORKED
AS-RECEIVED
Mo
29 hr IRRADIATED
0
100
200
300
400
TEMPERATURE IN °K

Fig. 35

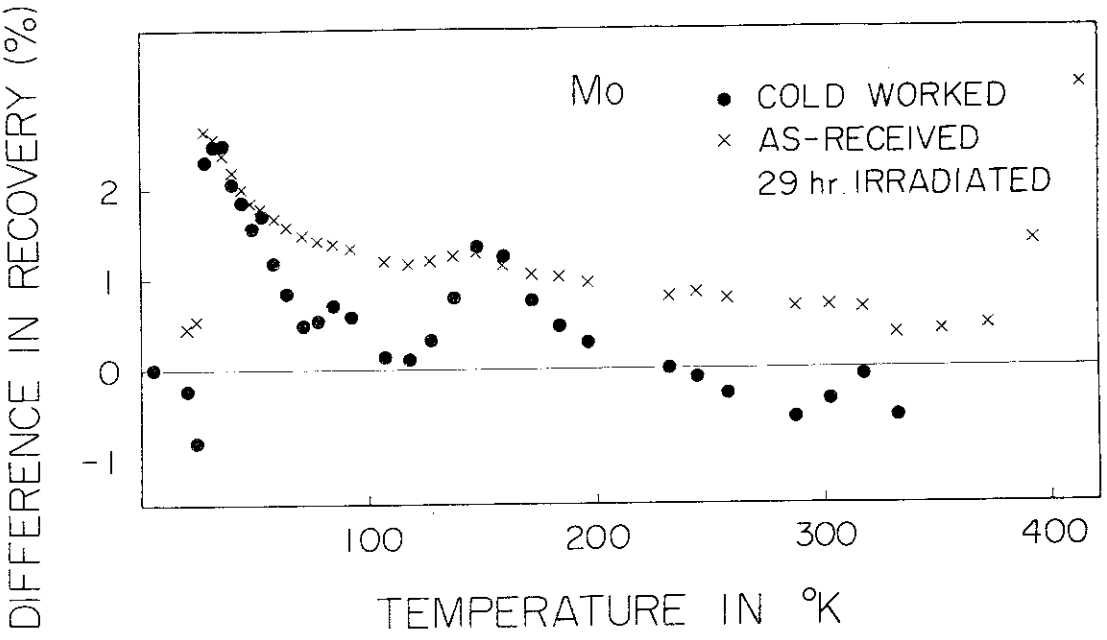
DIFFERENCE IN RECOVERY (%)
Mo
COLD WORKED
AS-RECEIVED
29 hr. IRRADIATED
2
1
0
−1
100
200
300
400
TEMPERATURE IN °K

Fig. 36

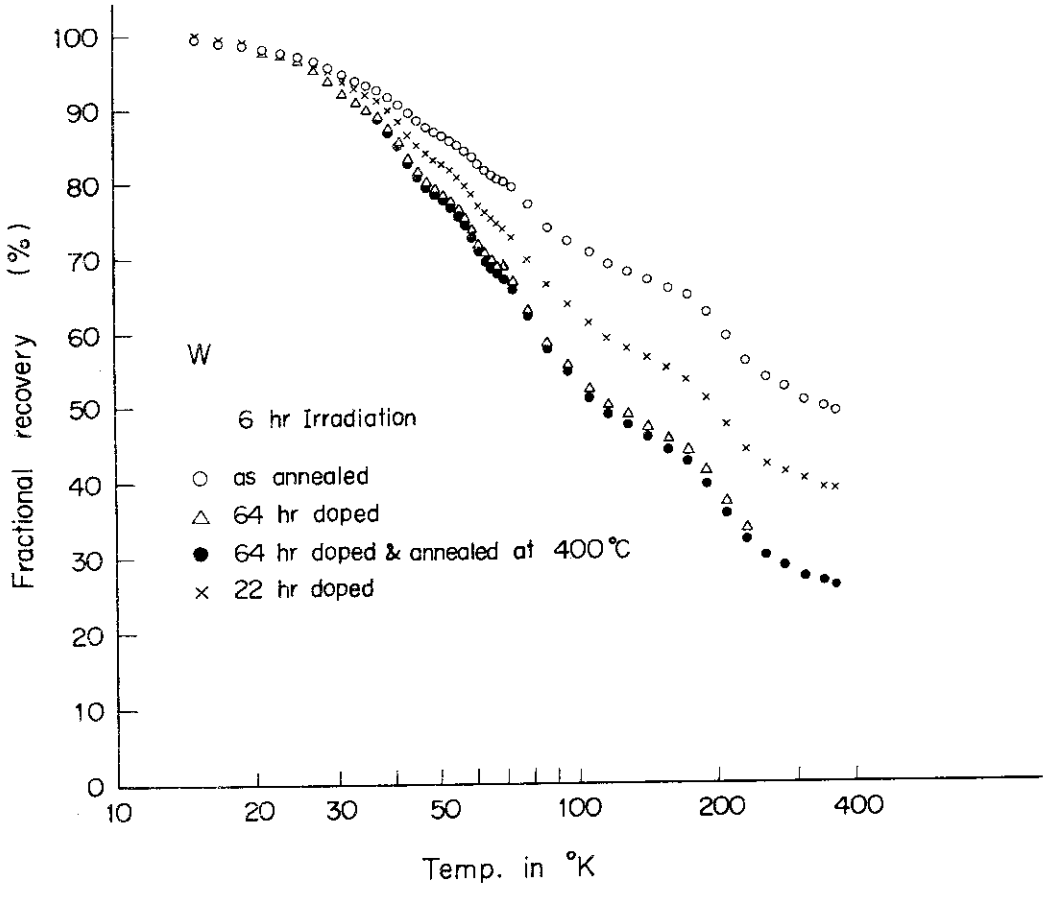
Fractional recovery (%)
W
6 hr Irradiation
as annealed
64 hr doped
64 hr doped & annealed at 400°C
22 hr doped
100
90
80
70
60
50
40
30
20
10
0
10
20
30
50
100
200
400
Temp. in °K

Fig. 37

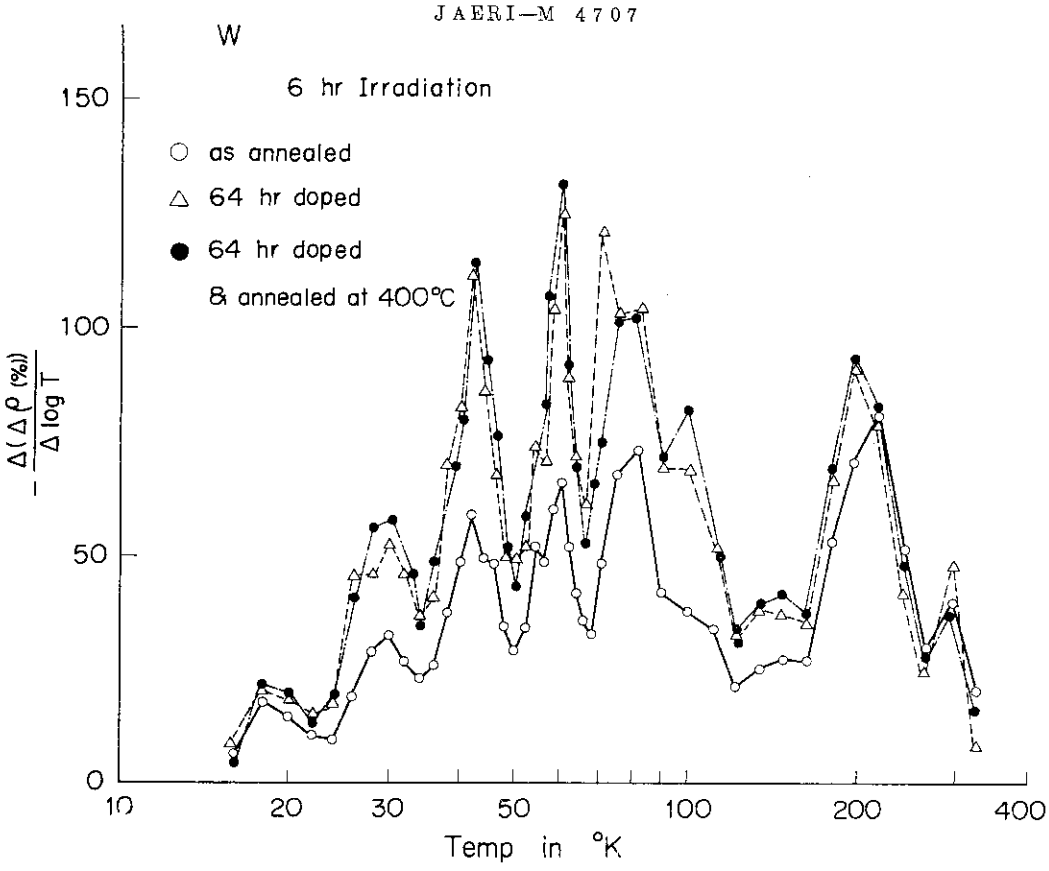
W
6 hr Irradiation
○ as annealed
△ 64 hr doped
● 64 hr doped
& annealed at 400°C
$-\frac{\Delta(\Delta\rho(\%))}{\Delta \log T}$
150
100
50
0
10
20
30
50
100
200
400
Temp in °K

Fig. 38

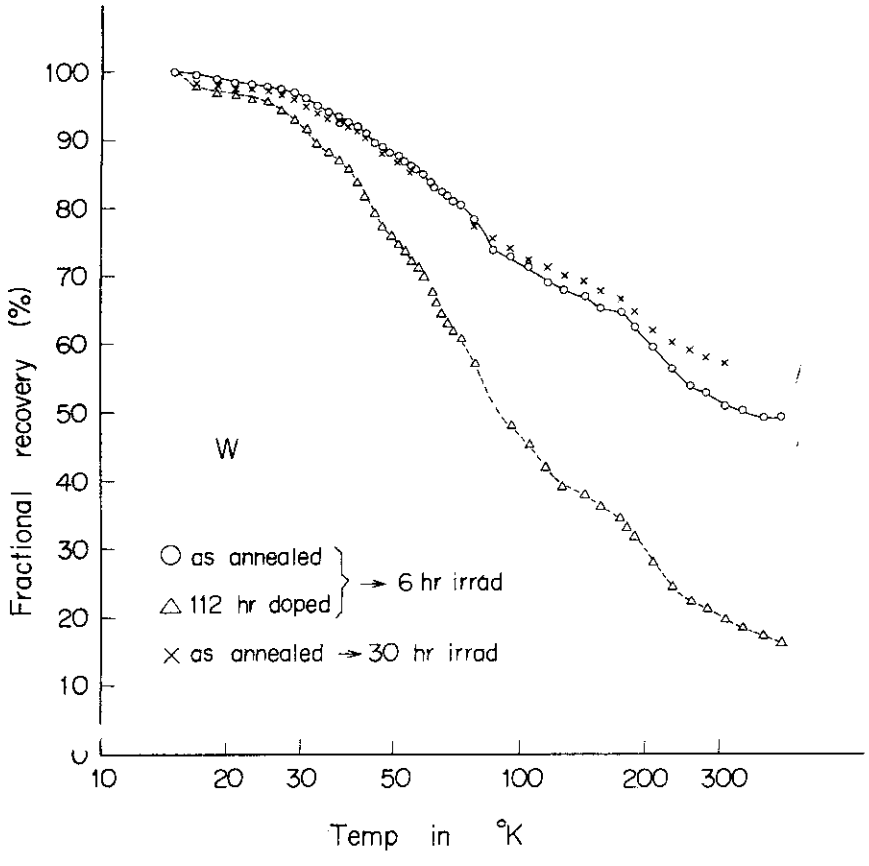
Fractional recovery (%)
100
90
80
70
60
50
40
30
20
10
0
W
○ as annealed
△ 112 hr doped
→ 6 hr irrad
× as annealed → 30 hr irrad
10
20
30
50
100
200
300
Temp in °K

Fig. 39

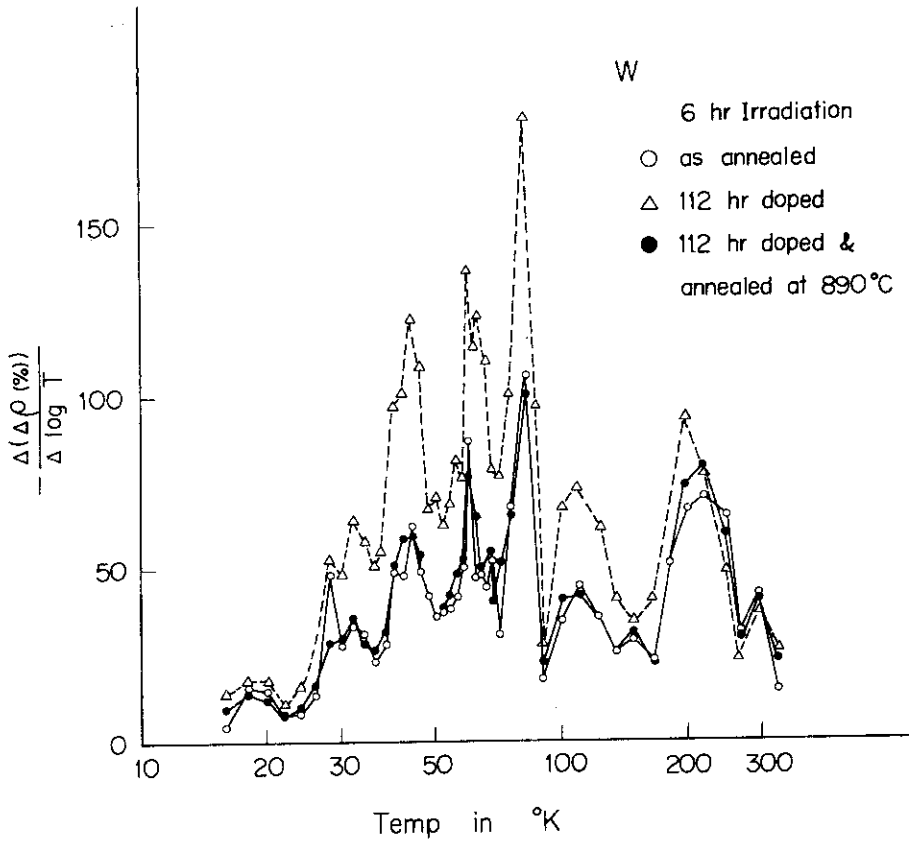
W
6 hr Irradiation
○ as annealed
△ 112 hr doped
● 112 hr doped &
annealed at 890°C
150
100
50
0
10
20
30
50
100
200
300
Temp in °K

Fig. 40

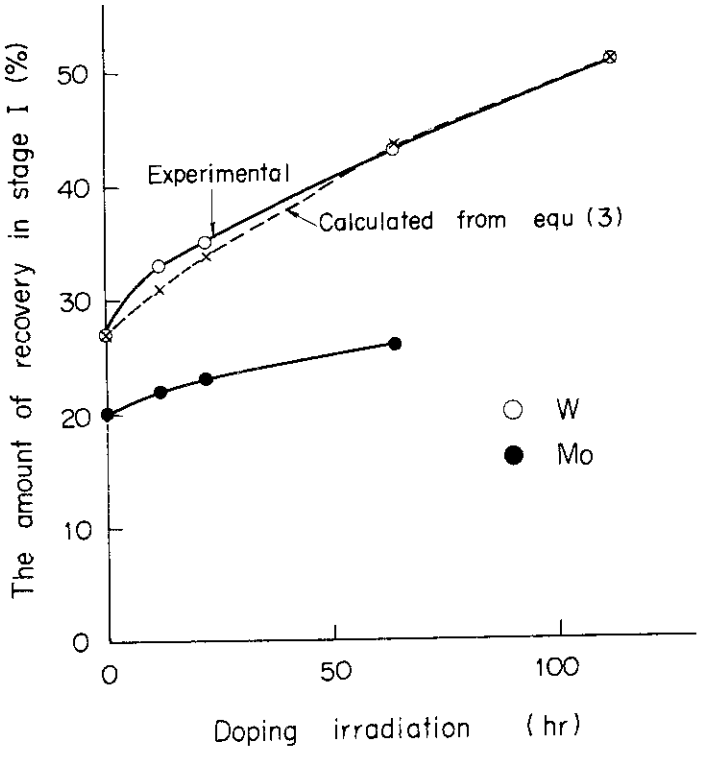
Experimental
Calculated from equ (3)
○ W
● Mo
50
40
30
20
10
0
0
50
100
Doping irradiation (hr)

Fig. 41

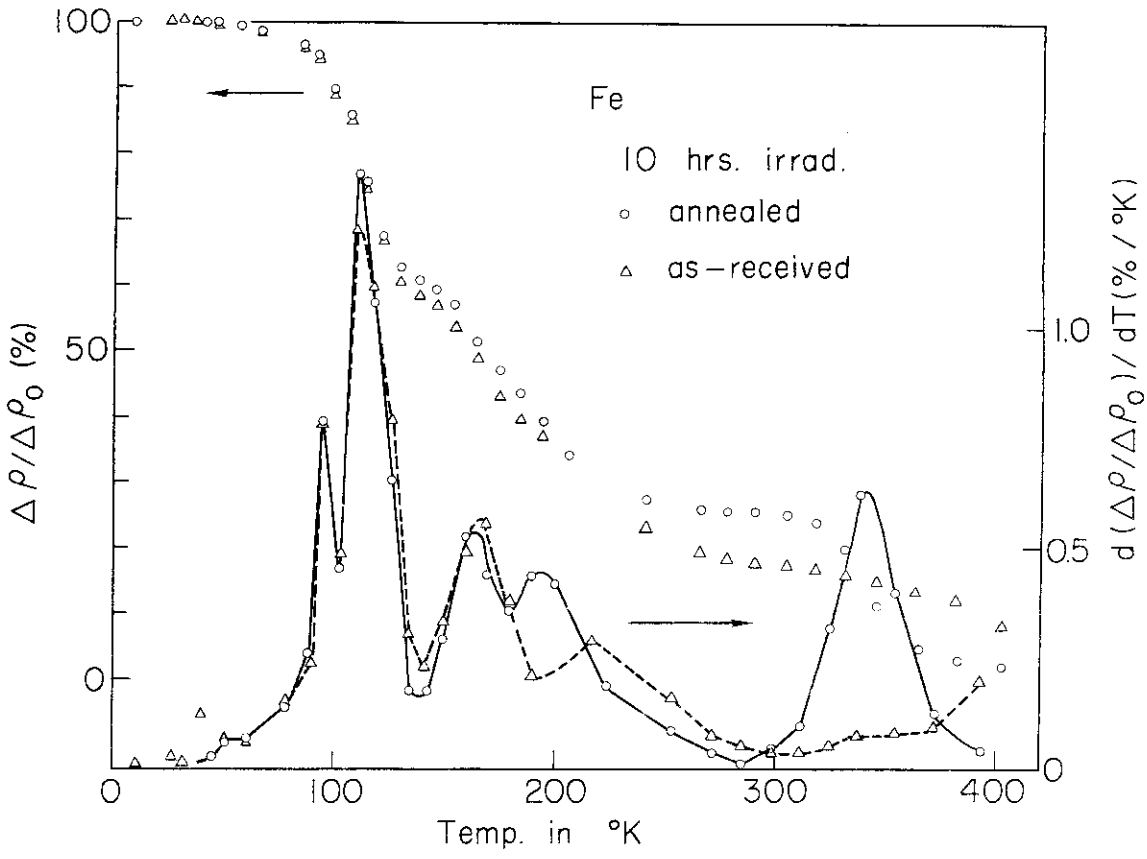
Fe
10 hrs. irrad.
annealed
as-received
Δρ/Δρ0 (%)
d(Δρ/Δρ0)/dT(%/°K)
Temp. in °K
100
50
0
1.0
0.5
0
100
200
300
400

Fig. 42

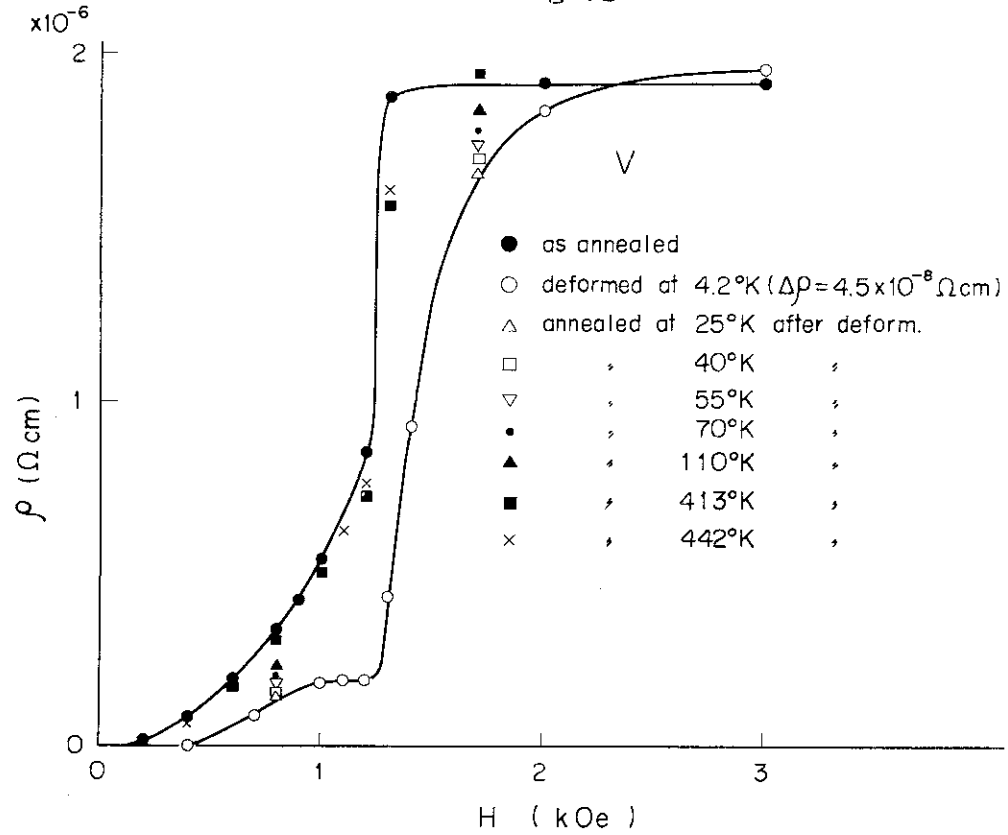
x10⁻⁶
2
1
0
ρ (Ω cm)
V
as annealed
deformed at 4.2°K (Δρ=4.5x10⁻⁸ Ωcm)
annealed at 25°K after deform.
40°K
55°K
70°K
110°K
413°K
442°K
0
1
2
3
H (kOe)

Fig. 43

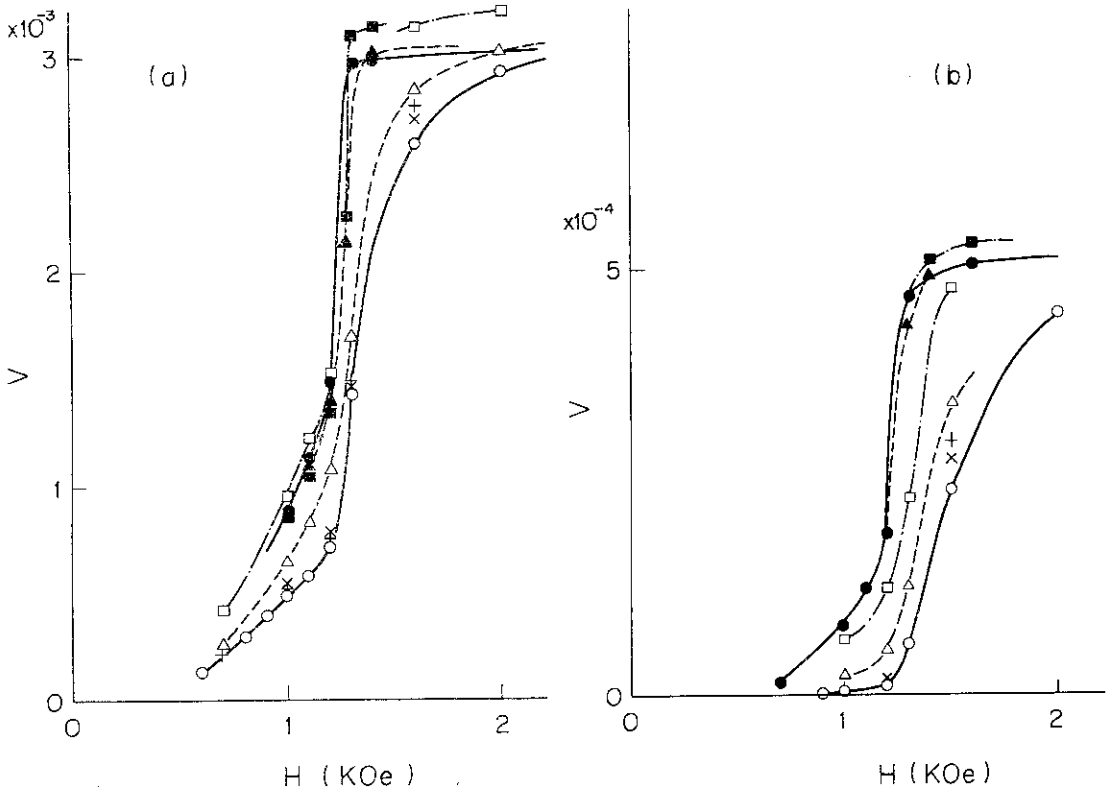
x10⁻³
3
2
1
0
V
(a)
0
1
2
H (KOe)
x10⁻⁴
5
0
V
(b)
0
1
2
H (KOe)

Fig. 44

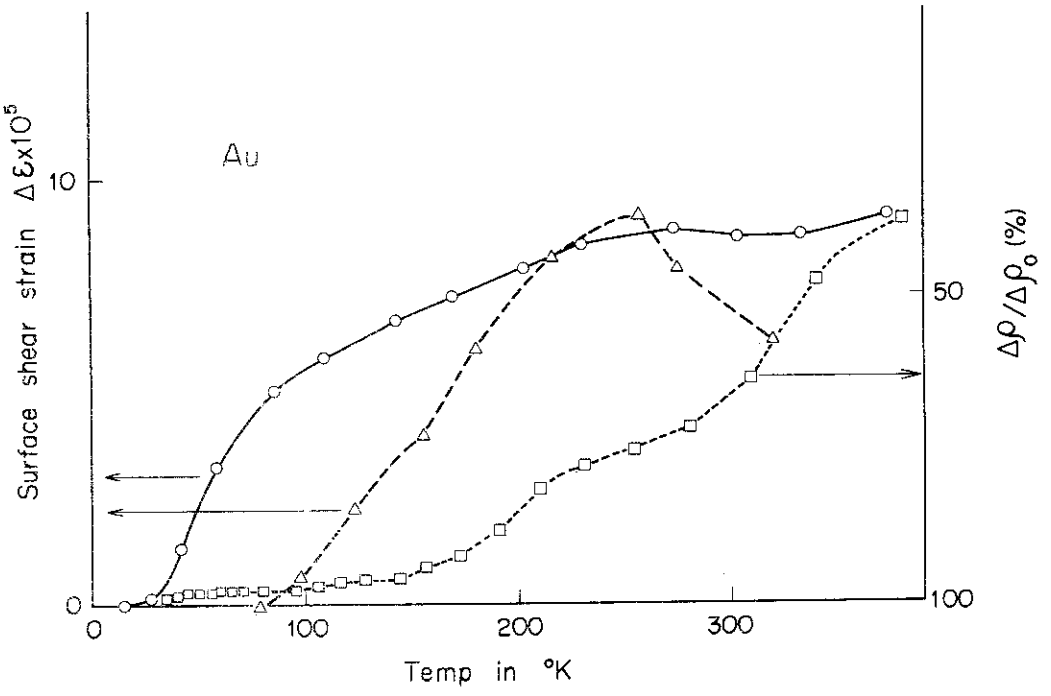
Au
Surface shear strain Δε x10⁵
10
0
0
100
200
300
Temp in °K
50
100
Δρ/Δρ₀ (%)

Fig. 45

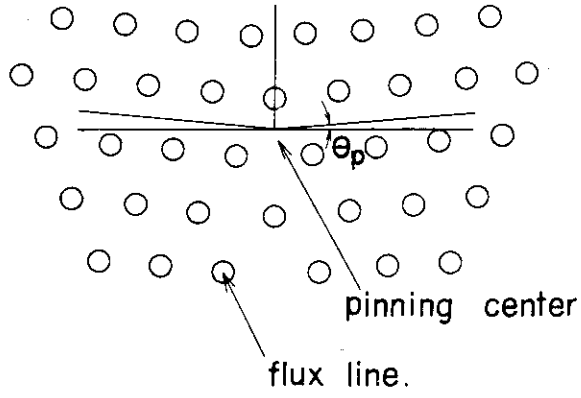
θ_p
pinning center
flux line.

Fig. 46

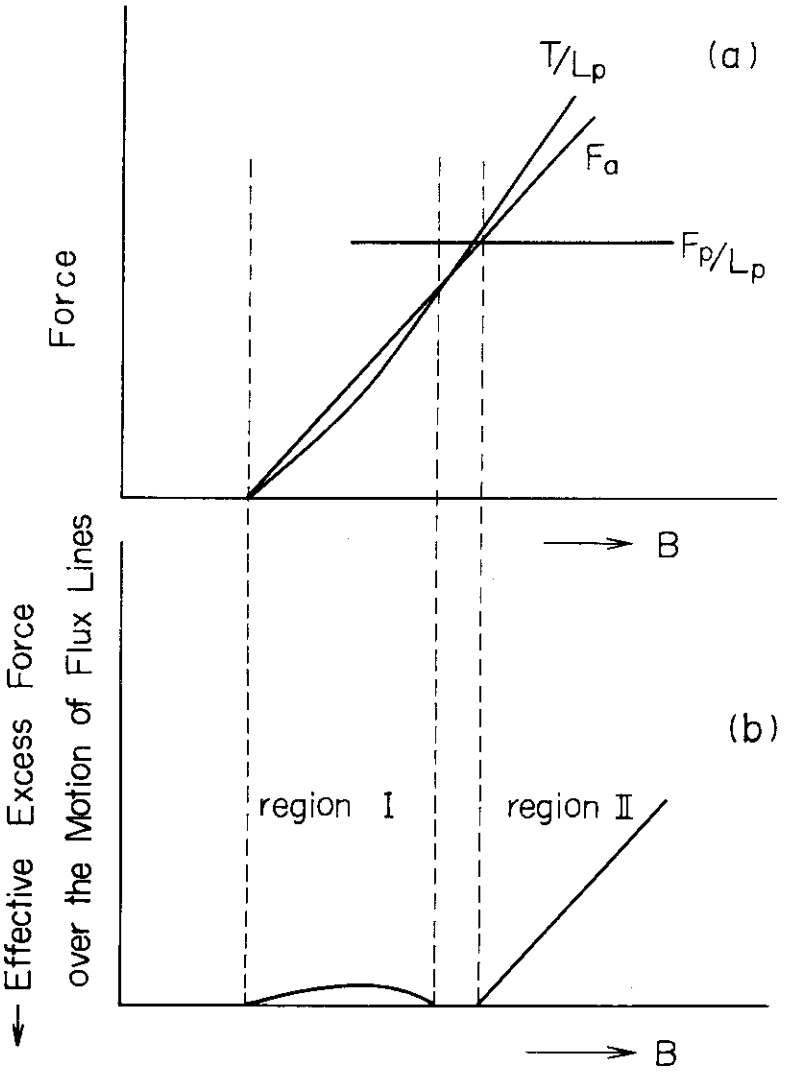
T/L_p
(a)
F_a
F_p/L_p
Force
B
(b)
region I
region II
← Effective Excess Force over the Motion of Flux Lines
B

Fig. 47